

## 6. SITE 923<sup>1</sup>

### Shipboard Scientific Party<sup>2</sup>

#### HOLE 923A

**Date occupied:** 7 January 1994

**Date departed:** 13 January 1994

**Time on hole:** 5 days, 10 hr, 39 min

**Position:** 23°32.556'N, 45°1.896'W

**Bottom felt (drill-pipe measurement from rig floor, m):** 2440.0

**Distance between rig floor and sea level (m):** 11.30

**Water depth (drill-pipe measurement from sea level, m):** 2428.7

**Total depth (from rig floor, m):** 2510.00

**Penetration (m):** 70.00

**Number of cores (including cores having no recovery):** 16

**Total length of cored section (m):** 70.00

**Total core recovered (m):** 40.76

**Core recovery (%):** 74.7

#### **Hard rock:**

Depth (mbsf): 70.00

Nature: Olivine gabbro, gabbro, troctolite, poikilitic olivine gabbro

Measured velocity (km/s): 5.40–6.58

**Principal results:** Site 923 is located on the western median valley wall of the Mid-Atlantic Ridge at 23°32.55'N, 45°01.90'W, about 6 km south of the Kane Fracture Zone and about 200 m north of Site 921 (Fig. 4, "Introduction," this volume). It is located a few meters upslope from an outcrop of massive gabbroic rocks with a slabby internal structure. At the outcrop scale, these rocks look very similar to the gabbroic rocks drilled at Site 922 and contrast with the more schistose outcrops at Site 921.

A total of 40.76 m of gabbroic rocks were recovered during drilling to a depth of 70.0 m (cumulative recovery 74.7%) in Hole 923A, the only hole at this site. Olivine gabbro, gabbro, troctolite, and poikilitic olivine gabbro are the dominant rock types recovered. These rock types are texturally heterogeneous and interlayered on scales of centimeters to meters, although in some cases long sections of core are composed of relatively uniform gabbro. Oxide gabbro and gabbro-norite are less common in Hole 923A than at Sites 922 and 921. Five lithological units have been distinguished on the basis of the dominant rock type present through vertical intervals of a few meters to tens of meters.

Layering in this gabbroic sequence is defined by variations in modal composition, grain-size, or both. Modal proportions of olivine vary over vertical intervals of meters to tens of meters and some poikilitic olivine gabbro intervals have crescumulate textures. Both green and brown clinopyroxene occur as interstitial phases in poikilitic olivine gabbro and troctolite. Large, anhedral, green clinopyroxene oikocrysts are rimmed by brown clinopyroxene. In contrast, brown clinopyroxene occurs as a cumulus phase in gabbro and in non-poikilitic olivine gabbro.

Alteration of variably deformed gabbroic rocks recovered from Hole 923A is strikingly low (10% average). Brown hornblende discontinuously rimming clinopyroxene, and as an interstitial phase, is the peak metamor-

phic mineral phase. Some of it may have crystallized as an igneous phase. Replacement of olivine by fine-grained oxide minerals, minor talc, cumingtonite, tremolite, smectite, and a trace of calcite and pyrite dominates alteration in most of the rocks recovered. Alteration of olivine is slight in most samples (<10%), with pervasive alteration typically limited to fine interstitial grains. In contrast to metagabbroic rocks from Sites 921 and 922, alteration coronas around olivine are generally absent, and chlorite is only a trace secondary phase. Clinopyroxene is generally slightly to negligibly altered to blebs and rims of brown hornblende, fine-grained magnetite, and a trace of actinolite. In rare, highly altered samples, clinopyroxene is overgrown by light green amphibole, and brown amphibole is rimmed by olive green amphibole. Similar to clinopyroxene, replacement of plagioclase by secondary phases is negligible in most samples. Alteration phases include minor chlorite and secondary plagioclase.

Rare, highly altered sections throughout the core are typically restricted to narrow mylonitic and cataclastic zones and to the vicinity of crosscutting felsic veins. In these zones, intense replacement by actinolite, chlorite, and smectite after mafic phases is ubiquitous, and plagioclase is in some places pervasively altered to prehnite, clay minerals, and secondary plagioclase with minor epidote. Many of these intensely altered zones are associated with fine veins, less than or equal to 1 mm wide, which form a network and are composed of chlorite, actinolite, rare prehnite, and epidote. Veinlets of clay and zeolite minerals also occur. Overall, such veinlets are less common and the general intensity of alteration is lower in the gabbroic rocks from Hole 923A than in those of Sites 921 and 922.

Trondhjemitic veins, 20–30 mm wide, are sparsely distributed throughout the cores. Primary minerals in these veins are commonly pervasively replaced. Actinolite and brown amphibole replace clinopyroxene, and secondary plagioclase, epidote, and prehnite are common after plagioclase. As in felsic veins from Sites 921 and 922, fluid inclusions typically record exsolution of brines and vapors concomitant with vein formation. Wall-rock alteration associated with these veins is variably developed, with actinolite, chlorite, secondary plagioclase, and a trace of epidote as common secondary phases.

Deformation microstructures in gabbroic rocks from Hole 923A are similar to those found at Site 921. Many gabbroic rocks contain essentially igneous textures including random shape fabrics and weak foliations and/or lineations defined by the preferred dimensional orientation of elongate plagioclase and/or clinopyroxene crystals. Crystal-plastic deformation is concentrated in centimeter- to decimeter-scale shear zones in which primary minerals commonly have undergone extreme grain-size reduction with little retrograde alteration. These include LS-tectonites in which the stretching lineation commonly plunges downdip. The foliation typically dips moderately (~35°) and kinematic indicators show normal displacement across the shear zones.

Brittle deformation is limited to minor cataclastic zones and several discrete generations of veins. Felsic and actinolite + chlorite veins are distributed through most of the core and most commonly dip either 25° or 60°. Faults, sheared veins, and cataclastic zones crosscut the earlier igneous or crystal-plastic fabrics, as well as the felsic veins. Normal displacement is documented for many of these features.

Gabbroic rocks sampled in Hole 923A are predominantly of reversed magnetic polarity, with some intervals of apparent normal polarity. The archive half-core data after 20 mT demagnetization indicate consistent negative inclinations to ~45 mbsf, with values very similar to the expected reversed polarity dipole inclination (~41°). Below this depth, the archive

<sup>1</sup> Cannat, M., Karson, J.A., Miller, D.J., et al., 1995. *Proc. ODP, Init. Repts.*, 153: College Station, TX (Ocean Drilling Program).

<sup>2</sup> Shipboard Scientific Party is given in the list of participants preceding the contents.

half-core data show both normal and reversed polarity. Comparison with discrete sample demagnetization results, however, suggests that many of these normal polarity intervals may represent a low-stability overprint.

Gabbroic rocks sampled in Hole 923A have grain densities between 2.77 and 3.03 g/cm<sup>3</sup> and porosities of 0.16% to 1.31%. Compressional-wave velocities commonly are higher in samples from this hole than in cores from holes at Sites 921 and 922. They range from 5.7 to 6.6 km/s down to Core 153-923A-13R (55.5 mbsf), and from 5.4 to 5.7 km/s below this depth. Gabbroic rocks at the bottom of the hole also have relatively high densities. Thermal conductivities range between 2.3 and 3.0 W/m°C and are typical of oceanic gabbroic rocks.

## OPERATIONS

### Site 922 Transit to Site 923

As the drill string was being retrieved from Hole 922B, Site 922 beacons were released and recovered. The vessel was then offset to a position approximately 150 m north of Hole 921E. A new positioning beacon was dropped at 1730 hr, 7 January, initiating Site 923.

### Hole 923A

A new rotary core barrel bottom-hole assembly (RCB BHA) was run in the hole. The VIT was lowered down the drill string and an 8 hr seafloor survey began. After locating an appropriate spudding location, the bit was set on the seafloor and a jet test performed. The bit was jettied in 4.5 m while pumping 350 gpm at 450 psi with 10,000 lb weight on bit (WOB).

While compensating the drill string the VIT was retrieved and Hole 923A was spudded at 0950 hr, 8 January. The bit walked downhill approximately 4.5 m during the initial stages of spudding the hole before it finally came to rest and began making the hole. The seafloor depth was determined by drill-pipe measurement to be 2440 mbrf (2428.7 mbsl).

The hole cored very slowly at 0.3 m/hr. The lower 20 m of the hole required reaming with elevated circulating pressures and high erratic torque was noted after each connection.

After Core 153-923A-15R at 2504.7 m (64.7 mbsf; Table 1), 2 hr of reaming and cleaning allowed coring operations to continue. The decision was made to cut one more core and then pull off bottom two singles before pulling the core barrel. The BHA had to be back-reamed out of the hole. On each connection high torque and high circulating pressures prevented recovery of the core barrel. Eventually the bit had to be pulled clear of the seafloor at 2258 hr, 12 January, ending Hole 923A and Site 923.

Hole 923A was cored 16 times to 2510 m (70 mbsf) recovering 40.03 m of gabbro for a 74.7% recovery rate.

### Camera Survey

Site 923 was located during an 8-hr VIT camera and sonar survey about 200 m north of Site 921 (Fig. 4, "Introduction," this volume). The survey was conducted to the north and east of outcrops identified during the 25 December survey for Site 921 (Fig. 1, "Site 921," this volume). It was undertaken to provide an alternative site for deep drilling in gabbroic rocks and deployment of a HRGB. As the survey proceeded, however, it became apparent that outcrops in the area had slopes that were substantially steeper than the operational limits of the guide base, and Hole 923A was spudded as an unsupported hole.

The area surveyed extends about 150 m in a north-south direction and about 50 m in an east-west direction (Fig. 1), except for a single longer (~100 m) westward traverse, which encountered only rubble buried in pelagic ooze. In the steeper, eastern part of the survey area, outcrops of gabbroic rocks form steep cliffs on the order of a few meters high. These appear to be minor steps that are bounded by moderately east-dipping tabular masses of rock similar to those observed near Site 922. This planar structure is much more widely spaced

than the schistosity observed in outcrops near Site 921. Planes of schistosity or faulting are commonly curved at a scale of a few meters, but dip consistently to the east, as in all other gabbroic outcrops surveyed during Leg 153. To the west, the slope is less steep and at least a few meters of rubble and pelagic ooze cover any basement exposures.

Hole 923A was spudded into moderately sloping seafloor covered by at least a few decimeters of rubble and sediment. The hole is situated at the slope break just a few meters above the crest of a steep gabbro outcrop. Extremely rapid progress during the first meters of drilling suggested that the drill bit may have skidded downslope some distance before actual coring began.

## Lithologic Units

Sites 921, 922, and 923 are located at a depth of 2500 m and lie along a line parallel to the axis of the Mid-Atlantic Ridge (Fig. 4, "Introduction," chapter, this volume). Site 923 was selected in order to explore lateral geochemical and structural heterogeneity northward along an isochron-parallel transect across the gabbro massif (Karson and Dick, 1983; Mével et al., 1991; Auzende et al., 1993). Hole 923A, the only hole at this site, penetrated to a depth of 70 mbsf with a cumulative recovery rate of 74.7% (Fig. 2). Of the holes drilled in this gabbro terrane that penetrated substantially more than 10 mbsf, Hole 923A had the highest total and percentage recovery.

The diverse suite of gabbroic rocks recovered from Hole 923A are different from those of the other holes in this area in that the rocks are relatively fresh and have relatively few highly deformed intervals. Substantial intervals of fresh igneous rocks with a wide range of magmatic textures were recovered.

A brief summary of the main lithologic units defined for Hole 923A is presented below. As for previous Leg 153 site summaries, the names of lithologic units presented in this discussion are highly generalized and are selected to describe the predominant rock type forming the unit (Table 2). No contacts between units were recovered; they all lie within intervals that were not recovered between individual pieces of the core.

Five lithologic units were defined within Hole 923A. Unit 1 consists of variably deformed gabbro and olivine gabbro. Primary magmatic textures in the upper part of this unit are intensely to moderately overprinted by a weak crystal-plastic deformation fabric. The tectonic overprint decreases in intensity downward and magmatic textures dominate in most rocks. The unit is characterized by cumulus brown clinopyroxene and grain-size layering that ranges from fine- to very coarse-grained on a scale of decimeters (Fig. 3). A predominantly magmatic, subhorizontal, shape-preferred orientation is common and is overprinted locally by the tectonic fabric. The boundary between Units 1 and 2 is marked by a sharp decrease in the modal abundance of clinopyroxene and a corresponding increase in modal olivine.

Unit 2 consists of interlayered olivine gabbro and troctolite (Fig. 4). Two distinct types of olivine gabbro appear in this unit. The predominant type is similar to that occurring in Unit 1, but grain-size layering is less well developed and deformation is localized within narrow intervals of 20–30 cm. Gabbro and olivine gabbro are interlayered with olivine-rich gabbro to troctolite in which plagioclase and olivine are the predominant cumulate phases, and brown clinopyroxene occurs as an interstitial phase. Grain-size layering is weakly developed to absent in the olivine-rich sections, but variations in modal mineralogy define a diffuse layering with gradational boundaries.

Unit 3 consists of very coarse-grained poikilitic olivine gabbro (Fig. 5) and troctolite that is extremely heterogeneous, both modally and texturally. Layering is poorly developed within this unit, although the top is relatively clinopyroxene-rich and the base olivine-rich. Overall, the unit is olivine gabbro, but locally, lithologies range from troctolite to anorthositic gabbro and feldspathic wehrlite. The unit is characterized by the presence of large poikilitic clinopyroxene that reaches up to 70 mm in size and the presence of very coarse-grained cumulate or crescumulate olivine. The pyroxene is commonly zoned, having green chadacryst-free cores and brown rims.

Table 1. Coring summary, Hole 923A.

Core	Date (Jan. 1994)	Time (UTC)	Depth (mbsf)	Cored (m)	Recovered (m)	Recovery (%)
153-923A-						
1W	09	1320	0.0–16.4	16.4	0.73	
2R	09	2025	16.4–19.2	2.8	1.99	71.1
3R	10	0335	19.2–21.2	2.0	2.00	100.0
4R	10	0940	21.2–23.0	1.8	1.37	76.1
5R	10	1550	23.0–24.7	1.7	2.49	146.0
6R	10	1935	24.7–26.9	2.2	1.57	71.3
7R	11	0230	26.9–29.0	2.1	2.06	98.1
8R	11	0930	29.0–31.9	2.9	2.92	100.0
9R	11	1620	31.9–36.5	4.6	3.09	67.2
10R	11	2225	36.5–41.2	4.7	4.10	87.2
11R	11	0245	41.2–46.0	4.8	2.53	52.7
12R	12	0800	46.0–50.8	4.8	2.98	62.1
13R	12	1220	50.8–55.5	4.7	3.45	73.4
14R	12	1630	55.5–60.3	4.8	1.86	38.7
15R	12	2010	60.3–64.7	4.4	3.23	73.4
16R	13	0305	64.7–70.0	5.3	4.39	82.8
Coring totals				53.6	40.03	74.7
Washing totals				16.4	0.73	
Combined totals				70.0	40.76	

The abundance of modal olivine decreases abruptly at the top of Unit 4, and gabbro and olivine gabbro are the most abundant rock types. The unit is characterized by a wide range in texture and grain size, as well as subtle gradational variations in modal mineralogy. Grain-size layering is nonetheless poorly developed. Abrupt grain-size discontinuities exist where microgabbro veins and/or intrusions crosscut gabbro and olivine gabbro. Deformation is highly localized and most intervals preserve magmatic textures.

Unit 5 is relatively homogeneous clinopyroxene-poor olivine gabbro and troctolite. The rocks are distinctive in their spotted appearance, which is due to the heterogeneous distribution of olivine oikocrysts, now partially altered to iron oxide minerals, within the white plagioclase-dominated rock. Green clinopyroxene and olivine typically enclose plagioclase poikilitically. Modal layering is well developed in some intervals. Deformation and grain-size layering, however, are only apparent at the bottom of the unit where there is a gradational contact with coarse-grained brown-clinopyroxene-cumulate gabbro displaying an increase in deformation toward the bottom.

## IGNEOUS PETROLOGY

### Lithologic Description

The principal rock types recovered from Hole 923A are similar to those from Holes 921A, 921B, 921C, 921D, 921E, and 922A and 922B. They are predominantly gabbro and olivine gabbro, but include minor oxide gabbro, troctolite, and felsic veins. Igneous textures within the gabbroic rocks range from equigranular to highly inequigranular, the latter particularly developed in poikilitic rock types.

There are two main lithologic groups within the rock units defined for each hole. One is gabbro and olivine gabbro in which prismatic brown clinopyroxene occurs as a cumulus phase. These have modal compositions similar to that of the lineated gabbro/olivine gabbro group from Site 921. As for Holes 921A, 921B, 921C, 921D, and 921E, this rock type is commonly deformed, but numerous intervals occur where the fabric is strictly magmatic. Grain-size layering, ranging from fine to very coarse, is a characteristic feature of these rocks (Figs. 3 and 6). This lithology predominates in Units 1, 2, and 3 and occurs in minor amounts in Unit 5. For convenience, this lithologic group will be referred to as brown-clinopyroxene gabbro in subsequent sections.

The other lithologic group consists of olivine gabbro and troctolite in which clinopyroxene is poikilitic and generally emerald green. Texturally, olivine varies from poikilitic, to harrisitic, to interstitial. These rocks have a spotted appearance owing to the heterogeneous distribution of olivine oikocrysts, now partially altered to iron oxide minerals  $\pm$  clay minerals  $\pm$  chlorite(?) within a white, plagioclase-rich rock.

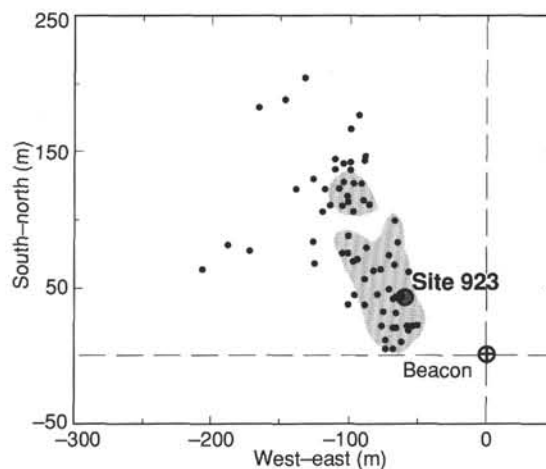


Figure 1. Map showing the location of the camera survey during which Site 923 ( $23^{\circ}32.55'N$ ,  $45^{\circ}01.90'W$ ) was located. Bold dots show locations where seafloor depths were estimated from the total length of the drill string. Outcrops are shaded.

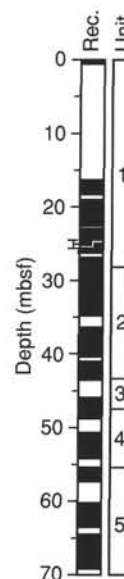


Figure 2. Columnar section showing the downhole recovery and lithological units in Hole 923A (black indicates recovered intervals). Note that bracket shown at approximately 26 mbsf indicates an apparent overcored interval. No duplication of cored material obvious from the rock recovered.

Because of the relatively high recovery in Hole 923A, fine-scale details of grain-size and modal layering have been recovered in some sections; similar variations were observed or inferred at Sites 921 and 922, but could not be as clearly documented there. These features will be described in some detail in a subsequent section.

### Brown-clinopyroxene Gabbros

The brown-clinopyroxene gabbro group of rocks consists of olivine gabbro and gabbro in which the texture and modal mineralogy are variable. The dominant rock type is olivine gabbro containing low modal olivine (average 7%) and approximately 30% clinopyroxene. The dominant characteristic of these rocks is the presence of cumulus, subhedral, brown clinopyroxene, and cumulus plagioclase (average 60%). Olivine is typically an interstitial phase, but in olivine-rich gabbro it is a coarse-grained primocryst phase.

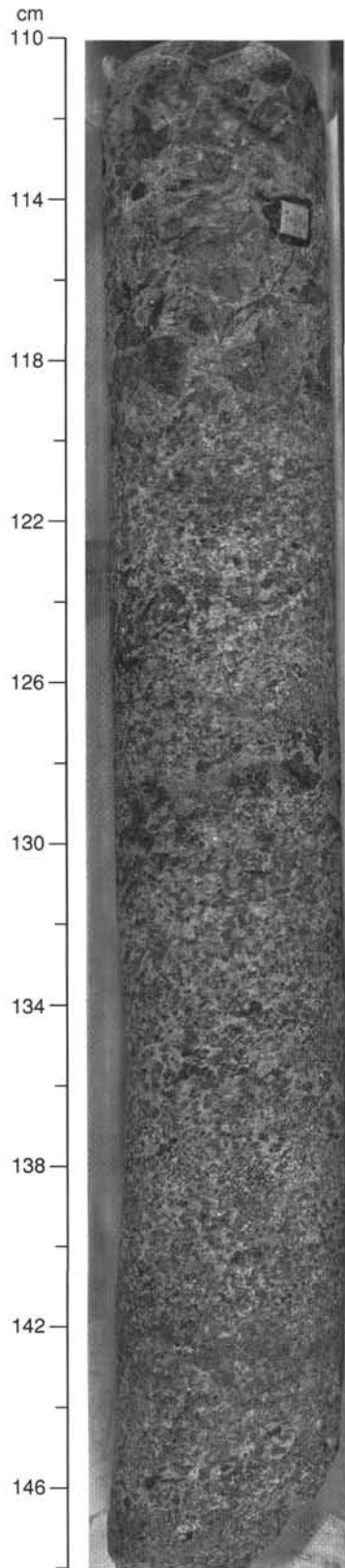


Figure 3. Gabbro to olivine gabbro of Unit 1 (Sample 153-923A-3R-1, 110–148 cm), showing typical grain-size layering with gradational boundaries. Top of interval is pegmatitic to very coarse-grained gabbro that grades downward into medium-grained olivine gabbro.

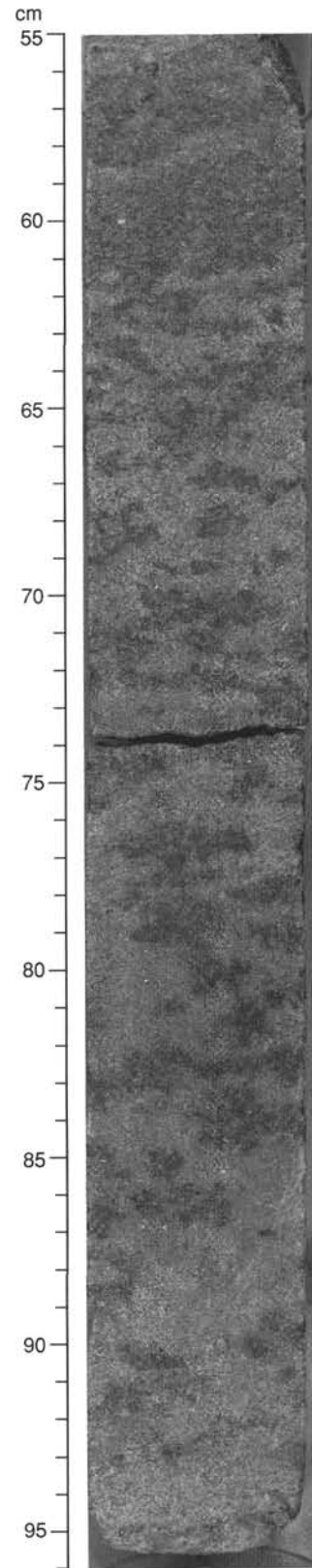


Figure 4. Layered olivine gabbro (55–62 cm) and spotted troctolite from Unit 2 (Sample 153-923A-9R-2, 55–96 cm). Dark, lobate olivine crystals have branching, dendritic, crescumulate textures and are surrounded by light-colored domains rich in randomly oriented plagioclase laths.

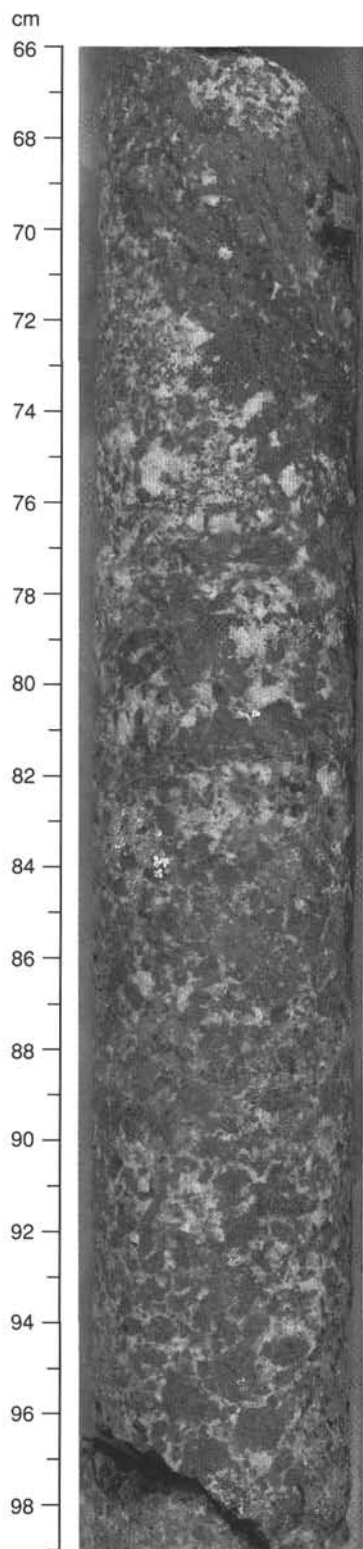


Figure 5. Heterogeneous, crudely layered, poikilitic olivine gabbro of Unit 3 (Sample 153-923A-12R-1, 66–99 cm). Dark interval at top (66–75 cm) is a layer of wehrlite to feldspathic wehrlite that grades downward into very coarse-grained poikilitic wehrlite. In the lower part of the interval (especially 90–98 cm), coarse dark crystals are olivine, which are commonly lobate in form. Coarse, medium gray, angular crystals in the middle of the interval (84–89 cm) are clinopyroxene oikocrysts.

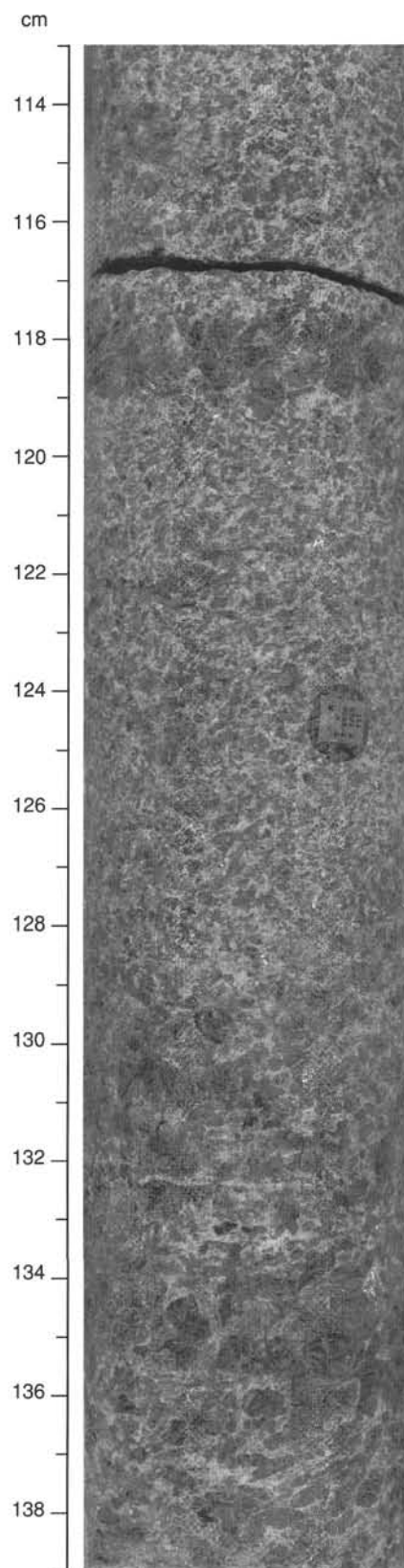


Figure 6. Grain-size layering within gabbro, Sample 153-923A-10R-2, 113–139 cm. Grain-size layering occurs on the scale of 2 to 10 cm, with medium-grained gabbro and coarse-grained gabbro in sharp contacts at ~118 and 130 cm. The contacts are horizontal in the core.

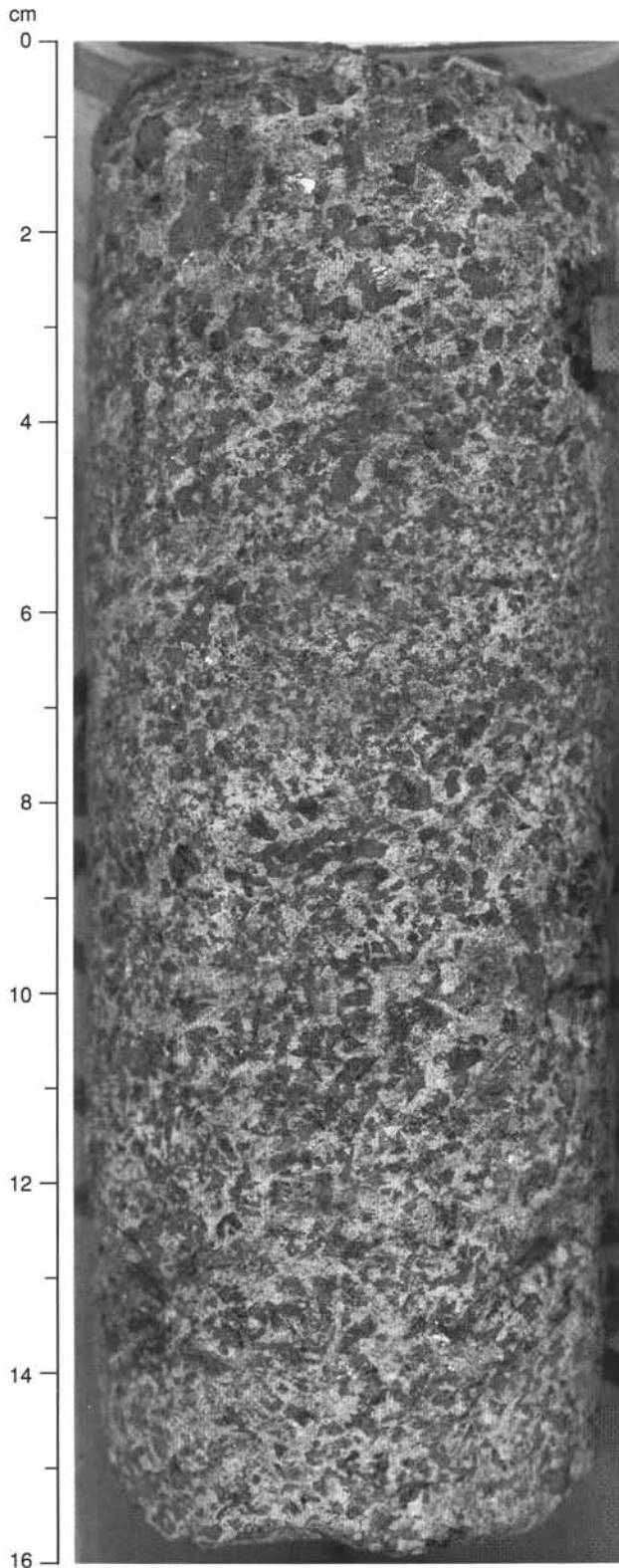


Figure 7. Subtle grain-size layering dips to the left about 30° in Sample 153-923A-8R-3, 0–16 cm. A thin, medium-grained gabbro ~2.5 cm thick is flanked above and below by coarser grained gabbro. The contacts are generally sharp, although somewhat irregular, and the modal abundances do not change across them. The upper contact of this medium-grained gabbro layer lies at 4 cm and the lower one at 6 cm.



Figure 8. Photomicrograph of Sample 153-923A-4R-1, 118–121 cm, showing subhedral to anhedral brown clinopyroxene largely surrounded by dynamically recrystallized plagioclase in a mildly deformed gabbro. Field length is 4 mm wide.

The grain size is dominantly medium to coarse (5 to 10 mm grain size). Plagioclase abundance ranges from 45% to 75%, although it predominantly falls within the 55% to 65% range. Where the olivine abundance is below 10%, clinopyroxene typically ranges from 25% to 40%. As olivine increases above this content, however, clinopyroxene decreases to as little as 20% in olivine-rich gabbro. Despite the inverse variation between olivine and clinopyroxene modal proportions, plagioclase abundance remains relatively constant, and independent of variations in the modal abundance of mafic phases.

A primary magmatic, subhorizontal, grain-size layering is characteristic of this group (Figs. 3 and 6). The layering shows a gradation from thin bands on a scale of 1 to 10 cm up to massive intervals on the scale of 1 m that show little internal layering. The boundaries between the layers are rarely accompanied by a significant modal variation (Fig. 7).

In thin section, plagioclase forms subhedral to anhedral cumulus grains that show varying degrees of development of mechanical twins in deformed rocks and preserved magmatic twins in less-deformed intervals. Optical determinations suggest that there is a limited range of compositions around An<sub>60</sub> in undeformed gabbros of this group. Clinopyroxene forms subhedral to anhedral, and rarely euhedral, cumulus grains (Fig. 8) that can exhibit magmatic twins. In places, cumulus clinopyroxene optically encloses small plagioclase laths. Olivine varies in texture from coarse, cumulus grains that are subhedral to interstitial and occasionally poikilitic in texture. Iron oxide minerals are minor or accessory in abundance. Brown amphibole is a common accessory phase occurring as rims on, and inclusions within, clinopyroxene.

A grain-shape preferred orientation is common and may be in part magmatic (Fig. 9), although it is overprinted in some places by a crystal-plastic fabric. In deformed samples, plagioclase is generally partially to completely recrystallized and clinopyroxene and olivine are typically partially recrystallized to an aggregate of neoblasts that are aligned parallel to the crystal-plastic fabric. Brown amphibole is more abundant within the deformed gabbro layers. Localized intense deformation zones are common above approximately 20 mbsf, and weakly to strongly lineated textures predominate in the interval (Figs. 10–12). Below this level, the deformation tends to be partitioned into shallow-dipping, high-strain zones tens of centimeters thick, in which localized mylonitic and gneissic textures occur and undeformed igneous textures are more common.

Microgabbro occurs within the top three sections and the last two sections of the hole as single pieces or intervals of several pieces. Microgabbro also occurs as 1- to 2-cm-wide veins (Figs. 13 and 14) and patches up to 8 cm wide at several locations. The microgabbro consists of a fine-grained, polygonal equigranular aggregate of clinopy-

**Table 2. Summary of lithologic units defined for Hole 923A.**

Unit	Name	Cored interval		Curatorial depth to top of unit (mbsf)	Recovered (m)	Recovery (approx. %)
		From	To			
1	Variably deformed gabbro and olivine gabbro	1R-1 (1)	7R-1 (12)	0.0	10.71	90.8
2	Interlayered troctolite and olivine gabbro	7R-1 (13)	11R-2 (10)	28.2	12.38	74.5
3	Poikilitic olivine gabbro and troctolite	11R-2 (11)	12R-1 (5)	43.9	0.80	62.1
4	Varitextured gabbro and olivine gabbro	12R-2 (1)	13R-3 (7)	47.5	4.85	65.0
5	Troctolite and poikilitic olivine gabbro	14R-1 (1)	16R-4 (8)	55.5	9.48	65.4

Notes: Recovery is approximate where unit boundaries fall within sections. Percent recovery excludes wash core for Unit 1. Total depth of penetration was 70.0 mbsf.

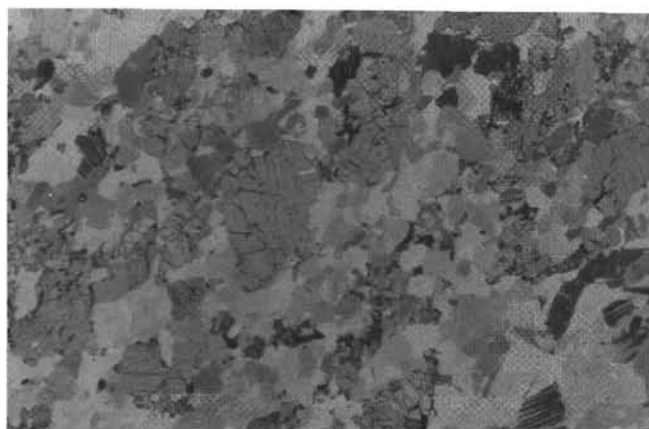


Figure 9. Photomicrograph of an olivine gabbro in Sample 153-923A-2R-2, 89–92 cm, showing the slight shape preferred orientation of clinopyroxene, olivine, and plagioclase, with adcumulus overgrowth. Field length is 4 mm wide.

roxene and plagioclase and variable abundances of brown amphibole. Microgabbro patches have interdigitating diffuse margins with the host rock, which may be a coarse-grained gabbro (Section 153-923-13R-3, Pieces 6 and 7; Fig. 14) or a troctolite (Section 153-923-8R-1, Pieces 3–5). Figure 14 shows a contact of microgabbro with gabbro and illustrates the complex nature of the boundary. The adjacent wall-rock gabbro has the appearance of a net-vein breccia in which thin bands of plagioclase-rich gabbro (possibly microgabbro) dissect the gabbro and individual pyroxene grains that appear fractured and invaded by the plagioclase-rich material. Plagioclase in these zones is partially to completely recrystallized, suggesting that the presence of the microgabbro and recrystallization of plagioclase are related. Unfortunately, because these zones are deformed, the former intrusive relationship has been obscured and any interpretation remains tentative.

#### Poikilitic Olivine Gabbros

The poikilitic olivine gabbros are variable in texture and modal mineralogy. They include rocks that range from olivine gabbro to troctolite. They are distinguished by the occurrence of oikocrystic clinopyroxene and/or olivine, which encloses euhedral to subhedral plagioclase laths. In some intervals, both olivine and clinopyroxene show poikilitic relationships in the same piece. In clinopyroxene-poor rocks, partially altered olivine oikocrysts are black. This gives the rock a spotted appearance in which dominant whitish plagioclase-rich gabbro regions are dotted by roughly spherical or elongate dark patches of olivine oikocrysts that are interstitial to plagioclase laths (Fig. 4). The rocks are typically gray-white to dark gray and exhibit a range of textural patterns from spotted to layered that corresponds with variations in modal mineralogy.

Plagioclase in the poikilitic olivine gabbro is clear to white and varies in texture from equigranular to, most commonly, subhedral

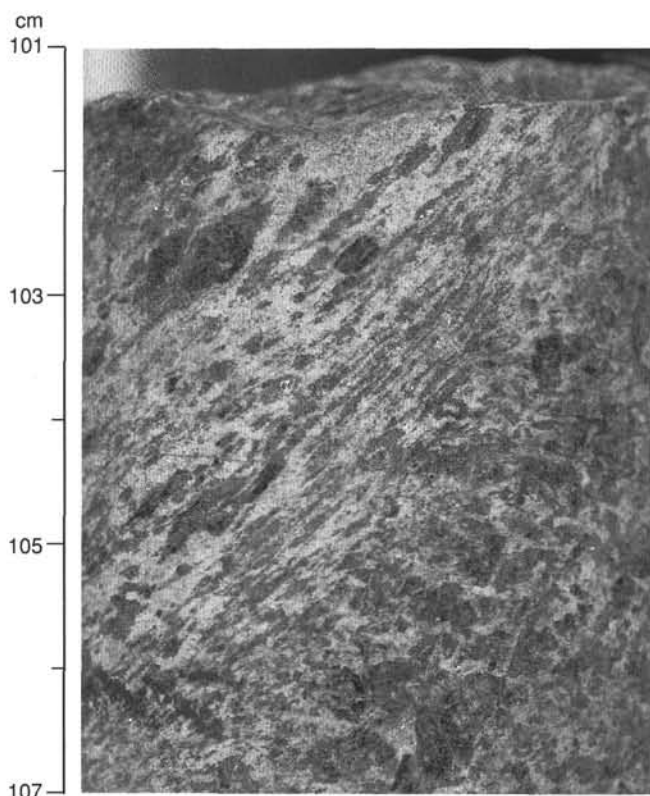


Figure 10. Gabbro, Sample 153-923A-11R-1, 101–107 cm, cut by a ductile shear zone dipping  $\sim 60^\circ$  showing a strong shape preferred orientation of clinopyroxene porphyroclasts and recrystallized clinopyroxene aggregates that define the foliation plane. Plagioclase shows marked grain-size reduction across the contact between little-deformed gabbro (below) and gneissic gabbro (above). The boundary between these two textural types occurs across a 5-mm zone. Lineations and kinematic indicators in this shear zone show a normal down-dip sense of displacement.

laths that are subophitically to ophitically enclosed by olivine and/or clinopyroxene (Figs. 15 and 16). In most examples, it also retains a magmatic crystal habit. In places, plagioclase crystals are randomly oriented, but in others they show a well-defined, magmatic shape-preferred orientation. The average composition is about  $An_{70}$ , estimated from optical properties.

Clinopyroxene occurs both as a cumulus and an interstitial phase, commonly within the same sample (Fig. 15). The most prominent habit is as coarse-grained, bright green oikocrysts that commonly are rimmed by brown clinopyroxene. Less commonly, clinopyroxene forms anhedral, pale brown interstitial grains within the matrix of olivine gabbro.

Olivine typically occurs as dark oikocrysts up to 60 mm in maximum dimension, particularly in troctolitic rocks. Where olivine is less

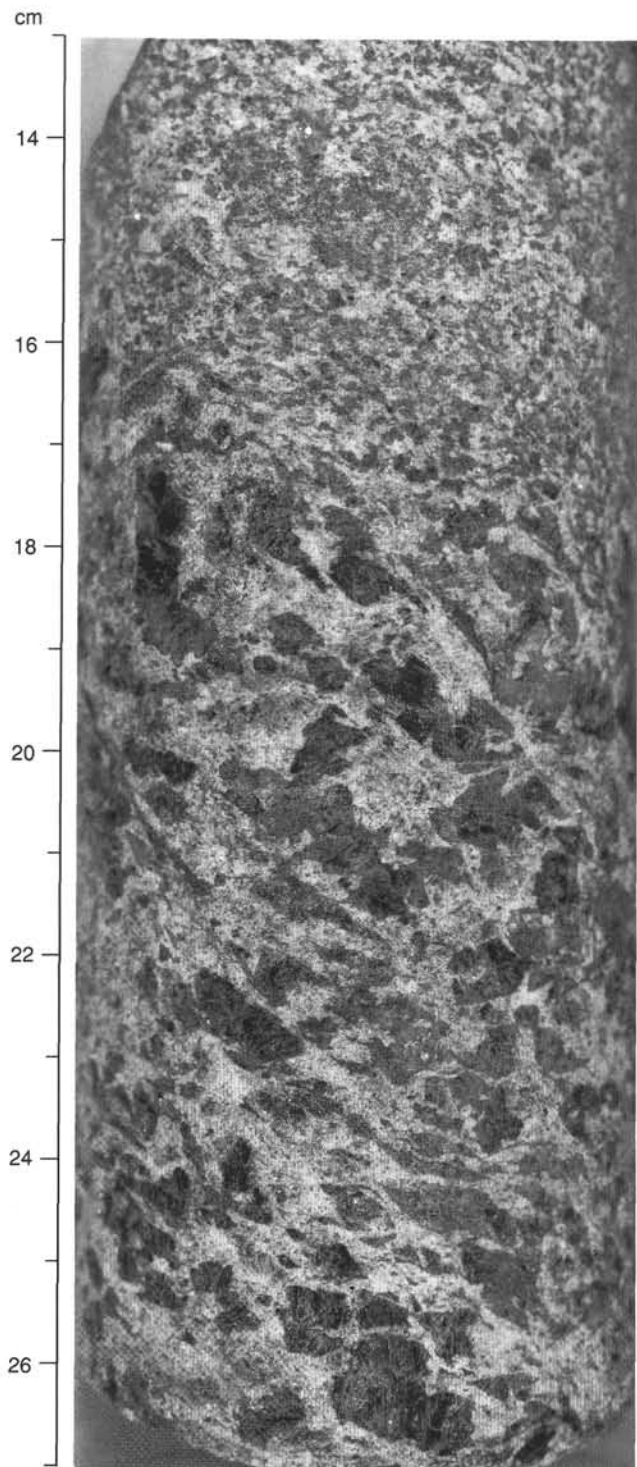


Figure 11. Contact between coarse-grained gabbro (below; i.e., 18–27 cm) and medium-grained gabbro (above; i.e., 13–27 cm) in Sample 153-923A-3R-2, 13–27 cm. The coarse-grained gabbro exhibits a weakly to moderately developed shape preferred orientation of clinopyroxene that is characteristic of the upper 20 m of Unit 1 of Hole 923A. Crystal-plastic strain is heterogeneously distributed, with some highly elongate clinopyroxene porphyroclasts (24 and 18 cm) and weakly deformed zones between them. Localized and planar zones only a few millimeters thick and dipping  $50^\circ$  to the right generally show evidence of intense ductile deformation. Two of these zones at 17–21 and 20–27 cm are confined to plagioclase-rich zones in gabbro.

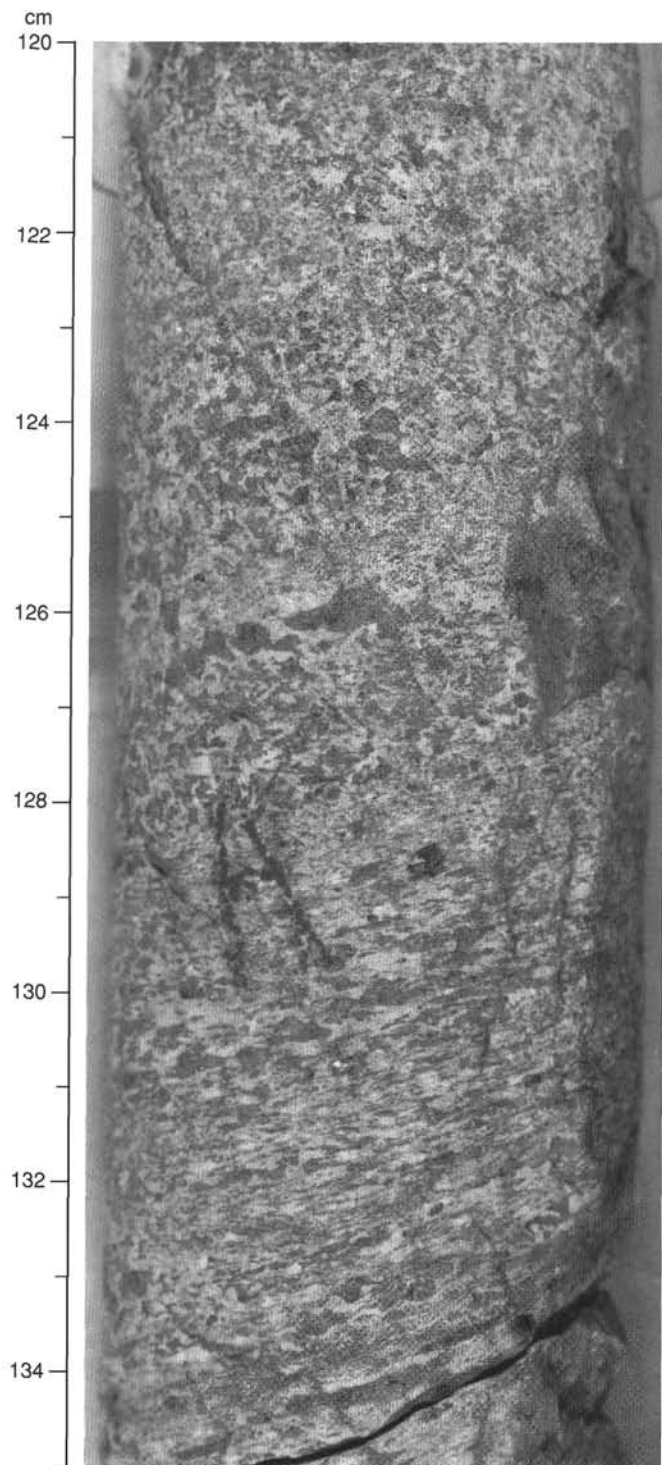


Figure 12. A crystal-plastic shear zone inclined at  $\sim 28^\circ$  (Sample 153-923A-13R-1, 120–135 cm), showing intense fabric development (mylonitic) at  $\sim 131$ –135 cm. This mylonite grades upward to a gneissic gabbro between 131 and 126 cm. The contact with little-deformed gabbro above 126 cm is sharp. Recrystallized aggregates of clinopyroxene or elongate clinopyroxene porphyroclasts define a downdip lineation, and kinematic indicators suggest a normal sense of shear.

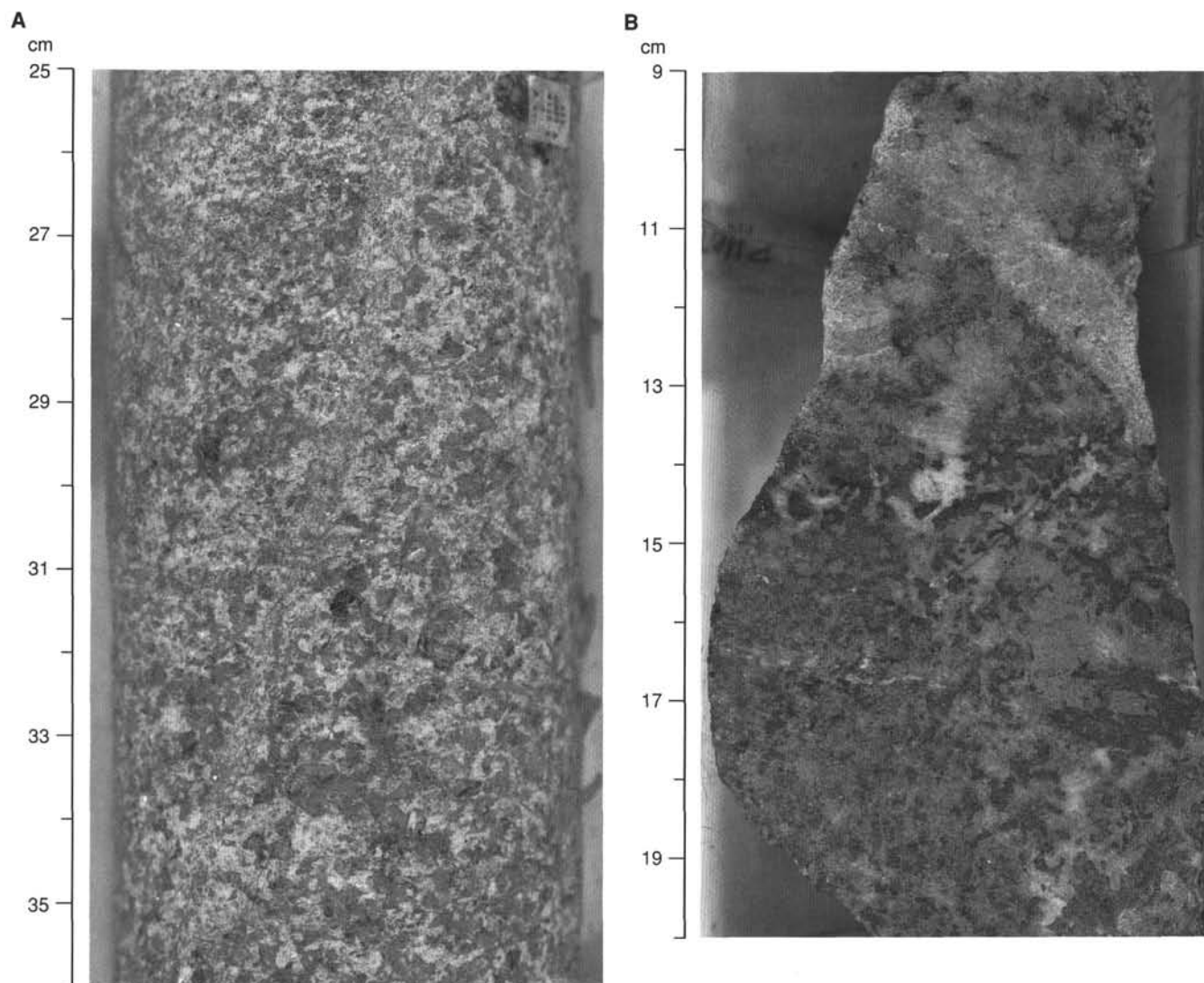


Figure 13. **A.** Coarse-grained olivine gabbro cut by a 5-mm-thick microgabbroic vein dipping  $70^\circ$  to the left, Sample 153-923-A-12R-2, 25–36 cm. **B.** Thin microgabbro vein cutting poikilitic olivine gabbro, Sample 153-923A-14R-1, 9–20 cm.

abundant, it occurs as anhedral interstitial grains. Several horizons have dendritic and elongate, blade-like olivine crystals that are also associated with coarse elongate, and in some places radiating, plagioclase laths (Fig. 16). In thin section these elongate olivines are optically continuous on the scale of 2 to 3 cm (Fig. 17) and are possible crescumulate textures.

In most oikocrystic rocks, relatively large (10–40 mm) crystals of clinopyroxene or olivine enclose chadacrysts of smaller plagioclase. The plagioclase grains form an interlocking network of subhedral to nearly euhedral crystals that are fully enclosed in the core of the oikocryst phase, but only partially enclosed near the rim (Fig. 18). The oikocryst phase is interstitial to this framework of plagioclase. This textural relationship is commonly interpreted as evidence that plagioclase is a cumulus phase and that the oikocryst is a post-cumulus phase (Jackson, 1961). In some cases, however, oikocrysts are totally devoid of a self-supporting plagioclase framework in the center of the crystals (Fig. 18); the poikilitic (or plagioclase-enclosing) relationship is restricted to the periphery of the large oikocrystic grain (the outer third or less of the grain margin). Thus, large parts of the grain are essentially inclusion-free and have elongate, branching extensions outward from a central inclusion-free core into the surrounding plagioclase framework. In thin section, this commonly appears as interstitial regions

between plagioclase grains filled with olivine that is optically continuous with an oikocryst core, but not connected within the plane of view (Fig. 17).

Another commonly observed textural relationship is one in which sparse, slender, and very elongate plagioclase laths are enclosed in the cores of clinopyroxene oikocrysts, but the plagioclase grain size outside of the core region of the oikocryst is three to four times that of the enclosed crystals. Distal from the core of the grain, clinopyroxene is interstitial to the plagioclase, indicating that although plagioclase and clinopyroxene grew simultaneously in these rocks, the nucleation rate for clinopyroxene (the oikocryst phase) was lower than that of the plagioclase. In addition, in spite of the lower nucleation rate, the growth rate of clinopyroxene was high enough relative to plagioclase that it engulfed small plagioclase nuclei, inhibiting further growth.

Very coarse (10–50 mm) green clinopyroxene crystals that are devoid of inclusions in their cores also occur (Fig. 18). In some places, as much as 30 mm of a crystal may be free of inclusions, yet their margins show a poikilitic relationship with plagioclase such that individual oikocrysts locally appear as isolated grains in an otherwise oikocrystic-textured rock. The margins of these large grains do, however, exhibit oikocrystic relationships with the surrounding framework of plagioclase grains, occupying the interstices with clinopyroxene

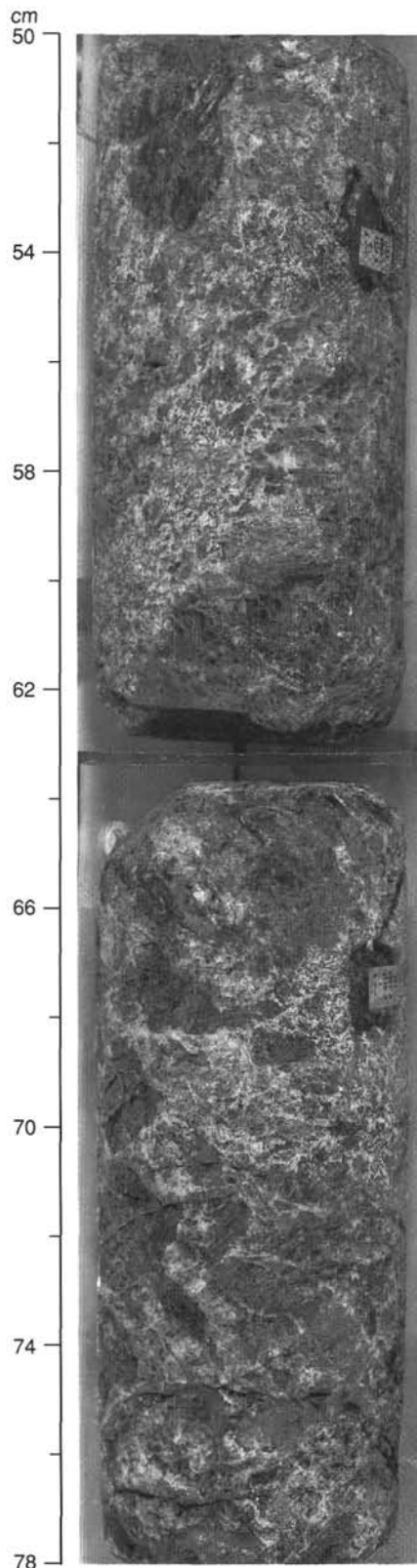


Figure 14. Sample 153-923A-13R-3, 50–78 cm. Coarse-grained gabbro (dark areas) intruded by microgabbro (light areas), which in places is part of a dike-like feature (right, 57–61 cm), and which elsewhere defines a fine net-veining through the coarse-grained gabbro (66–78 cm).

that is optically continuous with the large inclusion-free part of the crystal. Good examples of these large grains also occur in Sections 153-923A-14R-1 (Piece 2) and 16R-1 (Piece 2). These textural relationships are common in the core, and may reflect variations in nucleation and growth rates between plagioclase, olivine, and pyroxene.

The wide range in textures is reflected in the modal and grain-size heterogeneity of these rocks. Plagioclase is typically the most abundant phase, ranging from 35% to 75%, but most commonly between 56% and 72%. Clinopyroxene and olivine abundances tend to vary inversely, with clinopyroxene ranging from 2% to 45% and olivine from 3% to 55%. Primary opaque iron oxide minerals are present as rare, anhedral, interstitial grains. Variations in the grain size of the primary phases are also extreme, ranging from fine- to coarse-grained; maximum grain sizes reach 25 mm for plagioclase, 70 mm for clinopyroxene oikocrysts, and 48 mm for olivine oikocrysts.

Primary magmatic layering is defined by changes in grain size, but more commonly by modal mineralogy, on the scale of 1 cm (Fig. 19) to 10 cm and more (Figs. 5 and 20). The variations occur as layers that have margins ranging from relatively sharp to diffuse and gradational. These variations are discussed in detail in a subsequent section.

#### *Oxide Gabbros*

Oxide gabbros are a volumetrically minor, but not uncommon, lithology within the upper 20 m of Hole 923A; all reported occurrences are listed in Table 3. They are found exclusively within the brown-clinopyroxene gabbro group in rocks that typically contain less than 5% olivine; iron-titanium oxides constitute up to 10% of the assemblage. Oxide gabbro (total iron oxide abundance >5%) has not been observed within the poikilitic olivine gabbro group, although a deformed oxide-bearing gabbro cuts poikilitic olivine gabbro near the base of the hole (Fig. 21).

All oxide gabbros reported from this hole are associated with zones of crystal-plastic shear strain. Plagioclase is largely recrystallized, and clinopyroxene forms blocky to elongate porphyroclasts (up to 10 mm) that define a crystal-plastic foliation. Iron-titanium oxide minerals occur within these rocks as trails and aggregates of fine grains (0.1 mm), but also produce densely packed, elongate aggregates that form patches or semicontinuous stringers or layers 1–3 mm thick. Outside these oxide-mineral-bearing layers and stringers, the rock is modally similar to other pieces in the section, suggesting that the oxide mineral stringers are intrusive into the gabbro. In thin section, aggregates of iron-titanium oxides are commonly observed enclosing plagioclase and clinopyroxene neoblasts. Brown amphibole is generally present, replacing clinopyroxene and surrounding iron oxide minerals; orthopyroxene and apatite are commonly associated phases.

#### *Leucocratic Veins*

Several pieces in the core exhibit small (up to several centimeters thick) leucocratic veins. The composition of these veins varies from gabbro that contains long prismatic clinopyroxene or amphibole and coarse blocky plagioclase (e.g., Sample 153-923A-8R-2, Piece 1, 1–3 cm) to hornblende-clinopyroxene-plagioclase veins that are characterized by lower ratios of plagioclase to hornblende and/or clinopyroxene. No quartz-bearing felsic veins were observed in the core. Hornblende, apatite, and zircon occur mostly in very felsic rocks (>70%–80% plagioclase or altered plagioclase), suggesting that they are derived from very evolved melts. Leucocratic vein and oxide-gabbro occurrences (Table 3) appear to be mutually exclusive, with oxide gabbros occurring only in the upper part of the hole and leucocratic veins restricted to the lower part.

#### **Downhole Lithologic Variations**

Unit 1 (Fig. 2) consists entirely of gabbro and olivine gabbro of the brown-clinopyroxene gabbro group. The upper ~20 m of this unit are moderately deformed (to the base of Core 153-923A-3R, 21.2 mbsf)

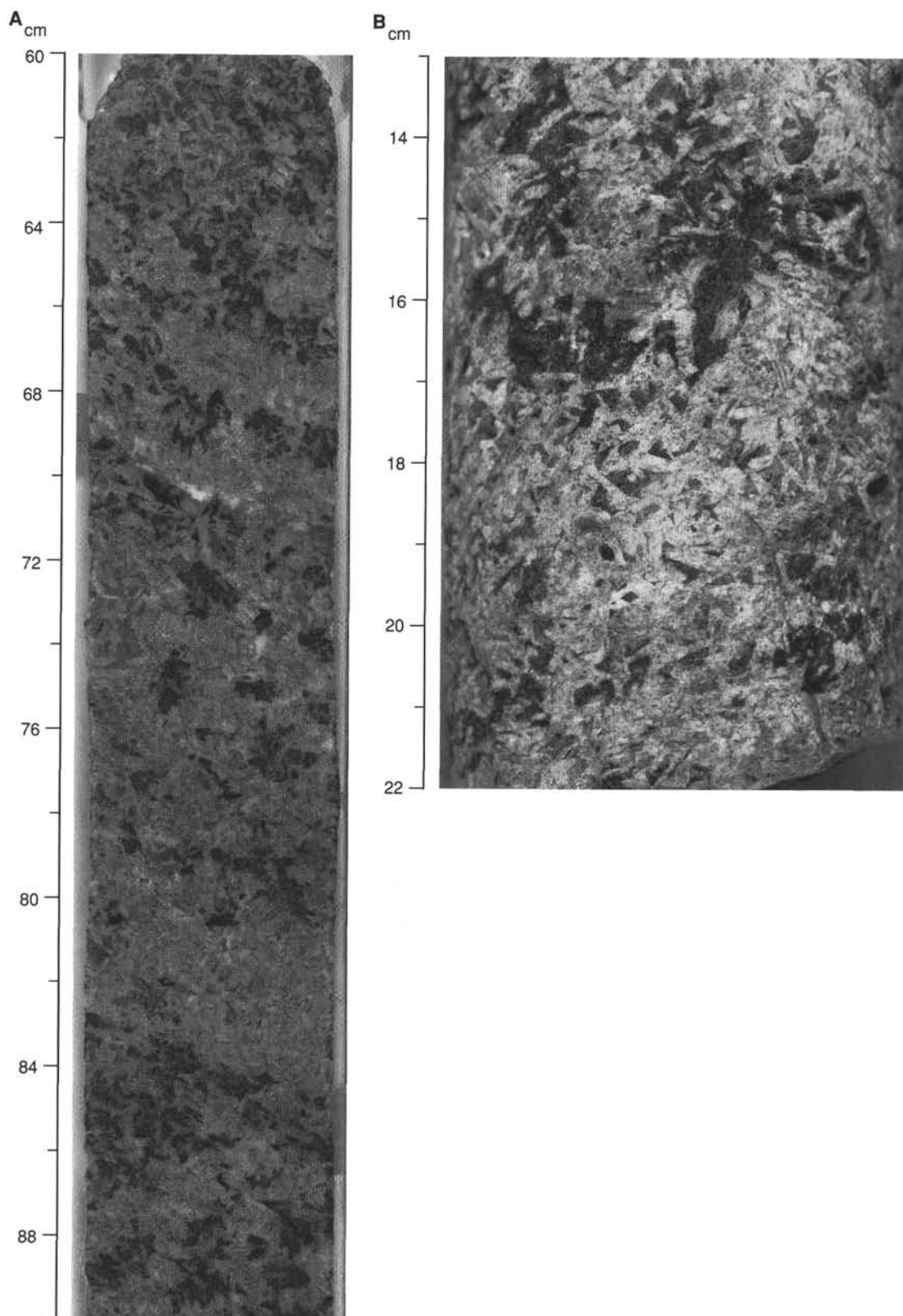


Figure 15. **A.** Sample 153-923A-16R-3, 60–90 cm. Interlayering of troctolite and olivine gabbro in which euhedral to slender subhedral plagioclase laths occur in radiating clusters and pyroxene oikocrysts are interstitial to the framework of interlocking plagioclase. The olivine and clinopyroxene grains have an oikocrystic relationship to plagioclase and the variation in the percentages of the oikocrystic mafic phases and the olivine/clinopyroxene ratio define the fine-scale layering. Darker bands are rich in olivine oikocrysts, and lighter bands are richer in clinopyroxene oikocrysts. The layering is inclined at 20°. **B.** Sample 153-923A-16R-3, 13–22 cm. Plagioclase framework with interstitial and poikilitic olivine (dark-gray to black) and clinopyroxene.

**Table 3. Distribution of veins and oxide gabbro from Hole 923A.**

Core, section	Leucocratic veins	Oxide gabbros
153-923A-1W-1		Piece 9
2R-1		Piece 1
3R-1		Pieces 2 and 5
4R-1		Pieces 1, 3, and 4
8R-2	Pieces 1, 2, and 3 (HLG)	
9R-1	Pieces 1 and 3 (HLG)	
10R-1	Piece 5 (LG)	
11R-2	Piece 7 (LG)	
12R-2	Pieces 3, 4, 7, and 8 (LG)	
14R-1	Piece 3 (LG)	
15R-2	Piece 3 (HLG)	
16R-1	Piece 1 (LG)	
16R-4	Pieces 1, 4, and 8 (LG)	

Note: HLG = hornblende leucogabbro, LG = leucogabbro.

and textures range from lineated and weakly deformed to gneissic (e.g., Fig. 11). Microgabbro is present in Sections 153-923A-1R-1 (Pieces 4–6) and 2R-1 (Pieces 3–5). With increasing intensity of crystal-plastic deformation, pyroxene becomes elongate and ultimately forms porphyroclasts within an intensely recrystallized matrix of plagioclase and olivine. Oxide gabbro occurs as discrete pieces within the top ~20 m of this unit.

Below 20 m depth (i.e., Core 153-923A-4R and below), the crystal-plastic deformation is strongly localized and the gabbro displays primary igneous layering and textures (Figs. 6 and 7). A weak, subhorizontal foliation defined by clinopyroxene shape-preferred orientation is probably a primary magmatic fabric. Grain-size layering on the scale of centimeters to meters is characteristic of this section.

Unit 2 is dominated by gabbro (brown-clinopyroxene gabbro), but includes discrete interlayers of olivine gabbro and troctolite. The upper boundary of the unit is placed at the top of the first occurrence of olivine-rich gabbro (Section 153-923A-7R-1, Piece 13). Recovery in this section was high (12.38 m, 75% recovery).

The top part of Unit 2 (Sections 153-923A-7R-1, Piece 13, to 8R-2, Piece 7) consists of olivine-rich (13%–24%) gabbro, minor troctolite, and gabbro. Olivine gabbro displays well-developed crescumulate textures (Fig. 4) and is anorthositic in small intervals and layers (e.g., Section 153-923A-8R-1, Piece 2; Fig. 19). Gabbro varies widely in texture in this interval, and microgabbro displays crosscutting relationships with troctolite (Section 153-923-8R-1, Pieces 3–5) and deformed brown-clinopyroxene gabbro (Fig. 22). The brown-clinopyroxene gabbro in this unit is typical of this rock type, including the presence of diffuse grain-size layering (Fig. 7) and of strongly localized zones of strain (Fig. 22).

Unit 3 consists of coarse-grained poikilitic olivine gabbro (poikilitic olivine gabbro and troctolite) that is extremely heterogeneous modally and texturally. The unit includes a total recovered length of 0.8 m and within that length, the modal proportion of plagioclase ranges from 5% to 70%, clinopyroxene from 3% to 45%, and olivine from 15% to 80%. Despite the wide range in modal proportions and the tendency for the base of the unit to be olivine-rich and the top of the unit clinopyroxene-rich, the interval is poorly layered. On average the unit is olivine gabbro (40% plagioclase, 40% olivine, and 20% clinopyroxene), but locally lithologies range from troctolite, to anorthositic troctolite, to feldspathic wehrlite (Figs. 5 and 23).

Although fine-grained layering and gradational grain-size variations occur in some intervals, most of the unit is uniformly coarse-grained. The unit is characterized by large poikilitic clinopyroxene (up to 70 mm) that is zoned from large green cores to thin brown rims. The cores of larger oikocrysts are chadacryst-free. In some places, both brown and green clinopyroxene occur as separate crystals, but toward the base of the unit only brown clinopyroxene occurs. Large clinopyroxene oikocrysts are locally surrounded by anorthositic zones that are to 0.5 cm wide. Olivine typically occurs as large cumulus crystals, but

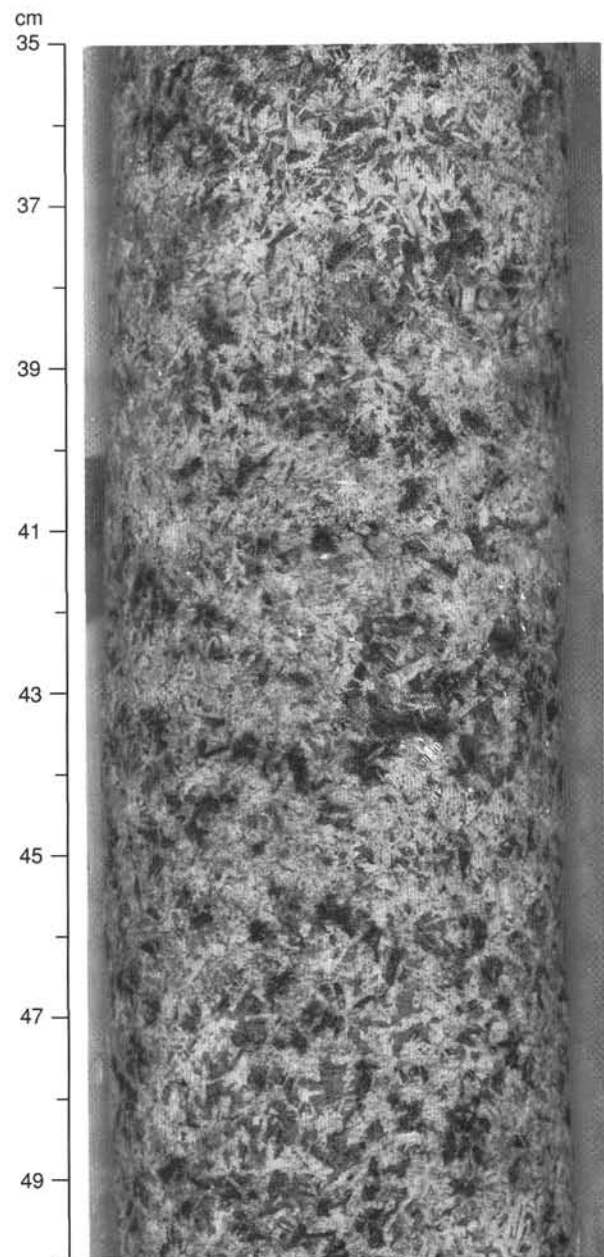


Figure 16. Poikilitic olivine gabbro, Sample 153-923A-16R-1, 35–50 cm, with large clinopyroxene grains enclosing slender laths of plagioclase. Plagioclase consists of slender radiating laths that form a network of interlocking grains with clinopyroxene oikocrysts or interstitial olivine.

it displays a crescumulate texture in some zones (Fig. 24). A layer in Section 153-923A-12R-1 (Piece 5; Fig. 23) contains coarse, euhedral olivine crystals in troctolite just above its base.

Unit 4 consists of brown-clinopyroxene gabbro and olivine gabbro with minor troctolitic gabbro, troctolite, and microgabbro. The top contact of the unit is not preserved, but is marked by a sudden change from olivine gabbro above to brown-clinopyroxene gabbro and microgabbro below the assigned unit boundary. The base of the unit is marked by a very coarse-grained brown-clinopyroxene gabbro in which plagioclase is moderately recrystallized. Thus, microgabbro veins and diffuse microgabbro patches are present at the top of the unit (Section 153-923A-12R-2, Pieces 1–2; Fig. 13) and at the base of the unit (Section 153-923A-13R-3, Pieces 6–7; Fig. 14). Two short intervals of troctolite (Section 153-923A-13R-1, Pieces 5–7) and olivine-

rich gabbro (Section 153-923A-13R-2) are present. Green clinopyroxene ranges from cumulus to oikocrystic, and green and brown clinopyroxene occur together within the middle of the unit (Sections 153-923A-13R-2, Piece 8, and 13R-1, Piece 13; Fig. 25). Green clinopyroxene also occurs within a layer or vein in Section 153-923A-13R-2. Within the olivine-rich rocks, olivine is typically cumulus to crescumulus textured.

Unit 5 is a coarse-grained olivine gabbro to troctolite (poikilitic olivine gabbro) unit showing subtle, but systematic, variations in modal mineralogy. The base of the unit is predominantly brown-clinopyroxene gabbro. The top of the unit is placed at the boundary between coarse-grained, pyroxene-rich gabbro (50% clinopyroxene) in the base of Section 153-923A-13R-3 and troctolite and olivine-rich gabbro in the top of Section 153-923A-14R-1. The troctolitic gabbro displays a relatively uniform, spotted texture formed by the presence of interstitial olivine patches within cumulus plagioclase. The modal proportion of plagioclase is relatively constant, ranging from 60% to 75%. The modal olivine content is also relatively constant at approximately 20% to 25% for most of this unit, but decreases in a gabbroic interval below Section 153-923A-16R-3 (Piece 5) where it ranges from 0% to 20%. The abundance of clinopyroxene is typically 10% to 25% in the olivine-rich gabbros, but increases dramatically in the pyroxene-rich gabbros at the base of the unit (up to 55% of the mode). Both olivine and clinopyroxene exhibit poikilitic textures, enclosing subhedral to euhedral plagioclase laths (Figs. 15, 16, and 18). Clinopyroxene oikocrysts have bright green cores and are zoned to brown clinopyroxene at the interstitial extremities; the oikocrysts are irregularly spaced within the rock. In some intervals, subhedral plagioclase exhibits a radiating habit associated with olivine oikocrysts (Fig. 26).

The bottom 1.2 m of Unit 5 consists of gabbro and olivine gabbro that are typical of the brown-clinopyroxene gabbro group. The rocks range from coarse-grained gabbro to olivine-free microgabbro and local intervals of deformation occur. A coarse-grained, strongly foliated, gabbroic layer (>2.5 cm) containing minor amounts of iron oxide minerals occurs, crosscutting poikilitic olivine gabbro in Section 16R-2 (Piece 1B; Fig. 21).

Although most of the unit is relatively fresh (total alteration <15%), Section 153-923A-15R-1 contains olivine metagabbro that is pervasively altered (65%–90%); the inferred protoliths were modally and texturally similar to the olivine gabbro in this unit.

Locally, olivine gabbro in Unit 5 displays significant modal layering (Fig. 12), gradational over tens of centimeters. Associated with the modal layering are changes in crystal habit of clinopyroxene that range from prismatic/interstitial grains in pyroxene-rich rocks to poikilitic in more olivine-rich lithologies.

The distribution with depth of poikilitic olivine gabbros vs. other gabbroic rocks is apparent in plots of modal composition as a function of depth and of the designated units (Fig. 27). There are significant increases in the maximum modal abundance of olivine at the top of Unit 2 and at the bottom of Unit 4. All of Unit 3 and most of Unit 5 are olivine-rich rocks. Clinopyroxene varies inversely with olivine (Fig. 27). The maxima in modal olivine correspond to intervals of poikilitic olivine gabbro and troctolite, whereas intervals of low modal olivine and high modal clinopyroxene correspond to sections of brown-clinopyroxene gabbro.

### Modal Layering and Cyclicity

The lithologic units described above were defined on the basis of the initial macroscopic inspection of the core. However, based on detailed analysis of the visual core descriptions, combined with data from thin sections, it was recognized that the rocks could be described in terms of a series of cycles consistent with an evolutionary magmatic sequence. Each of these cycles records a transition from a primitive olivine gabbro or troctolite at the base, upward through olivine gabbro in which green clinopyroxene occurs as an oikocryst phase, to olivine gabbro and gabbro in which brown pyroxene is a cumulus phase. This

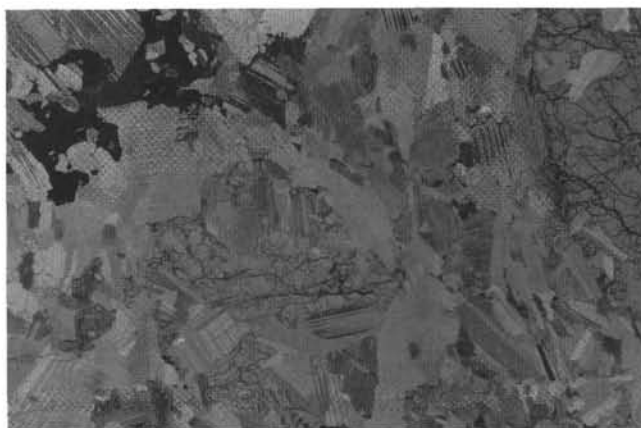


Figure 17. Photomicrograph of elongate, possibly crescumulate olivine in Sample 153-923A-7R-2, 1–2 cm. Width of frame is 4 mm.

lithologic progression is accompanied by a variation in the textural characteristics of the rocks. This section describes the macroscopic characteristics of these evolutionary “cycles” as far as they could be characterized within the constraints of shipboard activities. It was not possible to quantify this apparent cyclicity beyond the general textural characteristics aboard ship, nor was it possible to ascribe all of the observed macroscopic variations to the cyclic variation. The cycle designations presented below require detailed shore-based research before their validity can be established.

Eight large-scale cycles (Cycles 1–8) were documented on the basis of textures and modal proportions within the rocks. These eight cycles are listed in Table 4 and shown in Figure 27 in relation to the modal abundance of olivine with depth. The thickness of individual cycles varies from 2.2 m (Cycle 4) to more than 16 m (Cycles 6 and 8). Each cycle starts with a sharply defined boundary above which there is an accumulative, troctolitic base containing euhedral to subhedral olivine and interstitial plagioclase (olivine accumulative), or in which both euhedral to subhedral olivine and plagioclase are cumulus phases (olivine-plagioclase accumulative; Fig. 24). This is generally followed upward by an olivine-crescumulus troctolite containing large olivine oikocrysts (spotted troctolite; Fig. 4) that grades into poikilitic olivine gabbro in which large, green, poikilitic clinopyroxene is unevenly distributed but increases in abundance upward (Figs. 15 and 16). This clinopyroxene is zoned to brown rims.

The occurrence of euhedral cumulus plagioclase with olivine in olivine-plagioclase accumulates, and of poikilitic troctolite with large olivine oikocrysts (Fig. 4; Cycle 6) indicates that plagioclase was a cumulus phase at the start of each cycle and that olivine was generally also cumulus. The overlying poikilitic olivine gabbro contains sparsely distributed black patches (0.3–5.0 cm in diameter) of anhedral olivine that, in places, contain plagioclase inclusions. This texture suggests that the crystallization of crescumulus olivine is replaced in this section by crystallization of accumulative olivine that subophitically to poikilitically encloses plagioclase.

The upper part of each cycle is characterized by typical grain-size-layered (Fig. 6) olivine gabbro to gabbro (brown-clinopyroxene gabbro) that forms the bulk of the rock types present in most cycles (>80%). The texture is typically hypidiomorphic to allotriomorphic granular in which olivine is variably cumulus near the base but is invariably interstitial near the top of the cycle (Fig. 7).

Microgabbro sometimes occurs as veins and diffuse patches toward the top of the brown-clinopyroxene gabbro part of the cycle (Cycles 3, 4, and 5). It nonetheless occurs in one instance within the troctolitic base of a cycle (Cycle 8) where the contact between microgabbro and troctolite is steeply dipping and surrounded by a selvage of olivine gabbro (Sections 153-923A-8R-2, Pieces 1–3). The nature of this particular boundary is not entirely clear, but the presence of a selvage

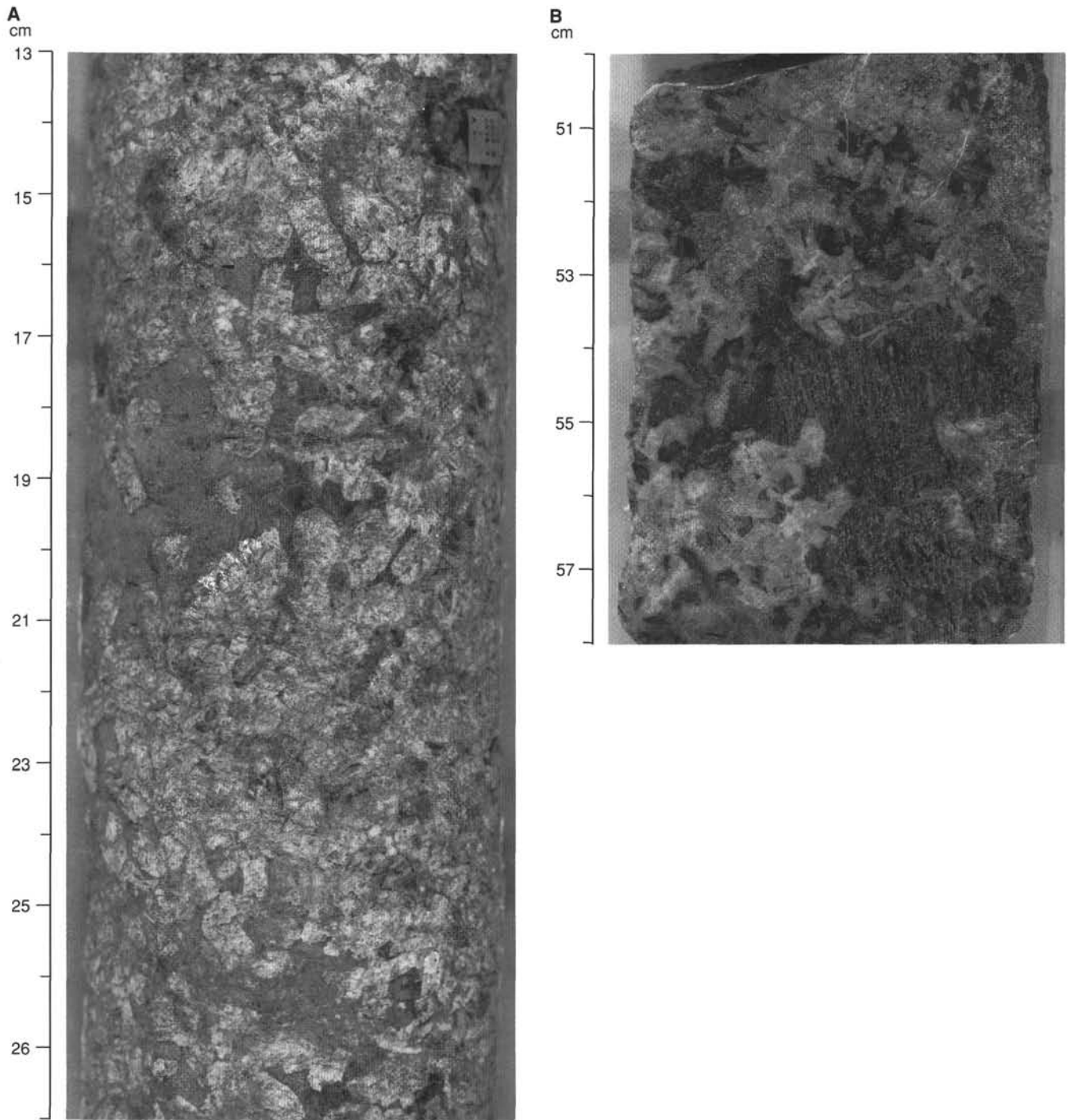


Figure 18. **A.** Sample 153-923A-3R-2, 13–27 cm, showing clinopyroxene oikocryst in olivine gabbro that has a large inclusion-free core. **B.** Sample 153-923A-16R-2, 50–58 cm, showing a large clinopyroxene grain at least 60 mm long that is largely chadacryst-free in its core, but rich in plagioclase chadacrysts toward its margin where it is interstitial between interlocking plagioclase grains.

intermediate in composition between microgabbro and troctolite suggests that the microgabbro has intruded and reacted with the troctolite.

Although the sequence of rock types and textures in each cycle is similar, the textural distinctions are not equally well developed in each unit. Gaps in the data recorded during macroscopic core description, in addition to irregularities within each of the cycles, tend to disrupt the general modal olivine trend of each cycle (Fig. 27), which is best observed in Cycle 7. Cycle 1 is incomplete and is represented only by brown gabbro rocks thought to be at the top of the cycle. Cycles 2 to 7 are relatively complete, although the boundary between Cycles 4

and 5 is difficult to place. Nonetheless, a transition from brown clinopyroxene below this boundary to green poikilitic clinopyroxene above the boundary is accompanied by a significant increase in modal olivine. The boundary between Cycles 2 and 3 is also poorly defined due to poor recovery and alteration within this interval, but the modal data above and below the boundary and textural characteristics strongly imply that a cycle boundary exists within this interval. Cycle 8 is incomplete, and dominantly brown-clinopyroxene gabbro.

Cycle 2 differs from the other cycles in texture and in being dominated by olivine-rich compositions. Olivine gabbro displays a

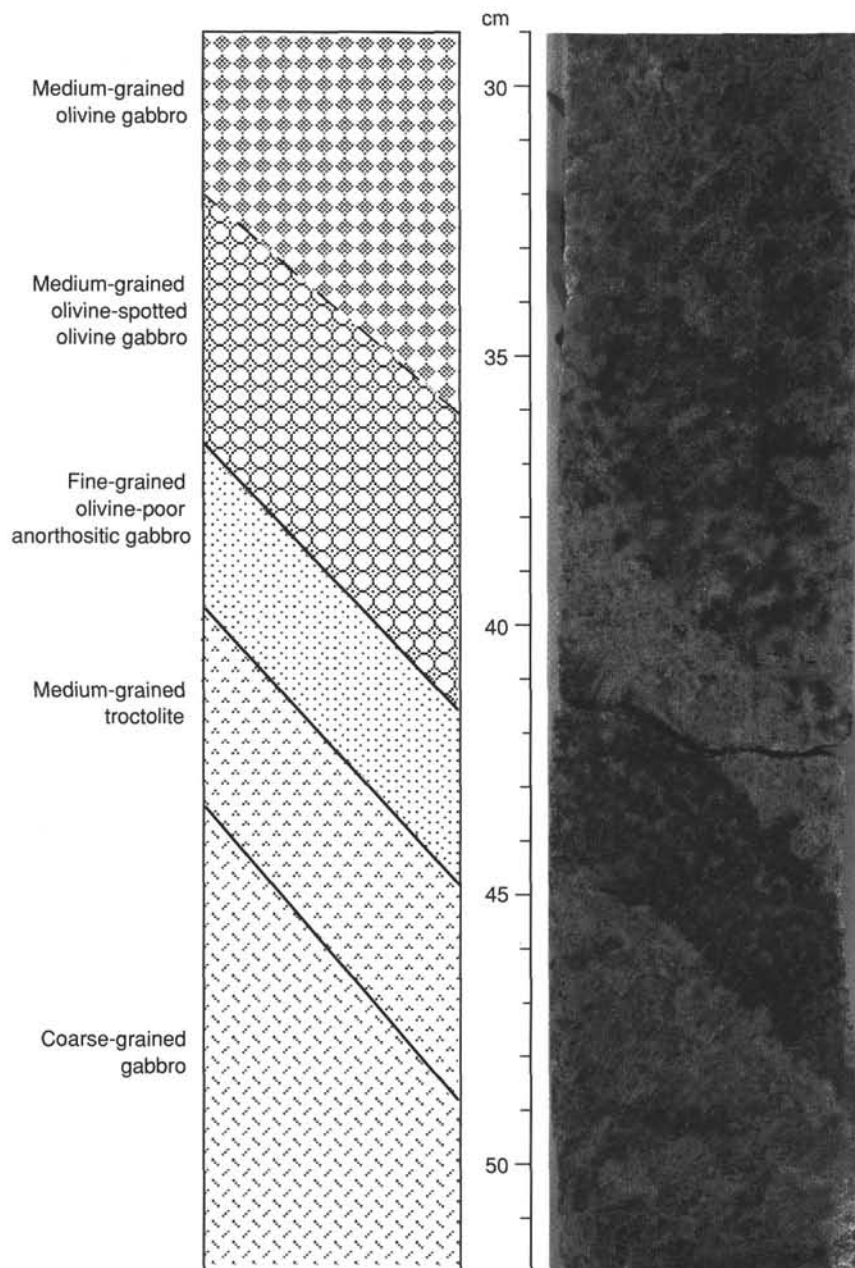


Figure 19. Modal layering between olivine gabbro and troctolite, Sample 153-923A-8R-1, 29–52 cm. The drawing shows the distribution of rock types and inclined contacts. The appearance or disappearance of clinopyroxene define the sharpest boundaries. Sharp boundaries are shown as solid lines; gradational boundaries as dashed lines.

spotted texture due to the presence of interstitial olivine, and a layering defined by interstitial phases rather than the cumulus phase (plagioclase). Interstitial to crescumulate olivine defines diffuse subhorizontal and subvertical layers (Fig. 15), whereas oikocrystic clinopyroxene produces an irregular layering due to its patchy development. The scale of this layering is less than 5 cm thick.

### Geochemistry

Fifteen whole-rock samples from Site 923 were analyzed by XRF for major element oxide compositions and abundances of the trace elements Nb, Zr, Y, Sr, Rb, Zn, Cu, Ni, Cr, V, Ce, and Ba (Table 5). Sample preparation techniques and analytical procedures are described in the introduction to the "Geochemistry" section of the "Site 921" chapter (this volume) and in the "Explanatory Notes" (this volume). Measured contents of Rb, Nb, Ce, and Ba mostly are near or below detection limits (Table 1, "Explanatory Notes," this volume). These values should be used with care because they have relatively large analytical

Table 4. Locations of textural cycle boundaries within Hole 923A cores.

Cycle no.	Interval	Depth (mbsf)
1	0 to 8R-2, Piece 7	0–31.3
2	8R-2, Piece 8, to 9R-2, Piece 8	31.3–34.4
3	9R-2, Piece 9, to 12R-1, Piece 5	34.4–47.5
4	12R-2, Piece 1, to 13R-1, Piece 7	47.5–51.3
5	13R-1, Piece 8, to 13R-2, Piece 7	51.3–53.5
6	13R-2, Piece 8, to 14R-2, Piece 8	53.5–60.3
7	15R-1, Piece 1, to 16R-3, Piece 5	60.3–68.6
8	16R-3, Piece 6, to 16-R, Piece 4	68.6–70.0

errors. Vanadium was also analyzed, but calibration problems produced unreliable data.

The main objective of the sampling strategy was to establish a chemical characterization of the recovered gabbro section. Samples were taken from pieces deemed to be representative. As a rule, the least altered samples were selected to reduce the problem of metamorphic

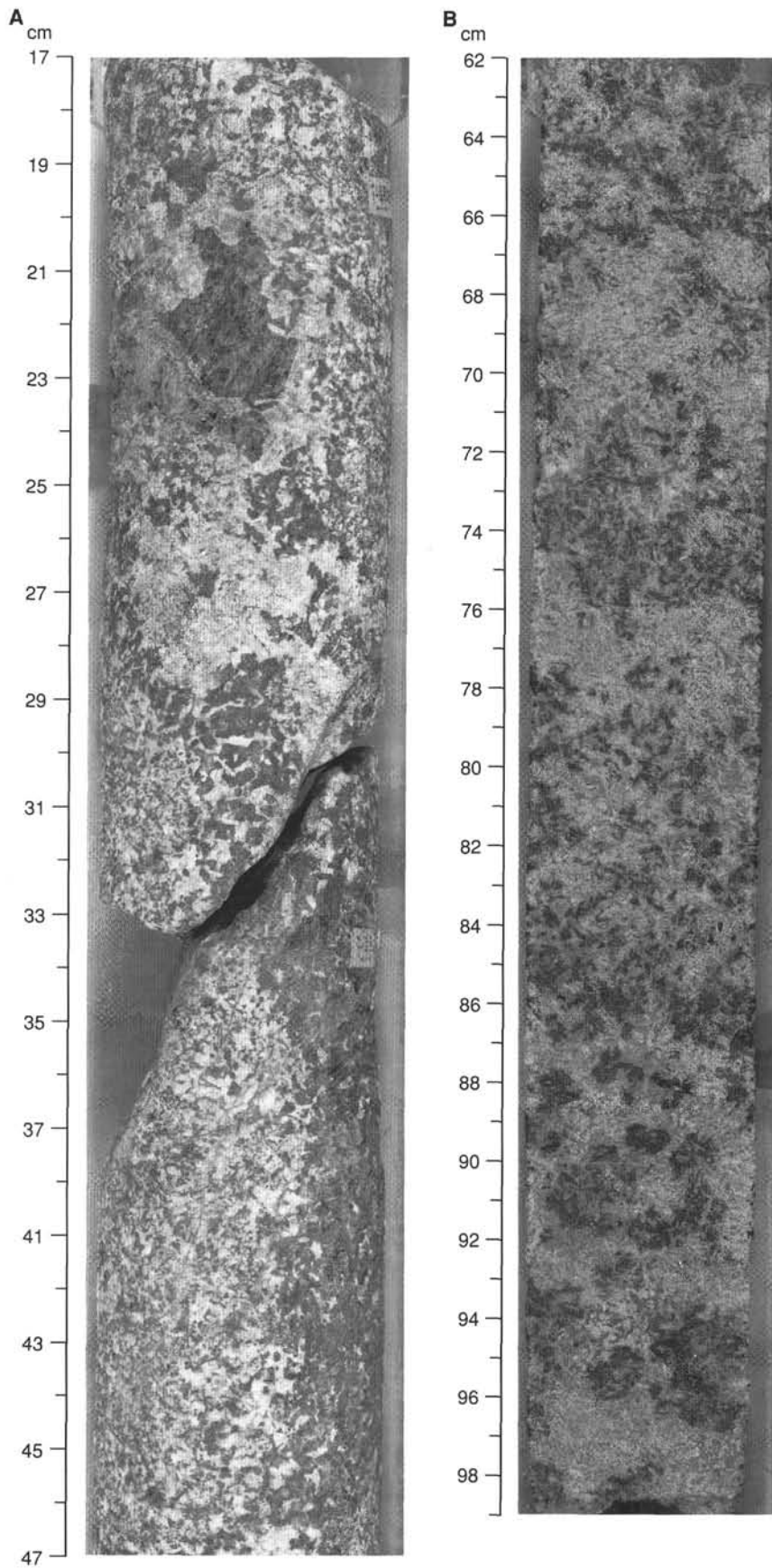


Figure 20. **A.** Sample 153-923A-12R-1, 17–47 cm. Modal layering in olivine gabbro in which a fine-grained olivine gabbro is in contact with a pegmatitic wehrlite layer containing olivine (black) and clinopyroxene (gray) that grades into gabbro containing a large (3 cm) clinopyroxene grain. **B.** Sample 153-923A-16R-1, 62–99 cm. Modal layering within olivine gabbro/troctolite. The layering is defined by variations in the ratio of olivine (black) and plagioclase (white).

Table 5. Major oxide and trace element analyses for Site 923.

Hole:	923A	923A	923A	923A	923A	923A	923A	923A	923A	923A	923A	923A	923A	923A	923A	
Core, section:	2R-1	2R-1	3R-1	4R-1	6R-1	5R-2	7R-2	8R-1	8R-3	10R-2	13-2	15R-1	15R-3	16R-3	16R-4	
Piece:	4	8	3	7B	7	2	1	5A	1	1C	7	14	1	5	7	
Depth (mbsf):	16.67	17.1	19.54	22.41	24.92	25	28.32	29.29	31.91	38.16	53.41	61.23	62.91	67.9	69.01	
Unit:	1	1	1	1	1	1	2	2	2	2	4	5	5	5	5	
Rock name:	MGAB	GAB	OLGAB	GAB	OLGAB	OLGAB	OLGAB	OLGAB	OLGAB	OLGAB	TRGAB	OLGAB	OLGAB	OLGAB	OLGAB	
Type:	1	1	1	1	1	1	2	2	1	1	2	2	2	2	1	
Major oxides (wt%)																
SiO <sub>2</sub>	51.17	52.49	51.79	51.66	50.92	51.79	48.49	50.21	52.03	51.55	47.98	47.85	48.60	49.59	50.21	
TiO <sub>2</sub>	0.32	0.58	0.38	0.55	0.35	0.44	0.63	0.36	0.34	0.42	0.25	0.58	0.16	0.27	0.35	
Al <sub>2</sub> O <sub>3</sub>	17.04	13.74	16.52	15.29	16.55	16.16	21.56	23.19	16.56	17.05	20.01	21.39	22.48	20.71	15.85	
Fe <sub>2</sub> O <sub>3</sub>	6.97	7.32	6.87	7.42	6.96	6.18	4.80	4.91	6.04	6.16	6.91	6.49	4.94	4.99	7.45	
MnO	0.14	0.16	0.14	0.15	0.13	0.13	0.09	0.08	0.12	0.13	0.11	0.11	0.08	0.09	0.13	
MgO	9.93	9.90	8.75	8.85	9.87	9.23	8.11	5.69	9.96	9.86	11.27	10.76	9.46	9.59	11.08	
CaO	12.50	14.13	12.82	12.99	12.98	13.77	13.33	12.12	13.93	13.51	10.54	10.60	12.12	12.94	12.42	
Na <sub>2</sub> O	2.41	2.30	2.54	2.44	2.32	2.40	2.11	2.88	2.21	2.23	2.30	2.27	2.24	2.09	2.10	
K <sub>2</sub> O	0.01	0.03	0.00	0.03	0.01	0.01	0.04	0.03	0.00	0.01	0.01	0.03	0.01	0.01	0.02	
P <sub>2</sub> O <sub>5</sub>	0.00	0.00	0.03	0.04	0.00	0.00	0.12	0.02	0.00	0.00	0.00	0.05	0.00	0.00	0.00	
Total	100.49	100.66	99.83	99.41	100.10	100.11	99.27	99.49	101.20	100.91	99.38	100.11	100.09	100.27	99.60	
LOI	0.71	0.27	-0.01	-0.09	0.20	-0.02	0.61	0.75	0.79	0.93	0.63	0.88	0.63	0.69	0.88	
CO <sub>2</sub>	0.02	0.05	0.05	0.04	0.04	0.01	0.04	0.05	0.06	0.04	0.03	0.06	0.03	0.07	0.05	
H <sub>2</sub> O	1.02	0.66	0.45	0.34	0.28	0.33	0.72	0.58	0.28	0.5	0.94	0.96	0.7	1.07	1.71	
Trace elements (ppm)																
Nb	0	1	0	1	0	0	1	0	0	1	0	1	0	0	0	
Zr	9	53	10	60	9	14	54	19	8	16	11	44	6	10	13	
Y	7	18	9	17	8	11	17	8	8	10	5	9	3	6	8	
Sr	160	116	152	135	144	143	146	188	141	145	151	151	162	144	122	
Rb	1	1	0	1	2	1	1	1	1	0	1	1	1	2	1	
Zn	34	36	29	37	32	28	24	23	23	26	33	36	20	21	37	
Cu	117	45	123	82	105	77	51	79	123	55	98	71	101	82	121	
Ni	99	68	82	78	114	90	199	141	117	99	215	262	220	207	157	
Cr	242	130	78	102	194	130	458	53	220	248	88	19	347	630	381	
Ce	0	0	0	0	0	0	0	0	0	0	0	0	0	0	0	
Ba	0	0	0	0	0	0	0	0	0	0	0	0	0	0	0	
Mg#	0.77	0.76	0.75	0.74	0.77	0.78	0.80	0.73	0.79	0.79	0.79	0.79	0.82	0.82	0.78	
Zr/Y	1.3	2.9	1.1	3.5	1.1	1.3	3.2	2.4	1.0	1.6	2.2	4.9	2.0	1.7	1.6	
Cr/Ni	2.44	1.91	0.95	1.31	1.70	1.44	2.30	0.38	1.88	2.51	0.41	0.07	1.58	3.04	2.43	

Notes: Mg number calculated as the molar ratio of Mg/(Mg + Fe<sup>total</sup>\*0.85). OLGAB = olivine gabbro, MGAB = microgabbro, GAB = gabbro, TRGAB = troctolitic olivine gabbro. Unit = lithologic unit defined on the basis of mineralogical characteristics. LOI = loss on ignition. Type = lithologic type defined on the basis of mineralogical and geochemical characteristics (see "Geochemistry," "Site 921" chapter, for discussion).

effects on the primary geochemistry. Samples that ranged from 35 to 55 g in weight were prepared from quarter-cores or from minicores used for measuring paleomagnetic and physical properties.

Table 5 shows the nominal depth in meters below seafloor, the unit number within the respective hole, and rock name code for each sample. A brief summary of the petrographic features of the samples analyzed is given in Table 6. The rock types analyzed are 11 olivine gabbros, 2 gabbros, 1 microgabbro, and 1 troctolite.

The two main lithologic groups at Site 923, described previously in this chapter, are directly comparable to the two principal lithologic and geochemical groups identified at Site 921: brown-clinopyroxene gabbros = Type 1, and poikilitic olivine gabbros = Type 2 (see "Geochemistry" section of the "Site 921" chapter, this volume). In particular, Type 1 gabbro (brown-clinopyroxene gabbros) typically contains higher contents of SiO<sub>2</sub>, Fe<sub>2</sub>O<sub>3</sub>, Na<sub>2</sub>O, and Zn (Table 5) and lower abundances of Al<sub>2</sub>O<sub>3</sub> and Ni than Type 2 gabbros (poikilitic olivine gabbros). The data for Zr and Y are less systematic for Site 923 gabbroic rocks than for Site 921 gabbroic rocks (Table 5), in that they show enrichments in four samples that do not correlate with indices of fractionation (e.g., SiO<sub>2</sub> or Mg#).

The geochemical variations within and between the lithostratigraphic units at Site 923 are shown graphically in Figure 28 where representative major element oxides and trace elements are plotted vs. Mg#. Shown for reference are the fields of gabbros recovered from Sites 921 and 735B. Collectively, the gabbros show well-defined negative correlations between SiO<sub>2</sub> and Na<sub>2</sub>O versus Mg# that are similar to those observed at Site 921, although Site 923 samples are more restricted in compositional range (Fig. 28).

Gabbro from Unit 1 has exclusively Type 1 compositions (see "Site 921" chapter, this volume, for Type 1, 2, and 3 definitions) and exhibits a restricted range of major element oxide and compatible trace element concentrations compared with other gabbro from Hole 923A. Type 2 gabbro from Units 4 and 5 is the most primitive in the

suite, and it exhibits a relatively tight grouping for most elements. In contrast, samples from Unit 2 span a range of compositions from the most evolved to among the most primitive. Section 153-923A-8R-1 (Piece 5A) from this unit is the most evolved sample analyzed from Hole 923A. These preliminary results highlight the lithologic heterogeneity of Unit 2 and the relative homogeneity of Units 1 and 5. Only one sample was analyzed from Unit 4, a troctolitic gabbro (Table 5), which is similar in composition to olivine gabbro from Unit 5.

Highly compatible trace elements (Ni and Cr) show a wide range in compositions over a small range in Mg numbers, similar to that seen at Site 921, although again exhibiting a more restricted compositional range, particularly for Cr. Cr abundances range to 630 ppm, whereas at Site 921 Cr contents are as high as 1900 ppm in poikilitic olivine gabbro. Brown-clinopyroxene gabbro from Unit 1 has the lowest abundances of Ni and Cr, whereas poikilitic olivine gabbro from Unit 5 contains the highest. Although poikilitic olivine gabbro from Site 923 has a wider range in Cr/Ni ratios than brown-clinopyroxene gabbro (Fig. 29), the range of values is more restricted than that observed in Site 921 poikilitic olivine gabbro.

The trend to high Cr/Ni with increasing Ni is attributed to the presence of Cr-rich clinopyroxene oikocrysts within the poikilitic olivine gabbros. The smaller degree of enrichment in Cr relative to Site 921 gabbro suggests either that clinopyroxene oikocrysts at Site 923 are not as Cr-rich as those from Site 921, or that Cr-rich poikilitic olivine gabbros were not sampled for XRF analysis.

Zr and Y are strongly enriched in four samples from Site 923 (Section 153-923A-2R-1, Piece 8, 4R-1, Piece 7B, 7R-2, Piece 1, and 15R-3, Piece 14) relative to other Site 923 gabbro and to gabbro from Site 921. This enrichment is independent of Mg number and SiO<sub>2</sub> content and occurs in both olivine-rich and olivine-poor gabbro. However, Zr-rich samples also show significant enrichments in Fe<sub>2</sub>O<sub>3</sub>, K<sub>2</sub>O, and TiO<sub>2</sub> (Table 5; Fig. 30). Gabbro containing less than 35 ppm Zr shows a positive correlation with TiO<sub>2</sub> indicating that the

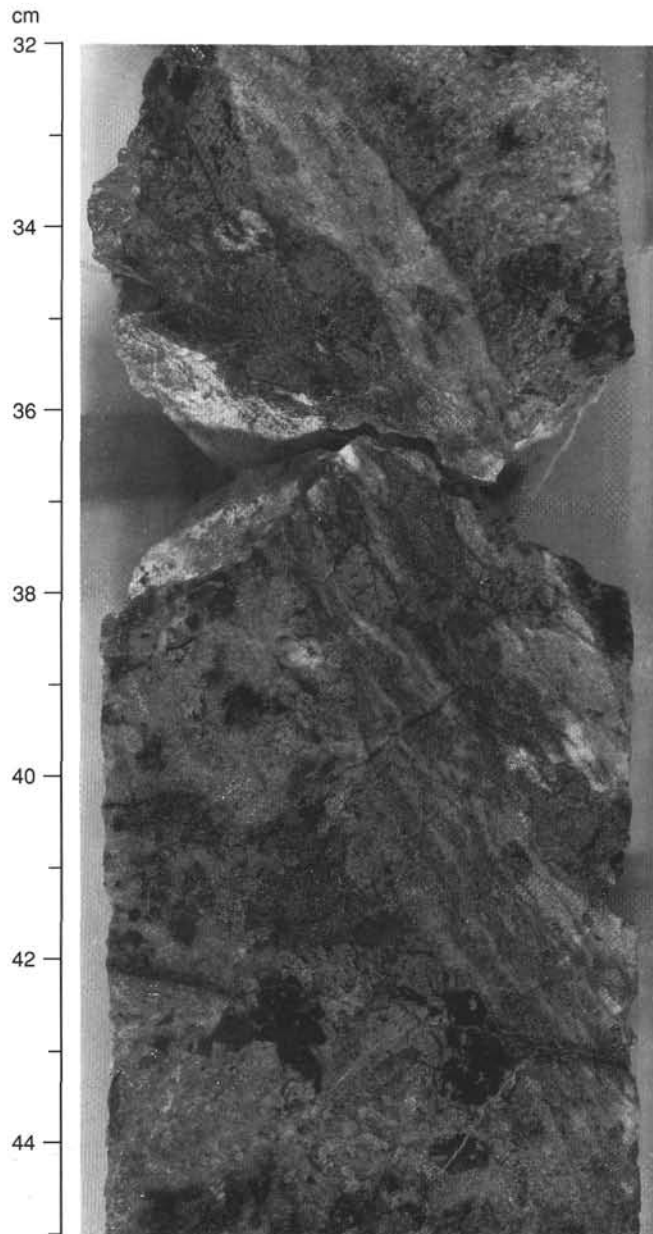


Figure 21. Sheared oxide gabbronorite in undeformed olivine gabbro, Sample 153-923A-16R-2, 32–45 cm.

Zr/Ti ratio does not vary within the group. However, a small group of samples with  $\text{TiO}_2$  contents greater than about 0.5 wt% are enriched in Zr relative to this trend (Fig. 30). A Site 921 sample that falls within this group is a cataclastic metagabbro in which the enrichment in high field strength trace elements (HFSE) was associated with the presence of observed zircon and apatite. High-Zr and high- $\text{TiO}_2$  samples are likely to have greater modal abundances of Fe-Ti oxide minerals and zircon, either because they crystallized from more evolved magmas, or because they have higher trapped melt contents. Given the fact that there is no correlation with Mg#, trapped-melt contents is a likely explanation.

### Discussion

Ternary plots of modal mineralogy illustrate the considerable mineralogical heterogeneity for gabbroic samples from Site 923, particularly for the poikilitic olivine gabbros, which show a greater degree

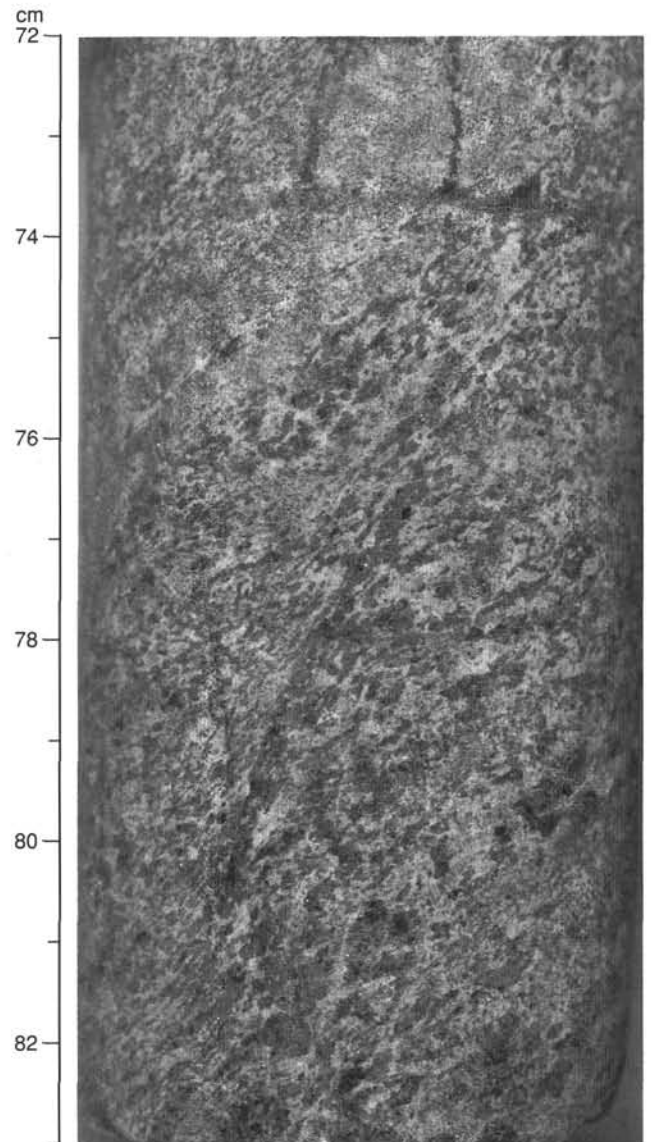


Figure 22. Gabbro and microgabbro contact at ~73 cm inclined at  $\sim 40^\circ$  (Sample 153-923A-11R-1, 72–83 cm). Crystal-plastic foliation in gabbro is subparallel to this contact, except near thin shear zone inclined at  $70^\circ$ .

of olivine enrichment (Fig. 31). There is, nonetheless, considerable overlap between the ranges of poikilitic olivine gabbro and brown-clinopyroxene gabbro. Unit 1 is relatively homogeneous gabbro and olivine gabbro that has generally low abundances of olivine (Fig. 31) with nearly constant plagioclase abundance. In contrast, olivine is always present in Unit 2 gabbro, and modal proportions of both plagioclase and olivine extend to higher levels. Unit 3 is uniformly more olivine-rich than either of the overlying units, and it has lower modal plagioclase and clinopyroxene contents. Unit 4 displays a bimodal distribution in which one group has compositions that are intermediate between those of the olivine gabbros and the gabbros (i.e., the brown-clinopyroxene gabbros). The other has compositions intermediate between the olivine gabbros and the troctolites. These differences are indicative of the interlayered nature of the gabbroic rocks in this unit. Finally, Unit 5 is almost uniformly olivine gabbro to troctolite, but includes a few gabbroic compositions from the bottom of the unit. As described in the section on layering and cyclicity (this section), some of this modal variation may be explained in terms of magmatic evolutionary processes.

Table 6. Petrographic summary of Hole 923A samples analyzed by XRF.

Core, section	Piece	Depth (mbsf)	Unit	Rock name	Olivine		Cpx		Opx		Plagioclase		Accessory minerals	
					Original	Relict	Original	Relict	Original	Relict	Original	Relict	Hornblende	Iron oxides
153-923A-														
2R-1	4	16.67	1	Microgabbro	3	3	20	20	6	5	70	70	1	0.2
2R-1	8	17.10	1	Gabbro	3	2	36	30	1	1	60	60		
3R-1	3	19.54	1	Olivine gabbro	10	10	30	30	0.3	0.3	60	60		0.2
4R-1	7B	22.41	1	Gabbro	3	2.8	30	29	3	2.8	64	63.5		0.5
6R-1	7	24.92	1	Olivine gabbro	8	8	27	27			65	65		0.1
5R-2	2	25.00	1	Olivine gabbro	5	5	30	30			65	65		0.1
7R-2	1	28.32	2	Olivine gabbro	16	15	8.5	7			73.5	73.5	2	0.1
8R-1	5A	29.29	2	Olivine gabbro	10	8	6	6	0.1	0.1	84	84	0.05	0.1
8R-3	1	31.91	2	Olivine gabbro	9	5	28	22			63	63		0.1
10R-2	1C	38.16	2	Olivine gabbro	17	14	17	15	0.3	0.3	66	64		0.2
13R-2	7	53.41	4	Troctolite	25	22	5	4.5	0.3	0.3	70	69	0.2	0.4
15R-1	14	61.23	5	Olivine gabbro	21	14	10	9	0.3	0.3	68	67	0.3	1.0
15R-3	1	62.91	5	Olivine gabbro	20	18	14	14	0.5	0.5	65	65		0.5
16R-3	5	67.90	5	Olivine gabbro	20	16	17	12			63	63	0.5	0.1
16R-4	7	69.01	5	Olivine gabbro	12	8	21	21			67	67		0.1

Note: All modes visually estimated from thin section.

Although the shipboard sampling density for XRF analysis is insufficient to fully test this hypothesis, the results are at least consistent with this model. Cr and Ni vary sympathetically within Unit 1, but below that depth, Ni and Cr vary inversely. The change in trends for these two elements reflects the different mineralogical character of the two principal lithologic groups identified at Site 923. Unit 1 consists exclusively of brown-clinopyroxene gabbro and in these rocks modal proportions of phases are relatively constant; variations in the abundance of Cr and or Ni probably reflect changes in the composition of the magmas with which these gabbros were in equilibrium. Most of the samples analyzed from Units 2 to 5 are from the poikilitic olivine gabbros. In these rocks, the proportion of Cr-rich clinopyroxene to Ni-rich olivine strongly controls the bulk-rock abundance of these compatible elements. The inverse relationship observed between these two elements is an indication of the varying modal proportions of these minerals in the bulk sample.

Enrichments in Zr, Y, TiO<sub>2</sub>, Fe<sub>2</sub>O<sub>3</sub>, and K<sub>2</sub>O observed in some gabbros from Site 923 apparently is not caused by crystallization from progressively more evolved magmas because they are not correlated with indices of magmatic evolution. They may arise from the presence of trace phase(s) that contain high abundances of these elements (e.g., zircon and apatite), and phases enriched in Fe<sub>2</sub>O<sub>3</sub>, Fe-Ti oxides, and K<sub>2</sub>O. One possibility is that these enrichments result from the presence of trapped melt, residual from in-situ crystallization of pore melts. Brown amphibole is commonly observed in interstitial areas and replaces clinopyroxene in these rocks. Although not observed, trace abundances of zircon or apatite may be associated with this mineral occurrence. Alternatively, the enrichment may be due to a later introduction of trace element-enriched melt. The common occurrence of magmatic veins that both crosscut and appear to infiltrate the gabbros (Fig. 14) is evidence that this process occurs at some scale. The correlation between TiO<sub>2</sub>, Fe<sub>2</sub>O<sub>3</sub>, K<sub>2</sub>O, and Zr, and Y enrichment may be evidence for the introduction of enriched melts into the gabbro column; shore-based study can confirm this.

## METAMORPHIC PETROLOGY

The relatively high recovery of gabbroic rocks from Hole 923A (~70%) allows preliminary characterization of the spatial variability of hydrothermal and deformational processes acting in the MARK area on vertical scales ranging from centimeters to tens of meters. The gabbroic rocks recovered from Hole 923A record a complex history involving substantial dynamothermal metamorphism that initiated at near magmatic temperatures and continued down to lower tempera-

ture conditions of the greenschist facies. Overall, however, static alteration associated with brittle failure is strikingly low (~10%).

In the following discussion, alteration mineral assemblages and textural relations within the gabbroic rocks from Hole 923A are described. Downhole variation of secondary phases between the gabbro, olivine gabbro, and troctolite are characterized and a summary of the metamorphic and hydrothermal history preserved in these rocks is presented.

## Alteration of the Gabbroic Rocks

The plutonic suite recovered from Hole 923A includes olivine gabbros, gabbros, rare oxide-bearing gabbros, and troctolites that are commonly slightly to moderately altered (10%–15%) (Fig. 32; Table 7). At least 68% of the gabbroic rocks recovered are affected by ~15% background alteration. Mineral assemblages defining distinct metamorphic zones are generally absent and alteration is heterogeneous. Secondary minerals reflecting high-grade thermal metamorphism are associated with highly deformed zones in olivine gabbros and indicate that dynamic metamorphism occurred under amphibolite to transitional granulite facies conditions. Overprinting of the ductile deformation fabrics by lower temperature secondary phases is generally slight, in contrast to that observed in similar zones at Site 922. Local intervals, which exhibit 80% to 100% replacement by secondary phases, are related to densely veined intervals of cataclastic deformation and rare alteration halos associated with felsic veins. In gabbroic rocks from Site 923, background static alteration is governed by replacement of olivine, followed by clinopyroxene, and more rarely orthopyroxene (Figs. 32 and 33).

## Olivine

In the gabbroic rocks, alteration of olivine is commonly slight to moderate with negligibly altered olivine present throughout many sections. Alteration is dominated by iron oxide minerals lining microfractures and rimming grain boundaries. The iron oxide minerals are commonly associated with talc (Fig. 34). Pervasively altered grains with abundant talc are restricted generally to fine interstitial grains, and there is a tendency for coarser grained olivine to remain less altered. Pervasively altered medium-grained to coarse-grained olivine that is widely distributed throughout the core is commonly associated with adjacent microfractures or veins of actinolite and chlorite (Fig. 35). In these zones, smectite, interlayered smectite and chlorite, and disseminated pyrite from pseudomorphs after olivine as dark green pods.

Table 7. Hole 923A metamorphic summary.

Mineralogy	
Primary	Secondary
Olivine	Iron-oxide, talc, tremolite, chlorite, smectite, pyrite
Clinopyroxene	Hornblende, actinolite, secondary clinopyroxene, iron-oxide minerals
Orthopyroxene	Cummingtonite, talc
Plagioclase	Secondary plagioclase, actinolite, chlorite, prehnite, rare epidote, and carbonate minerals
Apatite, zircon, magnetite	
Vein types	Facies intensity
Magmatic: plagioclase, amphibole, clinopyroxene	Transitional granulite to greenschist facies, <5%–70% altered
Hydrothermal: actinolite, actinolite + chlorite, rare prehnite ± epidote	

Brown amphibole partially rims olivine locally and occurs as an interstitial phase. In contrast to altered gabbroic rocks from Site 922, complex coronitic replacement in gabbroic rocks is generally absent in the rocks from Hole 923A. The style of olivine alteration, however, is similar to that observed in olivine in rocks recovered from Site 921.

### Clinopyroxene

Alteration of clinopyroxene is generally slight. Strongly pleochroic brown hornblende after clinopyroxene occurs as an interstitial phase and is pervasive throughout gabbroic rocks from Hole 923A (Fig. 33). It forms the earliest alteration phase after clinopyroxene, and occurs both as fine-grained brown inclusions within clinopyroxene and as discontinuous rims around clinopyroxene grain margins. Actinolite after clinopyroxene is not abundant except where clinopyroxene grains are cut by, or are adjacent to, vein networks. Secondary hydrothermal clinopyroxene occurs in magmatic veins and more rarely in the host gabbro and is characterized by abundant vapor-dominated fluid inclusions. In areas of ductile deformation, clinopyroxene occurs as neoblasts of fine-grained clear grains that generally lack alteration phases.

### Orthopyroxene

Orthopyroxene alteration is highly variable (<10% to 100%), and finer grains are commonly more highly altered. In slightly to moderately altered grains, cummingtonite(?) and fine-grained oxide minerals fill microfractures cutting orthopyroxene grains, form narrow rims around pyroxene grains, and occur as isolated intergrown fibrous patches within the grains. In highly deformed zones, orthopyroxene porphyroclasts are rimmed by fine stringers of iron oxide minerals and cummingtonite or tremolite.

### Plagioclase

In general, plagioclase alteration is strikingly slight throughout most of the sections recovered from Hole 923A. Pervasive alteration of plagioclase locally is associated with rare cataclastic zones, alteration halos associated with hydrothermal veins and veinlets (Fig. 35), and plagioclase grains hosted in felsic magmatic veins. Alteration in these zones predominantly involves the formation of secondary plagioclase with minor amounts of epidote, prehnite, and chlorite. In highly altered zones, plagioclase is typically turbid due to abundant fine-grained inclusions of chlorite, amphibole, and clay minerals. Secondary plagioclase commonly forms irregular microveinlets and patches that respectively crosscut and rim primary plagioclase grains. Pale green amphibole and chlorite veinlets also locally cut plagioclase grains. Trace amounts of epidote occur in magmatic veins and in

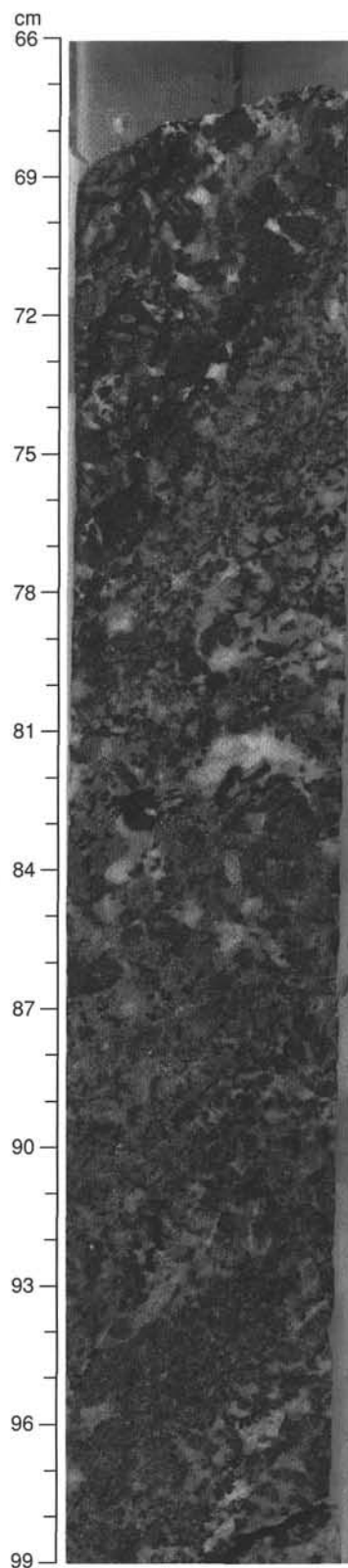


Figure 23. Zone near the bottom of Unit 3 containing olivine-rich troctolite and feldspathic wehrlite, Sample 153-923A-12R-1 (Piece 4B, 66–99 cm). The piece displays a contact at ~69 cm between a layer containing subhedral, coarse (>10 mm) olivine as a primocryst phase, surrounded by heteradcumulus plagioclase (above) and equigranular olivine-rich gabbro (below). The layering is inclined at ~50°.

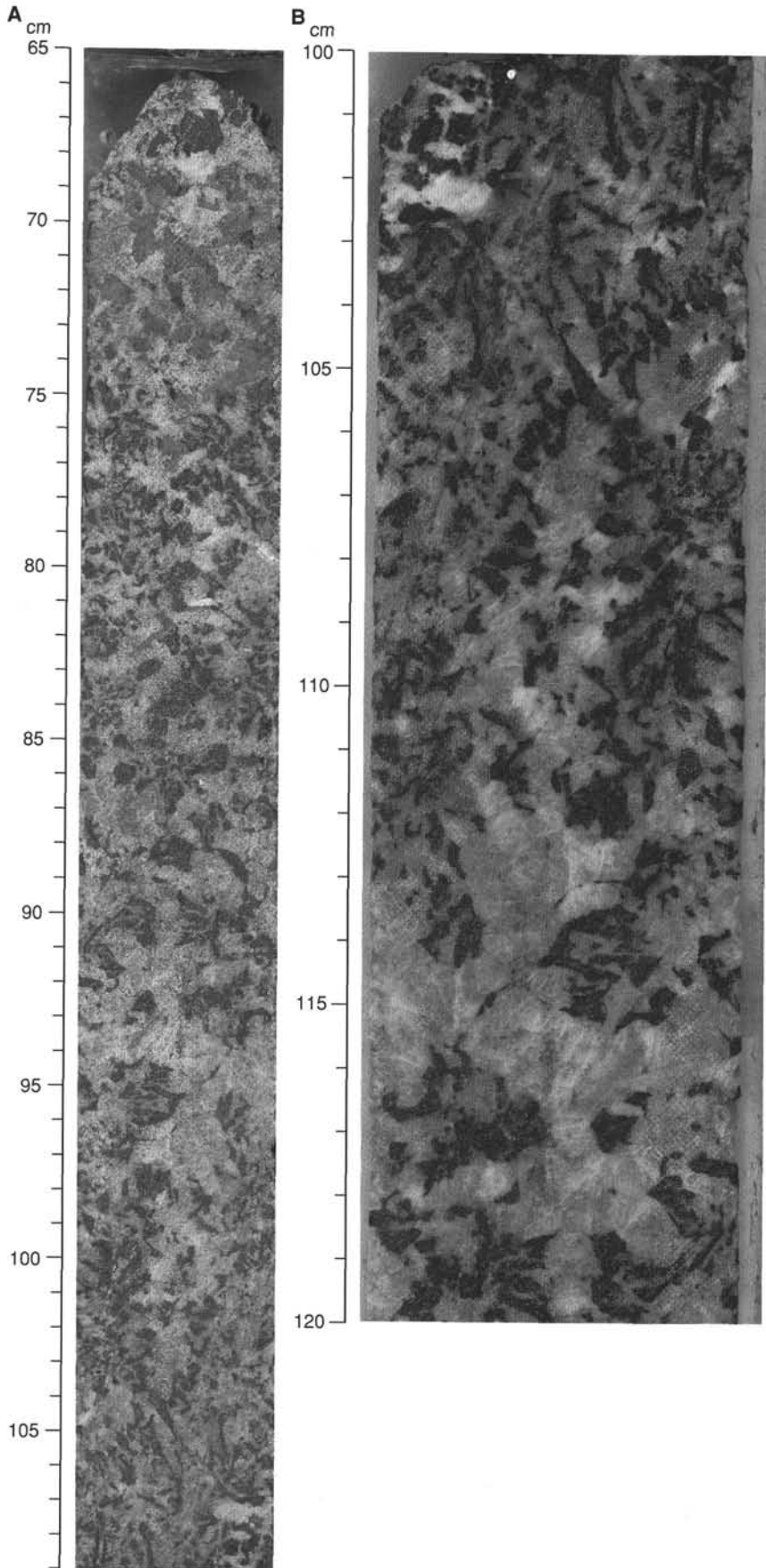


Figure 24. **A.** Olivine gabbro and troctolite, Sample 153-923A-12R-1, 65–109 cm, near the base of cyclic Unit 3, in part a “crescumulate” (Wadsworth, 1961). Note blade-like olivine grains at interval 104–109 cm. Clinopyroxene (gray) forms a large oikocryst between 66 and 77 cm. Elongate olivine (black) with slender grains up to 2 cm in length are observed at a high angle inclined at  $70^\circ$  to subhorizontal magmatic layering. This zone of elongate olivine between 89 and 103 cm gives way downward to a very coarse troctolite with space-filling olivine between large plagioclase (white) up to 25–35 mm in length. **B.** Close-up of Sample 153-923A-12R-1, 100–120 cm. Note bladed olivine (100–109 cm) and subtle layer boundary (112 cm) defined by changes in modal olivine and plagioclase, as well as a change in grain size.

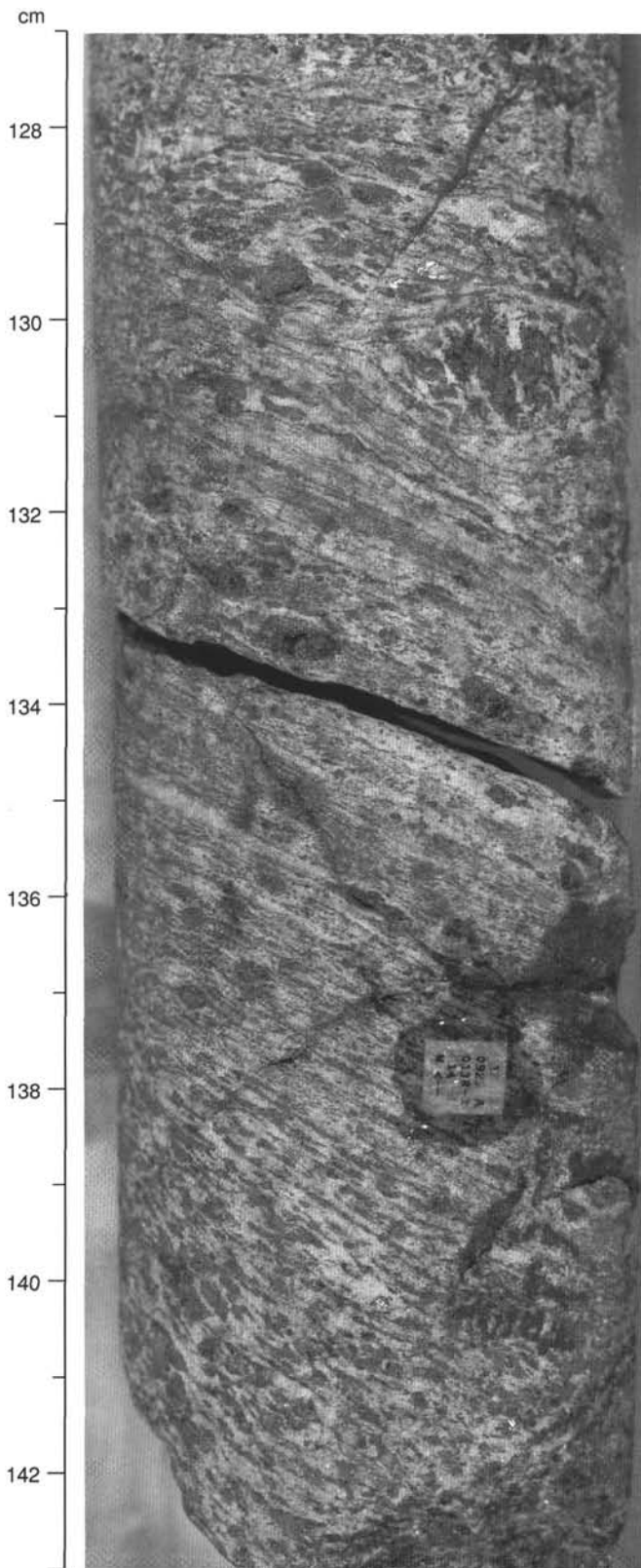


Figure 25. Sample 153-923-13R-1 (Piece 13, 127–143 cm). Large isolated green clinopyroxene porphyroclasts in a crystal-plastic shear zone that contains recrystallized brown clinopyroxene.

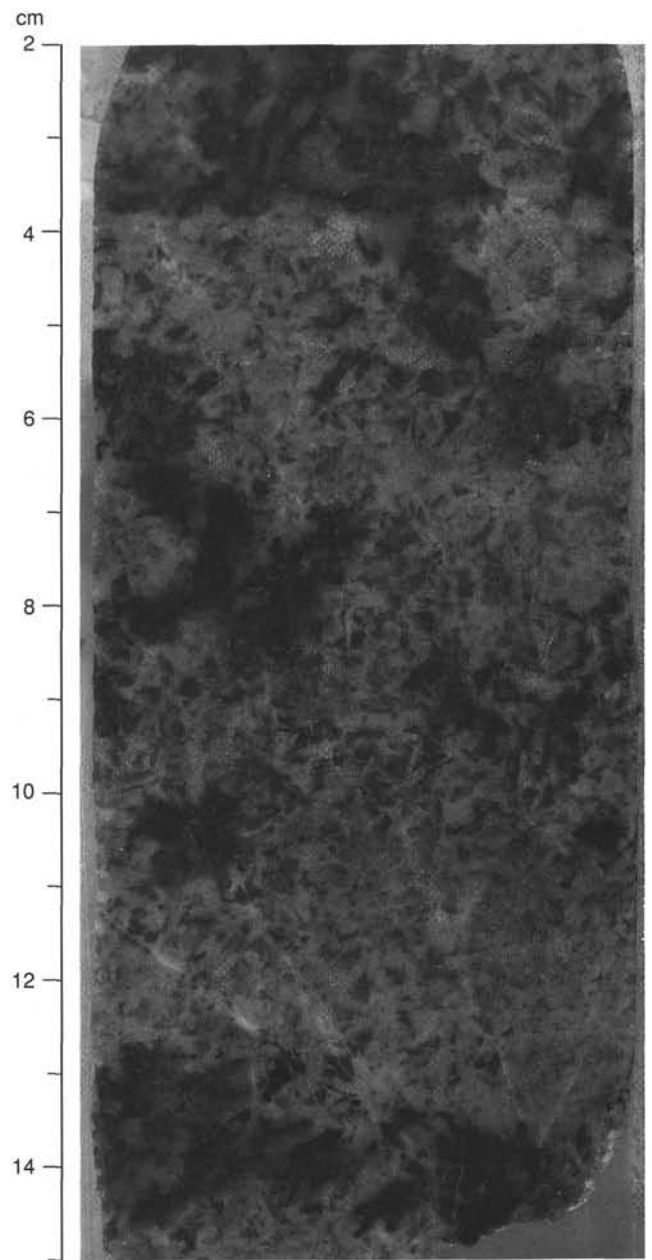


Figure 26. Sample 153-923A-14R-2, 2–15 cm, shows a troctolite with euhedral to subhedral radiating plagioclase, interstitial olivine, and darker patches of olivine relatively free of plagioclase. Two layer contacts, one near the top of the piece (4 cm) the other at the base (14 cm) are defined by an increase in olivine content. The top layer contact is nearly horizontal, whereas the basal contacts are inclined at  $\sim 15^\circ$ .

mylonite zones, form fine-grained, granular, pale green inclusions in plagioclase and are locally associated with prehnite.

#### Static and Dynamic Metamorphism of Gabbroic Rocks

The gabbroic rocks recovered from Hole 923A were affected by variable degrees of alteration and deformation that in the initial stages involved crystal-plastic deformation. This high-temperature deformation locally was overprinted by brittle deformation that resulted in the formation of millimeter-scale veins commonly consisting of actinolite and actinolite + chlorite. These vein sets, which locally form dense anastomosing networks, are rare, consistent with the low degree of

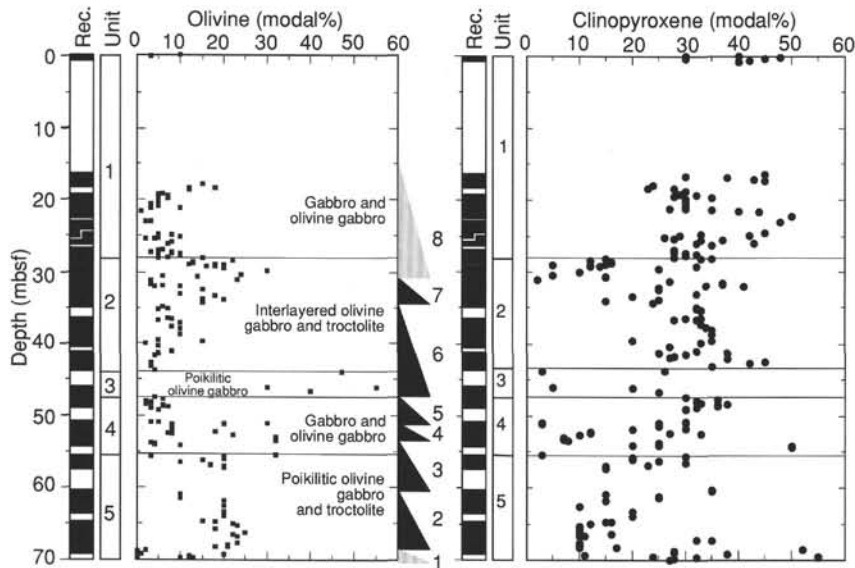


Figure 27. Plot of modal percentages of olivine and clinopyroxene against depth, showing unit boundaries and relationship to compositional/textural cyclic units (1–8) identified in the core.

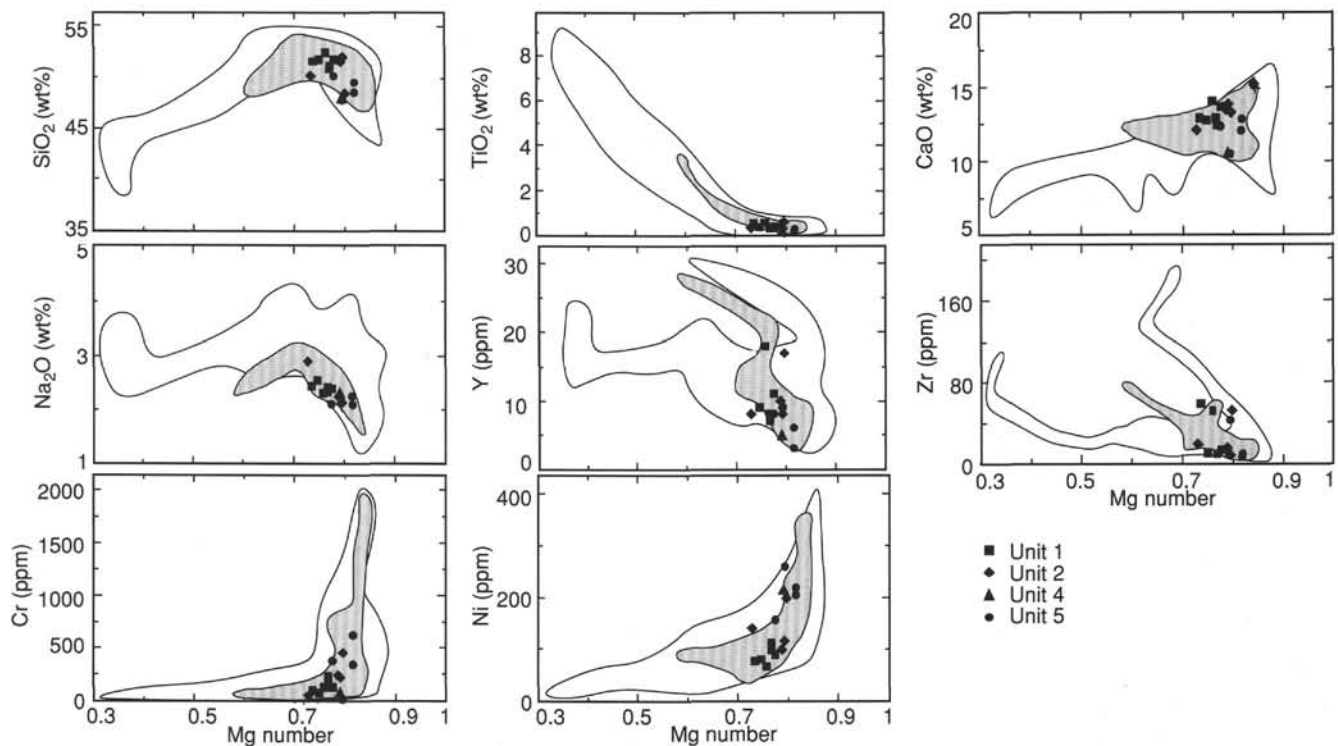


Figure 28. Bulk-rock major and trace element compositions plotted against Mg# for Site 923 samples. White field shows the range of compositions of Site 735B gabbros (Robinson, von Herzen, et al., 1989), and shaded field shows data from Site 921 (this volume).

alteration observed throughout most of these rocks. In the following discussion, mineral assemblages and deformational relationships are presented in terms of lithologic rock types.

#### Oxide Gabbro

Oxide gabbros constitute a minor component of the gabbroic rocks recovered from Site 923 and commonly exhibit moderate alteration intensities (15%; Fig. 21). Clinopyroxene hosts fine-grained brown amphibole and iron oxide minerals and locally is slightly altered to colorless to very pale green amphibole. In deformed zones, clinopy-

roxene neoblasts occur along grain boundaries as fine, clear grains with fine-grained blebs of brown hornblende and minor to well-developed rims of actinolite. Grain boundaries are rimmed by stringers of iron oxide minerals and orange clay minerals, which give the rocks an oxidized appearance. The stringers are discontinuous, and with elongate clinopyroxene and orthopyroxene aggregates, define a moderately well-developed foliation. Orthopyroxene grains are commonly rimmed by cummingtonite(?) and locally are moderately to pervasively altered to very fine-grained cummingtonite and talc(?). Plagioclase-rich zones are composed of fine-grained neoblasts that locally exhibit moderately to well-developed triple junctions, and

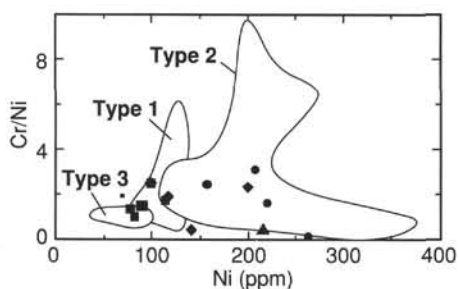


Figure 29. Bulk-rock ratio of Cr/Ni vs. Ni (ppm) in Site 923 samples. Symbols as in Figure 28. Types 1, 2, and 3 are defined in Figure 34 of the "Site 921" chapter (this volume). In Site 923 rocks, these types correspond to: Type 1 = brown gabbro group, Type 2 = poikilitic olivine gabbro group, Type 3 = gabbro-norites and oxide gabbros.

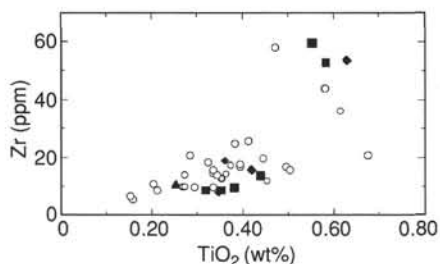


Figure 30. Zr (ppm) vs.  $\text{TiO}_2$  bulk-rock in Site 923 rocks. Open circles = gabbros from Site 921. Other symbols as in Figure 28.

porphyroclasts that exhibit deformation twins, sutured grain boundaries, and patchy extinction. Plagioclase grains form anastomosing discontinuous lenses that are bounded by mafic-rich zones.

### Gabbro

Undeformed gabbro is characterized by slight to moderate intensities of alteration (5%–20%). Clinopyroxene grains host hornblende blebs and fine-grained iron oxide minerals and are discontinuously rimmed by brown hornblende. Coarse clinopyroxene grains are locally replaced by actinolite and have dark cleavages lined by very fine-grained iron oxide minerals. Rarely grains are replaced by blue-green amphibole. In deformation zones, coarse clinopyroxene grains are replaced by neoblasts of fine-grained clear clinopyroxene, which generally lack alteration phases. Orthopyroxene grains are slightly altered to cummingtonite and talc(?), forming fine, narrow rims. Olivine alteration phases include iron oxide minerals along microfractures and rimming olivine, minor tremolite, talc, and smectite. Plagioclase is negligibly altered and exhibits undulatory and patchy extinction, and deformation twins.

Gneissic gabbro is a relatively common rock type in gabbroic rocks recovered from Hole 923A (Figs. 10, 12, and 36). Olivine in gneissic gabbro is highly recrystallized to very clear, medium-sized, strain-free grains and occurs as aggregates on the edges of pervasively altered coarser olivine grains. The olivine is highly to pervasively altered locally to iron oxide minerals that are intergrown with talc and fine-grained cummingtonite or tremolite. The grains lack corona structures. Coarse olivine grains commonly exhibit kink bands, and well-developed hornblende rims that are locally slightly altered to green amphibole. Clinopyroxene grains are typically only slightly altered, with alteration generally limited to inclusions of hornblende and coarse-grained discontinuous hornblende rims associated with oxide minerals and minor actinolite. Locally, the edges of clinopyroxene grains are dusty and turbid due to replacement by fluid inclusion-rich secondary clinopyroxene. Fine-grained actinolite

forms rare pale green interstitial patches. Plagioclase exhibits grain-size reduction in localized domains along elongate zones. It is generally negligibly altered to secondary phases; where secondary phases do occur they are generally related to fine, chlorite  $\pm$  actinolite veins.

Rare zones of cataclastic gabbros occur in rocks recovered from Site 923. The cataclastic zones are characterized by anastomosing veinlets of pale green actinolite with alternating lenses of plagioclase, chlorite, clay minerals, epidote, and prehnite. The cataclastic zones are typically associated with well-developed crosscutting actinolite and chlorite veinlets. Alteration intensities are pervasive in these zones (see "Structural Geology," this chapter).

### Olivine Gabbro

Olivine gabbro recovered from Site 923 commonly exhibits slight to moderate alteration intensities (<10%–15%). In slightly altered samples, olivine is generally fresh to moderately altered (10%). Secondary phases include iron oxide minerals and talc that line microfractures and rim grain boundaries, respectively (Fig. 34). Locally, fine olivine grains are pervasively replaced (100%) by smectite and iron oxide minerals that form fine, green patches sporadically throughout the sections. In rare samples, clinopyroxene is pervasively replaced by secondary hydrothermal clinopyroxene that contains abundant fluid inclusions. More commonly, clinopyroxene grains are partially rimmed by brown hornblende, and host fine hornblende blebs. Hornblende also occurs as a rare interstitial phase and is locally replaced by pale green amphibole, and traces of chlorite where adjacent to plagioclase. Alteration of plagioclase is rare.

Lineated olivine gabbro (see "Structural Geology," this chapter) is common throughout Section 153-923A-2R-2 and is characterized by slight to moderate alteration intensities. Alteration is dominated by slight to pervasive replacement of olivine. Fine-grained olivine in these rocks is pervasively altered (90% to 100%) to iron oxide minerals, which exhibit a dendritic to feathery habit, talc, and olive green smectite. Alteration phases typically do not develop coronas. Coarser grained olivine in some samples is pervasively altered to talc and fine-grained amphibole. Clinopyroxene alteration is only slight and limited to fine blebs of brown hornblende, discontinuous rims of hornblende, and fine-grained iron oxide minerals along cleavage planes. Where clinopyroxene is recrystallized, it is fine-grained, clear, and hydrous phases are absent. Highly strained plagioclase grains exhibit deformation twins, and undulatory and patchy extinction.

Shear zones up to 20–30 cm in thickness exhibit a well-developed fabric (Fig. 37), that in some samples is defined by discontinuous, narrow stringers of pale green to dark green fibrous amphibole that are associated with fine-grained opaque minerals. Clinopyroxene porphyroclasts are lensoidal in shape with dimensions of up to 2 mm in width and 10 mm in length and are replaced by green, fibrous amphibole. Rare grains have also been partially replaced by brown amphibole cores. These are rimmed by fibrous actinolite. The clinopyroxene porphyroclasts occur in discontinuous narrow bands less than a millimeter wide that are paralleled by rare magnetite stringers and more commonly by fine-grained neoblasts of plagioclase. Rare, undeformed, coarse-grained clinopyroxene porphyroclasts are only moderately altered, with amphibole along the edges and in fine veins. Clinopyroxene neoblasts locally occur along grain boundaries and form domains of mosaic textured grains. Plagioclase neoblasts also exhibit moderate development of a mosaic texture. Rounded lenses containing neoblastic olivine with mosaic textures are not altered. Aggregates of clinopyroxene, pervasively altered to amphibole, form mottled green lenses. Rarely, clinopyroxene in these domains contains blebs of brown hornblende. Typically, however they are pervasively altered to actinolite and fine-grained iron oxide minerals. Clinopyroxene is locally pervasively altered to secondary clinopyroxene. Elongate aggregates of clinopyroxene and rare recrystallized olivine with traces of magnetite that alternate with plagioclase-rich layers define a moderately well-developed foliation in these rocks.

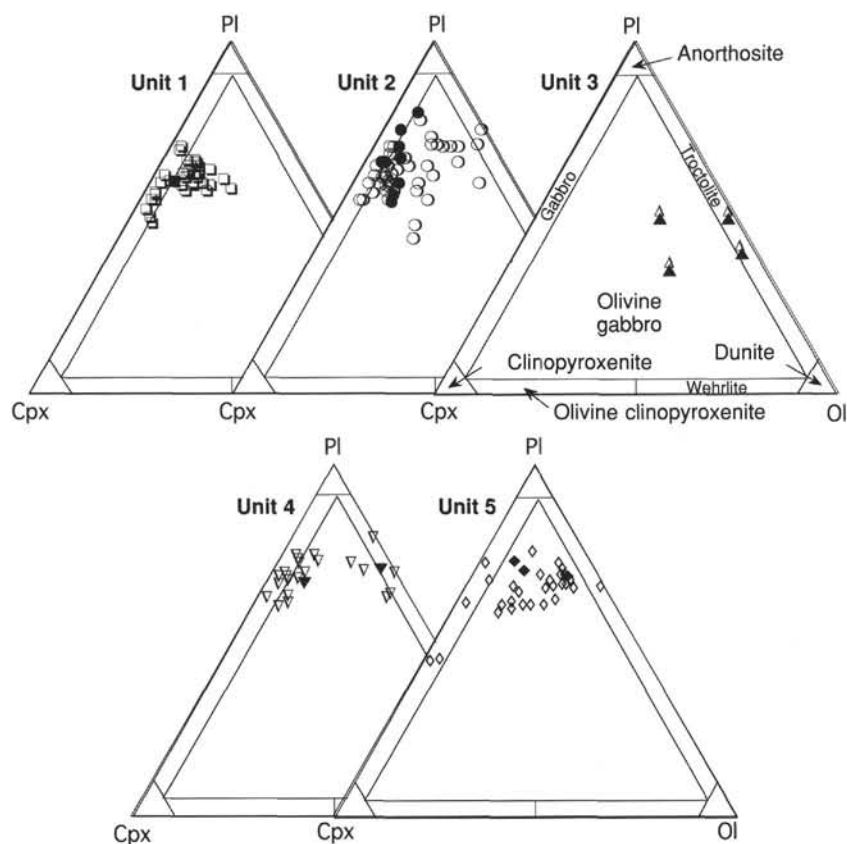


Figure 31. Modal proportions of olivine, plagioclase, and clinopyroxene plotted on the rock classification scheme used for this report ("Explanatory Notes," this volume). Note that the modal estimates for Unit 3 are averages of extremely heterogeneous pieces with compositions from 10% to 80% olivine, 5% to 70% plagioclase, and 0% to 20% clinopyroxene. Open symbols = modal estimates from macroscopic core descriptions; closed symbols = modal estimates from thin sections.

### Amphibolite

Amphibolite is rare in gabbroic rocks from Hole 923A, where it is limited to an interval of 34 cm recovered in Section 153-923A-2R-1 (Fig. 38). The amphibolite is fine-grained and exhibits a foliation defined by fine-grained olivine and clinopyroxene grains. The mafic phases exhibit slight to locally moderate replacement by greenschist facies mineral assemblages. Fine-grained aggregates of olivine and clinopyroxene with minor rims of hornblende are elongate to lensoid in shape and form "stringers" that are enclosed in plagioclase-rich zones. Olivine is replaced locally by fine-grained iron oxide minerals and minor interlayered smectite and chlorite. Plagioclase in these zones is fine-grained and exhibits a well-developed mosaic texture; however, twinning is present locally as well. Plagioclase grains that are not twinned are highly strained with patchy and wavy extinction. Fine-grained orthopyroxene is altered to cummingtonite (90%). The amphibolite is cut by very fine, branching, chlorite veinlets that locally exhibit evidence for shearing. The association of olivine, clinopyroxene, and brown hornblende, in near textural equilibrium with plagioclase, indicates formation temperatures of 700°C–900°C (Spear, 1981). Minor replacement of clinopyroxene and hornblende with fine-grained actinolitic hornblende coupled with the occurrence of actinolite and actinolite + chlorite veinlets indicates that later, limited interaction with fluids occurred under greenschist facies conditions.

### Troctolitic Gabbro

Troctolitic rocks recovered from Hole 923A consistently exhibit negligible to slight alteration intensities (<10%) (Figs. 16 and 24). Olivine is generally altered less than 10%, but locally, and adjacent to veins, alteration is pervasive. In these highly altered zones pseudomorphs after olivine have been formed by smectite, chlorite, and fine-grained pyrite. Alteration minerals in less altered zones include talc and fine-grained iron oxide minerals along fractures and rimming grains. Clinopyroxene is fresh to slightly altered with fine blebs and

discontinuous rims of brown hornblende. Plagioclase generally lacks secondary phases.

### Veins in the Gabbroic Rocks

Macroscopic veins are relatively rare throughout the gabbroic rocks recovered from Hole 923A. Hydrothermal veins are typically dominated by green amphibole and chlorite, though variable amounts of other phases are locally present as well. These minerals include epidote, prehnite, clay, and carbonate. In the following sections, the mineralogy and relative chronology of the veins are described.

### Magmatic Veins

Felsic magmatic veins constitute less than 1% of the core recovered from Hole 923A and are associated with pervasive alteration of the host gabbros (Fig. 39). The veins are generally either subhorizontal or subvertical and exhibit sharp boundaries with the gabbroic host rocks. The felsic veins are commonly 20–40 mm wide and exhibit compositional zonation with clinopyroxene and amphibole-rich cores with accessory phases consisting of apatite, zircon, and iron oxide minerals. The cores are bordered by selvages of variable width consisting of plagioclase, and they exhibit diffuse to sharp boundaries with the pervasively altered bounding host rock (Fig. 39). Primary minerals within the veins are typically highly to pervasively replaced by variable amounts of coarse-grained actinolite, secondary plagioclase, granular epidote, and prehnite. The wall rock alteration along the margins of these veins is variably developed, with actinolite, chlorite, secondary plagioclase, and trace amounts of epidote common as secondary phases (Fig. 39). Brown hornblende forms well-developed rims around clinopyroxene adjacent to the veins and locally rims host-rock olivine grains. In the olivine gabbros and poikilitic olivine gabbros, intrusion of these veins and attendant alteration have resulted in the development of coarse-grained talc and magnetite ± smectite-rich pods after olivine. Plagioclase in the veins and adjacent host rock is

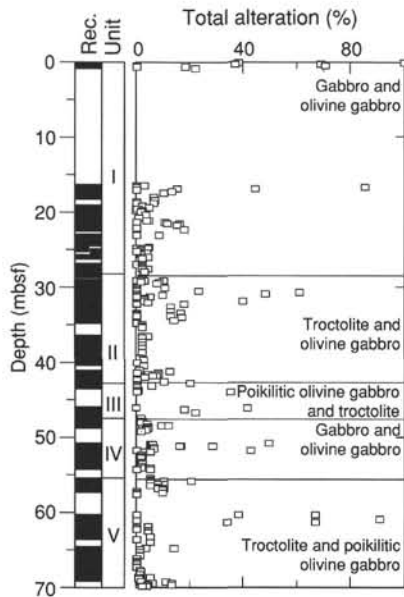


Figure 32. Depth vs. abundance of secondary minerals in percent, as estimated in core samples, for Hole 923A. Unit numbers correspond to units described in "Igneous Petrology," this chapter. The corresponding core recovery is indicated by black bars. Scale of figure differs from others of this site because of the amount of data shown.

highly to pervasively altered to secondary plagioclase, which rims grain boundaries and occurs along jagged and irregularly shaped fractures cutting plagioclase. Typically, the plagioclase in these zones is dusty in appearance due to abundant fine grains of clay minerals(?) and abundant liquid-dominated fluid inclusions.

**Hydrothermal Veins within the Gabbros**

Composite macroscopic veins are rather rare throughout the gabbroic rocks recovered from Hole 923A and commonly contain variable amounts of actinolite, actinolite + chlorite, and chlorite. On the basis of crosscutting relationships, three to four distinct vein generations are recognized. Each of the vein sets is described below (also see "Structural Geology," this chapter).

**Actinolite + Chlorite Veins**

Actinolite + chlorite veinlets are the most common veins in the gabbroic rocks and govern the background static metamorphism. The veins are typically ~1 mm or less wide; they are dark green and associated alteration halos are rare. They commonly form fine, anastomosing networks that locally pervasively crosscut and rim plagioclase grains.

**Chlorite Veins**

Chlorite veins generally form fine (<1 mm wide), dark green veins, in anastomosing networks cutting plagioclase grains and are most abundant in highly deformed samples. The veinlets are commonly discontinuous and contain dark green, well-crystallized chlorite; associated wall-rock alteration is typically absent.

**Epidote ± Prehnite Veins**

Epidote and epidote æ prehnite veinlets (1–2 mm wide) are rare in the gabbroic rocks and are associated with pervasive alteration of the adjacent host rock. They form subvertical veins that cut highly deformed zones. Associated wall-rock alteration with this vein set includes pervasively altered plagioclase grains that are partially re-

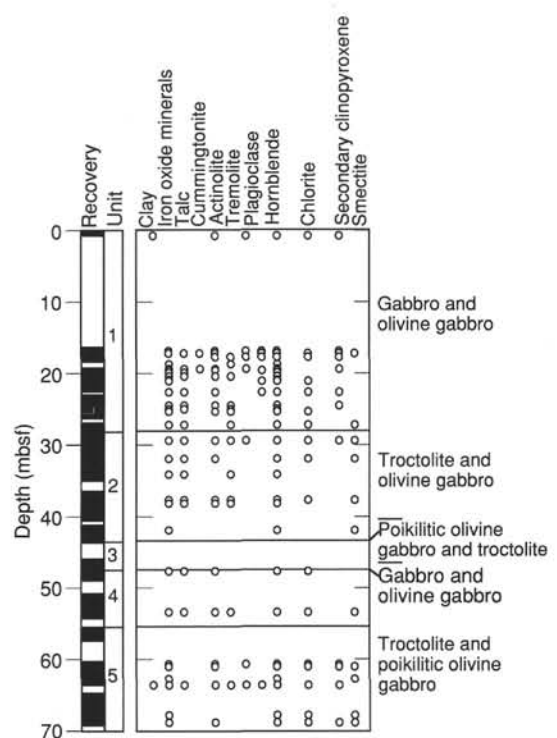


Figure 33. Occurrences of secondary minerals with depth in the gabbroic rocks recovered from Hole 923A.

placed by medium-grained apple-green epidote, prehnite, and lesser amounts of secondary plagioclase.

**Downhole Variation in Alteration**

Alteration is most intense in the top and bottom portions of Hole 923A where there are localized cataclastic zones. Alteration intensities of Units 1–5 are all similar, though isolated intervals of gabbro and olivine gabbro locally exhibit somewhat higher alteration intensities (Fig. 32). Overall, there is no apparent difference in the occurrences of alteration minerals downhole and intensities are broadly similar (Fig. 33).

**Discussion**

Alteration of variably deformed gabbroic rocks recovered from Hole 923A is strikingly low, with alteration intensity averaging only ~10%. In general, brown hornblende discontinuously rims clinopyroxene and as an interstitial phase marks the peak metamorphic mineral phase indicating temperatures of 700°–900°C (Spear, 1981). It is well preserved in these rocks with little mineralogical evidence for significant retrograde alteration. Replacement of olivine by secondary phases dominates alteration in most of the rocks recovered from this site, with fine-grained oxide minerals and minor talc, cummingtonite, tremolite, smectite, and traces of carbonate and pyrite making up the major secondary phases. Alteration intensity of olivine is low in many samples (<10%) and pervasive alteration typically is limited to fine interstitial grains. In contrast to olivine replacement observed in gabbroic rocks recovered from Site 922, alteration coronas are generally absent in gabbro at this site, and chlorite occurs only in trace abundances as a secondary phase. Clinopyroxene is generally slightly to negligibly altered to blebs and rims of brown hornblende, fine-grained magnetite, and trace amounts of actinolite. In rare, highly altered samples, clinopyroxene is overgrown by massive, light green amphibole, and brown amphibole is rimmed by olive green amphibole. Similar to clinopyroxene, replacement of plagioclase by secondary phases is

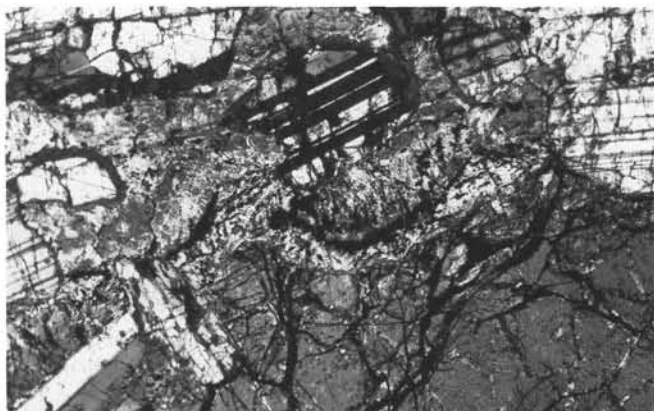


Figure 34. Photomicrograph showing an olivine grain rimmed by talc and cut by fine-grained iron oxide-bearing veinlets (Sample 153-923A-7R-2, Piece 1, 1–7 cm). Field length is 1.5 mm.

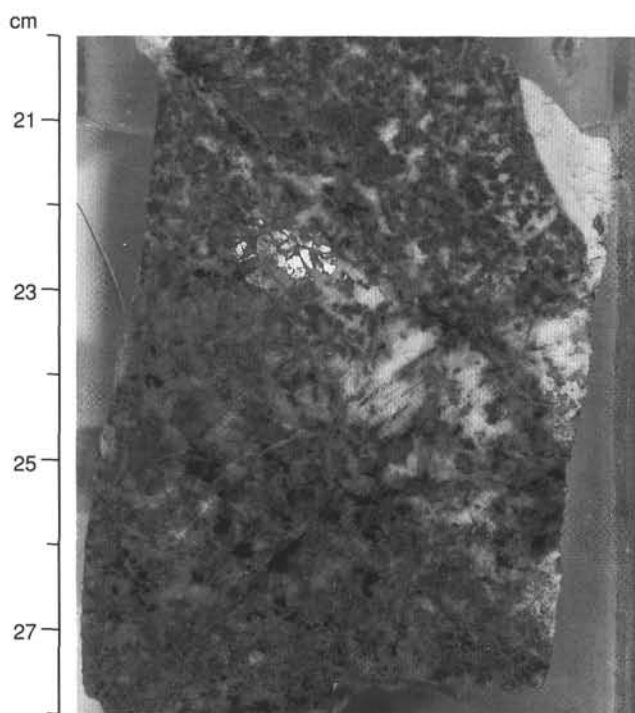


Figure 35. Sample 153-923A-1W-1 (Piece 3, 20–28 cm). Intense alteration in the gabbro near actinolite-chlorite veins is characterized by secondary plagioclase, actinolite-tremolite, chlorite, smectite, and minor prehnite. Chlorite and smectite replacement after olivine forms dark irregular patches. Also, notice the shining poikilitic clinopyroxene grain in upper left part of photograph.

negligible in most samples. Alteration phases include minor chlorite and secondary plagioclase.

Rare, highly to pervasively altered sections throughout the core are typically restricted to narrow mylonite and cataclastic zones (e.g., mylonites in top of Sections 153-923A-1W-1, 15R-1, and 16R-2) and crosscutting felsic veins. In these zones, intense replacement by actinolite, chlorite  $\pm$  smectite after mafic phases is ubiquitous, and plagioclase is locally pervasively altered to prehnite, clay minerals, secondary plagioclase, and minor epidote. Many of these intensely altered zones are associated with fine, <1-mm- to 1-mm-wide veins that typically form networks and are composed of chlorite, actinolite, rare prehnite  $\pm$  epidote, and veinlets of clay  $\pm$  zeolite.

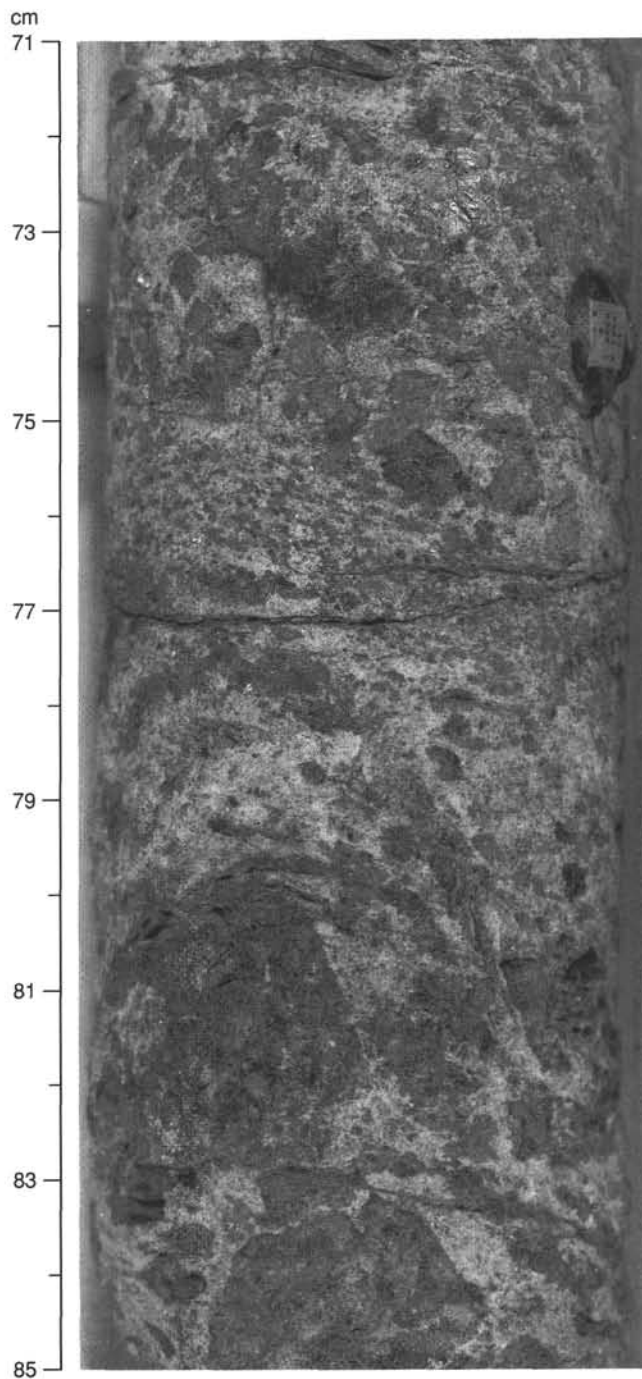


Figure 36. Gneissic gabbro in Sample 153-923A-2R-1 (Piece 6, 71–85 cm). Coarse-grained pyroxene porphyroclasts are enclosed in a finer grained matrix of partially recrystallized plagioclase. Finer grained pyroxene in the center of sample may have resulted either from magmatic grain-size variations, or from grain-size reduction during crystal-plastic deformation.

Magmatic veins are generally rare, but occur as felsic veins, 20–30 mm wide, sparsely distributed throughout the sections. Primary minerals are commonly pervasively replaced and actinolite  $\pm$  brown amphibole after clinopyroxene, and secondary plagioclase, epidote, and prehnite are common after plagioclase. As in felsic veins from other sites, fluid inclusions typically record exsolution of brines and vapors concomitant with vein formation. Associated wall-rock alteration along the margins of these veins is variably developed, with actinolite, chlo-

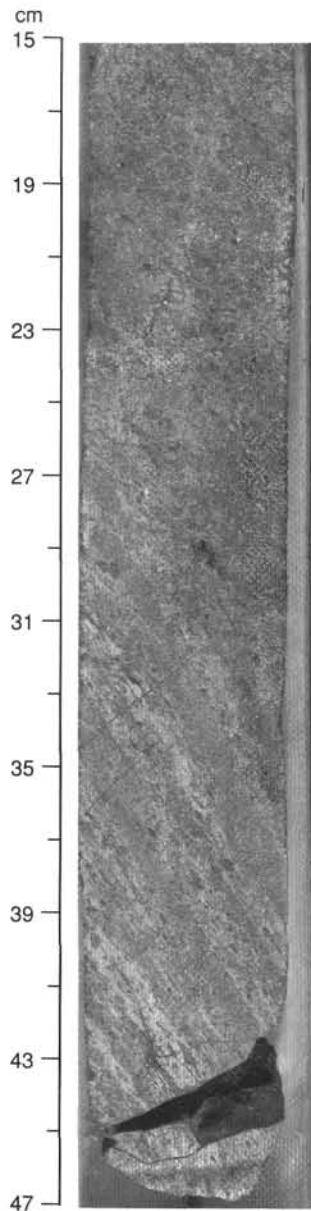


Figure 37. Shear zone in olivine gabbro (Sample 153-923A-2R-2, Piece 1, 15–47 cm). Crystal-plastic deformation intensity increases downward. Alternating pyroxene and olivine-rich bands and leucocratic plagioclase-rich bands define a well-developed layering in the mylonitic gneiss (30–47 cm).

rite, secondary plagioclase, and trace amounts of epidote common as secondary phases. Fine <1-mm-wide actinolite and actinolite  $\pm$  chlorite veinlets are less commonly observed in the gabbroic rocks from Hole 923A than in rocks from Sites 921 and 922, consistent with the lower alteration intensities observed in the Hole 923A rocks. In localized, highly deformed zones, the occurrence of olivine, clinopyroxene, and more rarely orthopyroxene, which are in apparently near textural equilibrium with hornblende and plagioclase, indicates that peak metamorphism occurred under near transitional granulite to amphibolite facies conditions. Minor overprinting of these high-temperature mineral assemblages by greenschist facies minerals indicates that subsequent penetration by hydrothermal fluids was generally weak.

### STRUCTURAL GEOLOGY

The 40.76 m (58.2% recovery) of compositionally and texturally variable gabbros recovered from Hole 923A contain a range of struc-

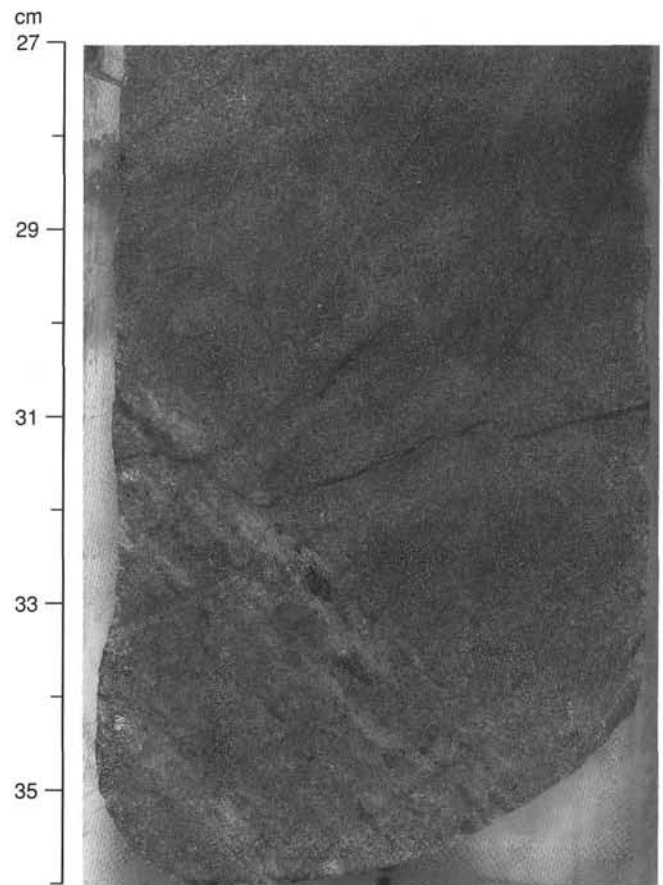


Figure 38. Amphibolite in Sample 153-923A-2R-1 (Piece 4, 27–36 cm). Sample is cut by millimeter-wide en-echelon chlorite-actinolite veinlets that pervasively alter the adjacent host rock.

tures and fabrics that closely resemble those encountered at Sites 921 and 922. Rocks from Hole 923A, however, are distinct from those recovered from Sites 921 and 922 in that they also contain thick (over 30 cm) mylonitic shear zones.

As outlined in the “Explanatory Notes,” a fabric was described as “magmatic” if the mineral grains had a shape-preferred orientation but there was no evidence of grain-scale crystal-plastic deformation. This does not necessarily imply a uniquely magmatic origin for the fabric. Penetratively-deformed rocks where all the minerals have a strong shape preferred orientation and display evidence for grain-shape distortion and intracrystalline deformation were termed “crystal-plastic,” and pieces containing these characteristics were assigned a fabric intensity value ranging between 1 and 3 (see “Explanatory Notes,” this volume).

Many rocks in the core contain fabrics that are gradational between the strongly developed crystal-plastic deformation and the undeformed magmatic fabric. These rocks have a variably developed shape preferred orientation with a limited occurrence of grain-shape distortion and intracrystalline deformation.

### Magmatic Fabrics

Magmatic fabrics in gabbroic rocks from Site 923 commonly have a shape preferred orientation, a preferred alignment of both plagioclase and, less commonly, pyroxene grains. Olivine grains rarely show a preferred alignment, but there are some locations where olivine oikocrysts occur as irregular, elongate crystals, with their long axes oriented subparallel to the plagioclase and pyroxene alignment (e.g., Fig. 4). The preferred mineral alignment commonly defines a weak folia-

tion, although linear fabric was also observed. Where this fabric is weakly developed it was difficult to assess the relative strengths or orientations of the planar and linear fabrics. The magmatic foliation is generally flat lying throughout Hole 923A (Fig. 40). For example, in Section 153-923A-12R-2 (Piece 13) the foliation dip is about  $3^\circ$ .

A comparatively rare textural type is represented by a polygonal equigranular fabric that is characterized by anhedral mosaics of equant plagioclase and pyroxene; trains of equant pyroxene grains locally form a crude banding. This fabric is unique to Hole 923A and was not recognized at Sites 921, 922, or 924. One example is in Sample 153-923A-12R-2 (Piece 2, 25–36 cm) wherein the fine-grained granular texture is located in a steep magmatic vein (10 mm wide; Fig. 13A). One margin of the vein is a sharp contact (Fig. 41) but the other margin is diffuse (Fig. 42). In this section, plagioclase contains straight magmatic twins (simple and albite twins). Plagioclase has a pronounced crystallographic preferred orientation, and the twins in different grains are roughly aligned parallel to one another. Trains of equigranular pyroxene grains define a weak banding in the vein.

### Crystal-plastic Fabrics

Porphyroclastic to gneissic textures have been recognized in Site 923 core, and are attributed to crystal-plastic deformation. The porphyroclastic texture is defined by a bimodal grain size distribution. Porphyroclasts consist mainly of elongated pyroxene and olivine that commonly have well defined, fine-grained tails 1–20 mm long. Plagioclase is mainly (80%–95%) found as a mosaic of small neoblasts with a sugary texture, surrounding olivine and pyroxene porphyroclasts. Minor olivine, pyroxene, and amphibole are also found as small grains in the mosaic matrix. Stringers of oxide minerals also locally parallel the foliation (e.g., Section 153-923A-2R-1, Piece 11).

A gneissic texture is found in some samples where alternating plagioclase- and pyroxene/olivine-rich horizons form a well defined banding (Fig. 37). Samples 923A-2R-2, 1–48 cm and 923A-13R-1, 120–135 cm also show a progressive increase in the gneissic texture downcore. Gneissic equigranular textures are mostly seen in fine-grained rocks; average grain size is less than 1 mm and can be much smaller, as seen in Sections 153-923A-2R-2, Piece 1 (Fig. 37), and 13R-1, Piece 13 (Fig. 25), whereas medium- and coarse-grained rocks (3–15 mm) commonly have a porphyroclastic texture. Gneissic intervals were not sampled for shipboard thin sections. Equigranular and porphyroclastic deformation fabrics in Site 923 gabbroic rocks correspond most closely to either pervasive or localized crystal-plastic fabrics (textural Groups 3 or 4; Fig. 17, "Explanatory Notes," this volume) microstructures, respectively.

Strongly developed crystal-plastic fabrics typically show a subequally well-developed foliation and lineation (LS-tectonite). The foliation generally dips  $40^\circ$ – $50^\circ$  (Fig. 40) and the lineation is most commonly oriented downdip as seen in Section 153-923A-13R-1 (Piece 13; Fig. 25). The relationship of the foliation to the compositional and/or textural layering is variable (Fig. 11). For example, in Section 153-923A-8R-3 (Pieces 1 and 3) a foliation defined by the shape preferred orientation of pyroxene and plagioclase grains dips at  $18^\circ$  and is subparallel to a banding defined by grain-size variations. In Section 153-923A-15R-2 (Pieces 1–3) both the primary igneous layering and the crystal-plastic foliation dip about  $40^\circ$ . A strong localized porphyroclastic fabric is subhorizontal and coincides with a sharp grain-size variation (medium-grained gabbro to pegmatitic gabbro) in Section 153-923A-10R-2 (Piece 2B). In Section 153-923A-12R-2 (Pieces 7–8) there is a well-developed elongate porphyroclastic texture concordant with the foliation in a fine-grained gabbro. In Piece 4 of this same section, however, a contact between the fine- and medium-grained gabbro dips  $60^\circ$  and is discordant to the crystal-plastic foliation. At the contact, however, the foliation progressively changes orientation toward parallelism with the contact.

The crystal-plastic foliation becomes intense (923A-11R-1, 103–107 cm) (Fig. 10) in some intervals, showing tails of pyroxene

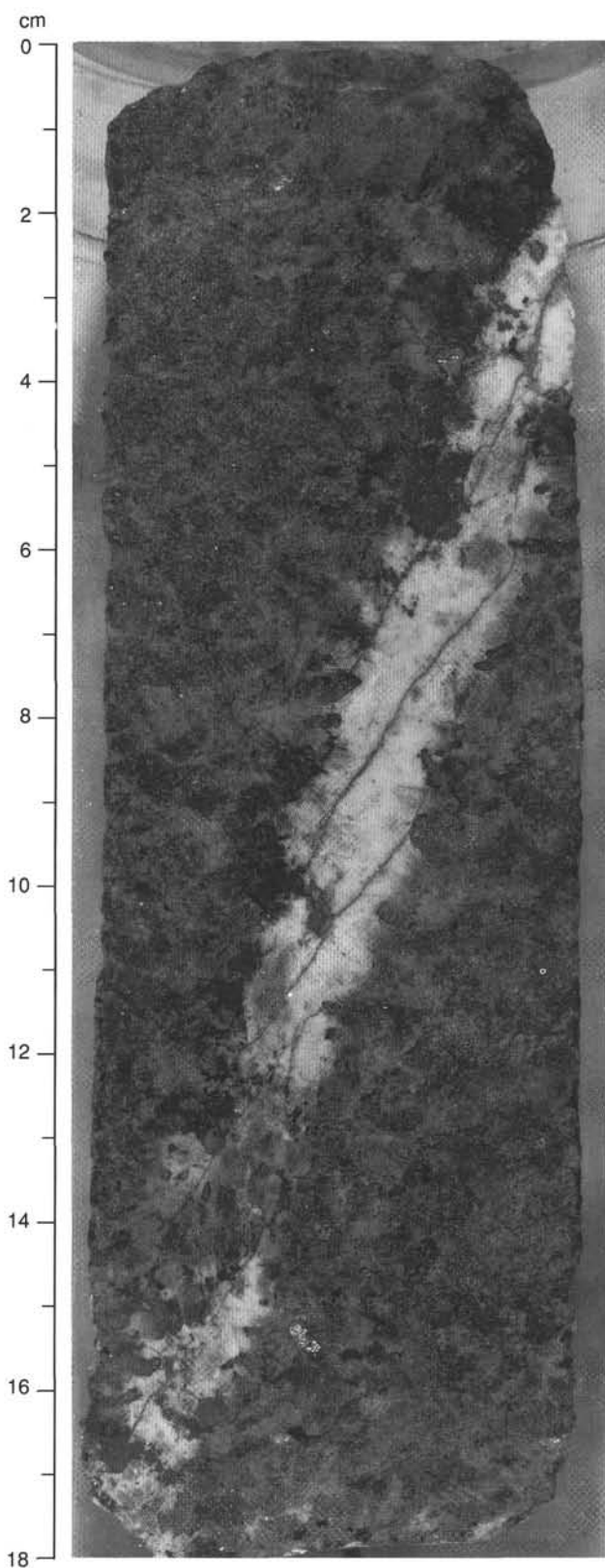


Figure 39. Felsic magmatic vein in Sample 153-923A-9R-1 (Piece 1, 0–18 cm), cut by actinolite  $\pm$  chlorite veinlets. Alteration of both vein and wall rock minerals is pervasive.

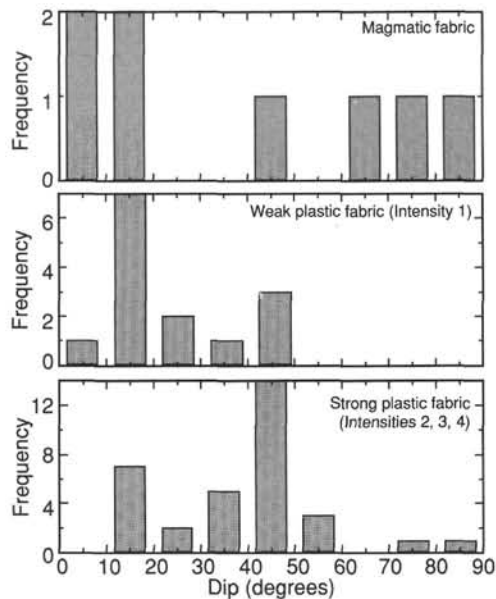


Figure 40. Histograms of foliation dip for magmatic, weak crystal-plastic, and strong crystal-plastic fabrics. The total number of data points for the magmatic foliation is low because it was commonly too weak to be measured accurately. Note that vertical scales are different on all three histograms.

neoblasts. A mylonitic texture occurs in several pieces (e.g., Section 153-923A-2R-1, Pieces 2–4). Shear-sense indicators in these shear zones include asymmetric pyroxene and olivine porphyroclasts and narrow synthetic shear zones oblique to the main foliation (Fig. 22, Sample 923A-11R-1, 76–83 cm). All of the kinematic indicators observed in shear zones at Site 923 indicate a normal shear sense.

One of the major shear zones is located in Section 153-923A-13R-1. Pieces 11 and 12 of this section are medium-grained with a subtle subhorizontal grain-size layering on the scale of 1 to 5 cm. The foliation intensifies toward Piece 13 (Fig. 25) where over 20 cm extreme grain-size reduction produces a mylonitic texture in olivine gabbro. Asymmetrical tails on clinopyroxene porphyroclasts suggest a normal shear sense. An augen on the back of the working-half of this piece consists of green poikilitic clinopyroxene, subophitically enclosing plagioclase. Another gradation of fabric intensity toward a shear zone occurs over a few centimeters in Piece 1 of Section 153-923A-2R-2.

In contrast, a shear zone with a sharp boundary occurs in a gabbro layer within the undeformed olivine gabbro (Section 153-923A-16R-2, Pieces 1–2; Fig. 21). This shear zone shows a normal shear sense. In Section 153-923A-2R-1 (Pieces 2–4) the contact between strongly deformed porphyroclastic gabbro and the mylonitic gabbro is sharp. The porphyroclastic gabbro contains millimeter- and centimeter-scale shear zones. Discrete shear zones also occur in coarse-grained gabbros. For example, in Section 153-923A-3R-2 (Piece 2) irregular, branching shear zones are defined by plagioclase aggregates that wrap around pyroxene porphyroclasts. Discrete centimeter-scale porphyroclastic mylonite shear zones containing fine-grained pyroxene are also present.

Weak crystal-plastic fabrics display a shape preferred orientation similar to that of some magmatic fabrics. In contrast to the “magmatic” fabric, this shape preferred orientation is primarily defined by aligned pyroxene and olivine grains and less commonly by plagioclase. Although pyroxene typically occurs as single crystals with continuous cleavages, weak grain distortion and neoblast development are locally visible with the aid of a hand lens or binocular microscope. Plagioclase primarily occurs as anhedral grain mosaics. Individual grains commonly have a vitreous luster and visible twins. Subhedral plagioclase crystals are not common but locally occur partially included in poikilitic pyroxene. In thin section, 10% to 30% of the plagioclase consists

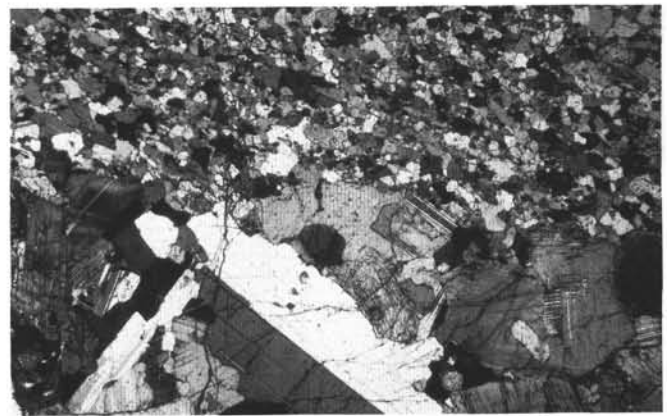


Figure 41. Sample 153-923A-12R-2, 24–26 cm. Field length is 8.6 mm. Sharp contact between magmatic vein with polygonal equigranular texture (Fig. 13A) and country rock (medium-grained gabbro).

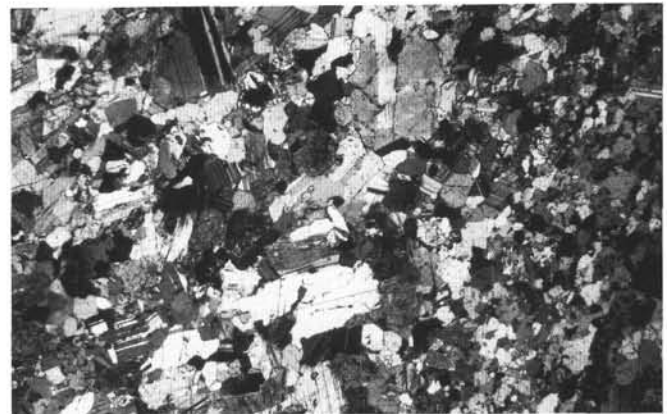


Figure 42. Sample 153-923A-12R-2, 24–26 cm. Field length is 8.6 mm. Diffuse contact between dike with polygonal equigranular texture (Fig. 13A) and gabbroic country rock. Opposing margin of the same dike shown in Fig. 41.

of fine-grained neoblasts. The neoblasts are located most commonly along the larger plagioclase/plagioclase grain boundaries. Neoblasts are also located along microshear zones. Neoblast size varies from about 100  $\mu\text{m}$  to 1 mm. A weak distortion of the lattice of primary igneous phases is present and plagioclase exhibits mechanical twins. Olivine exhibits subgrain boundaries and undulose extinction, and slightly elongated olivine and pyroxene grains show a weak alignment. Igneous textures are preserved locally in these rocks, identified by the subhedral habit of larger (>1 mm) plagioclase crystals, magmatic twins (combination of albite and simple twins in plagioclase and simple twins in augite), interstitial and/or poikilitic habit of clinopyroxene and olivine. Plagioclase laths within these zones sometimes show a weak shape preferred orientation. The best examples of this texture have been seen in thin sections taken in Cores 153-923A-8R, 9R, and 10R.

Well-defined linear shape preferred orientations are not typical in weak crystal-plastic fabric though a faint lineation may be present in Section 153-923A-9R-2 (Piece 2). The weak foliation defined by pyroxene grain alignment is the most commonly measured crystal-plastic fabric and it generally dips between 10° and 50° (Fig. 40).

### Mixed Brittle and Crystal-plastic Fabrics

In several locations, pyroxene grains are surrounded by fine-grained plagioclase with a saccharoidal texture. In many instances, the plagioclase “matrix” appears to have filled fractures cutting the pyrox-

ene porphyroclasts (Fig. 43). The term “semi-brittle” was used to describe the occurrence of both brittle and crystal-plastic microstructures in rocks which in Hole 923A were generally associated with coarse-grained units. Similar textures have been observed in the gabbroic rocks of Sites 921 and 922 (see Fig. 9, “Site 921” chapter, this volume) but they generally have a more brecciated appearance. A shape preferred orientation of microcrystalline plagioclase (<1 mm) is commonly visible under the binocular microscope. Pyroxene grains, however, display only a weak preferred orientation with angular to subangular grains. Some of the pyroxene grains appear to have separated along crystal cleavages and intragranular cracks to produce smaller fragments. In some places, coarse-grained subophitic textures in angular plagioclase and pyroxene, where no fracturing has occurred, appears very similar to the semi-brittle texture. In these cases, however, intact twins in primary, undeformed plagioclase grains are visible.

A spectrum of the mixed brittle and crystal-plastic textural relations outlined above appears in rocks from Hole 923A. At one end of the spectrum the pyroxene fragments show no mesoscopic evidence for intragranular distortion and no shape-preferred orientation. Gradually, over intervals of tens of centimeters, the pyroxene grains display a weak to moderate shape preferred orientation. In the same zones, the irregular, branching plagioclase veinlets become weakly aligned parallel to the weak shape preferred orientation of pyroxene grains and fragments (e.g., Sections 153-923A-11R-1, Piece 1, and 3R-1, Pieces 2–5). Some of these zones of weakly-aligned plagioclase veinlets coincide with larger-scale grain-size changes. Intervals with semi-brittle fabrics also grade vertically into zones of variably lineated and/or foliated crystal-plastic fabric in the same core piece. Narrow zones (<0.5 cm) of semi-brittle texture with finer-grained minerals than surrounding wall rock also occur within otherwise texturally isotropic lithologies (e.g., Section 153-923A-5R-2, Piece 1E). The highest concentration of pieces with semi-brittle textures in Hole 923A is found in Core 153-923A-8R.

### Downhole Variations

#### Magmatic and Crystal-plastic Fabrics

Core from Hole 923A displays distinct fabric-intensity and inferred strain-partitioning characteristics. Figure 44 shows variations in fabric intensity, the location of brittle features, and igneous unit boundaries. The locations of shipboard thin sections are also shown in Figure 44 and their microstructural characteristics listed in Table 8.

Core from the upper portion of the hole (down to Core 153-923A-4R) commonly contains rock with a strong crystal-plastic fabric (Fig. 44). A noteworthy mesoscopic example of a gradient in the intensity of the crystal-plastic fabric is found in Section 153-923A-2R-2 (Piece 1). The top of the piece has a well developed elongate porphyroclastic fabric that grades into a mylonitic gneiss at the base of the piece (Fig. 37). Strain gradients also occur over tens of meters: crystal-plastic fabric intensity decreases from Core 1R toward the bottom of Core 4R and only weak crystal-plastic fabrics are present in Section 153-923A-4R-1.

From Core 5R to the middle of Section 153-923A-8R-2, the rock is characterized by predominantly magmatic fabrics. Starting at the bottom of Section 153-923A-8R-2 through Section 923A-10R-4 the rock is characterized by a weak crystal-plastic fabric that commonly overprints a “magmatic” preferred orientation of crystal shapes. The change from no crystal-plastic fabric to weak crystal-fabric at the bottom of Section 923A-8R-2 coincides with a marked change in lithology from medium-grained troctolite to medium- to coarse-grained olivine gabbro with less than 10% olivine.

Several zones of intense crystal-plastic fabric occur in Sections 923A-11R-1, 12R-2, 13R-2, and 16R-2. A shear zone with sharp boundaries is located in Section 153-923A-11R-1 (Piece 9B), where the transition from a mylonitic texture to an igneous texture with weak crystal-plastic overprint occurs over 2 mm (Fig. 10).

The core below Section 923A-13R-2 contains predominantly random igneous mineral shape fabrics with narrow zones ( $\leq 20$  cm of

**Table 8. Shipboard thin sections and textural grouping from Hole 923A.**

Core, section, interval (cm)	Microstructure
153-923A-	
1W-1, 44	1a/1b
1W-1, 81	3
2R-1, 27	3
2R-1, 70	4a
2R-2, 2	3
2R-2, 44	3
2R-2, 89	3
3R-1, 10	3
3R-1, 34	3
3R-1, 54	3
3R-1, 95	1
3R-2, 5	3
3R-2, 34	3
4R-1, 118	3
5R-2, 35	2a
5R-2, 109	2a
5R-2, 123	2a
6R-1, 22	2b
7R-2, 1	1b
8R-1, 29	2a
8R-3, 10	3
9R-2, 70	3
10R-1, 106	1a
10R-2, 39	2b
11R-1, 69	3
12R-2, 24	1a
13R-2, 113	1a
13R-2, 113	2a
15R-1, 51	2a
15R-1, 93	2a
15R-3, 4	1a
15R-3, 88	2b
16R-2, 110	1a
16R-3, 74	1a
16R-4, 60	1a
16R-4, 60	2b

Note: Classification scheme is described in the “Structural Geology” section of the “Explanatory Notes” chapter (this volume).

recovered section) of strongly developed crystal-plastic fabrics. Most shear zones are observed in gabbro and olivine gabbro with cumulus pyroxene. No shear zones have been observed in the poikilitic olivine gabbros. The best example of this occurs in Section 153-923A-16R-2 (Pieces 2A and 2B). The sheared gabbro layer in this sample is bounded by undeformed poikilitic olivine gabbro (Fig. 21).

In summary, the upper part of the core from Hole 923A shows a strong variation in crystal-plastic fabric intensity within gabbroic rocks that show little change in modal mineralogy or grain size. By contrast, the rock from the lower part of the hole exhibits a coincidence between fabric intensity and lithologic variations.

The intensity of magmatic and crystal-plastic fabrics is reflected by systematic variations in the dip of the foliation (Fig. 45). Intense crystal-plastic fabric and moderate foliation dip ( $40^{\circ}$ – $50^{\circ}$ ) occur in rocks from the top and bottom of the hole. Shallow foliation dips ( $<20^{\circ}$ ), magmatic fabric, and weak crystal-plastic fabric predominate in rocks from the middle part of the hole.

#### Brittle Features

Brittle deformation in gabbroic rocks from Hole 923A is represented by a similar suite of mesoscopic structure as that encountered at Sites 921 and 922. These include faults, joints, cataclastic zones, distributed cracks, discrete veins and vein meshworks.

#### Distributed Fractures

Fracture networks, distributed over several centimeters are commonly present in core from Hole 923A. These fracture networks have no strong preferred orientation, although they locally follow crystal cleavages and grain boundaries. They are most evident in medium- to

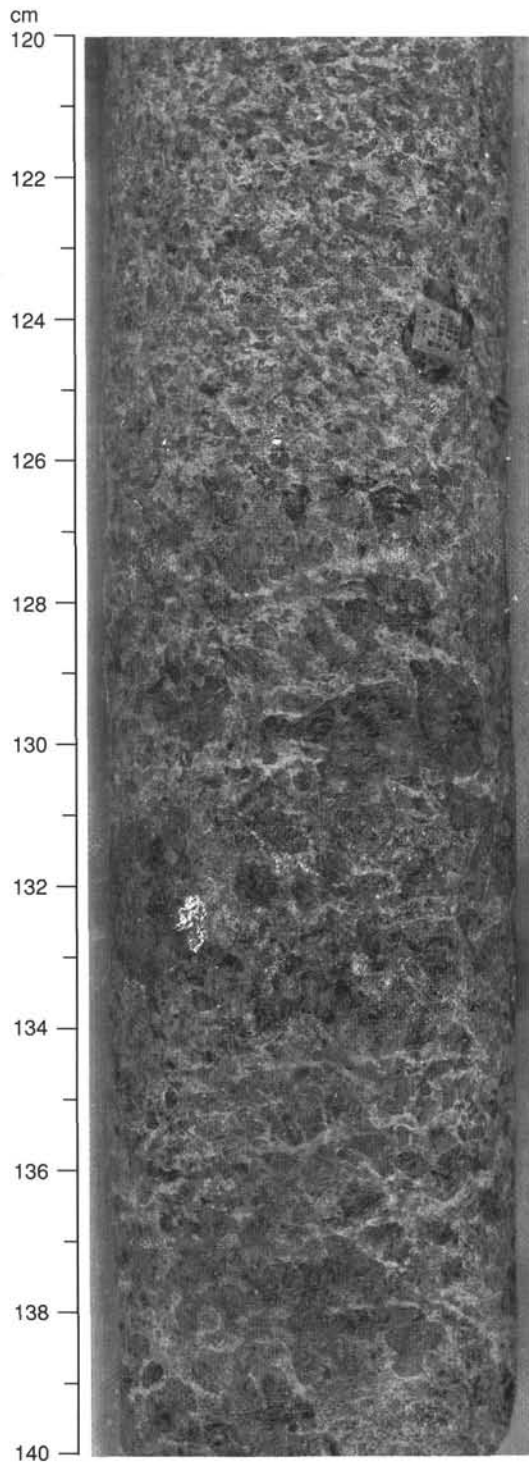


Figure 43. Sample 153-923A-10R-2 (Piece 2, 120–140 cm). Mixed brittle and crystal-plastic fabric. Fractures filled with fine-grained plagioclase surround coarse-grained pyroxene porphyroclasts in the lower part of the piece.

coarse-grained gabbros. They occur predominantly in plagioclase but are also found in pyroxene grains. Fractures do not appear to accommodate significant displacements but the fracture density is variable and locally high.

Distributed fractures locally grade into discrete plagioclase veins. For example in Piece 5 of Section 153-923A-8R-1, interconnecting distributed fractures filled with plagioclase in altered gabbro appear

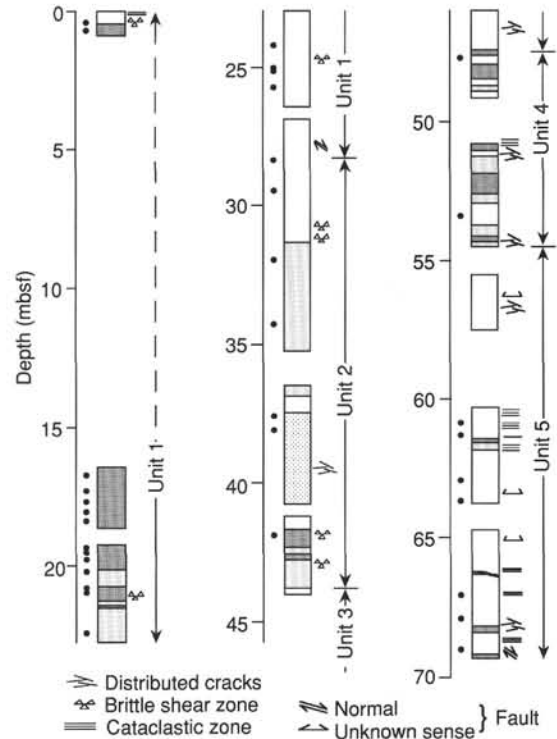


Figure 44. Downhole variations in the distribution and fabric intensity of crystal-plastic and brittle structures in core from Site 923. Boundaries of the igneous units shown. Locations of shipboard thin sections are shown by solid dots along depth axis. Dark gray boxes show areas of core with strong crystal-plastic fabric (Intensity 2 and 3). Light gray boxes represent core with weak crystal-plastic fabric (Intensity 1) and blank boxes represent core with only a magmatic fabric. Empty spaces in the diagram are intervals of no recovery.

to diminish toward the base of the piece becoming discrete plagioclase veins in Piece 6. A similar gradient in the fracture density occurs within Section 153-923A-8R-2 (Piece 8), but in this case the fractures merge into a zone of mixed brittle and crystal-plastic deformation.

In some locations, the fracture network is dominantly intragranular with limited intergranular fractures and no separation of grains. In these cases the plagioclase grains are commonly clouded by microfractures filled with chlorite and clay minerals. In some sections, intracrystalline fractures in clinopyroxene are filled with actinolite (e.g., Section 153-923A-3R-1, Piece 2). Similar to occurrences of distributed fractures at Sites 921 and 922, dense zones of microfractures localize along and overprint crystal-plastic shear zones (Section 153-923A-11R-1, Piece 9B). A corresponding increase in the abundance of chlorite and actinolite, formed from the breakdown of clinopyroxene and plagioclase, occurs in these zones. Similarly in Piece 3 of Section 153-923A-9R-1 microfracture density increases from a zone of weak brecciation to discrete veins that are associated with an increase in the abundance of green smectite/chlorite patches. The most extensive distributed fracturing in Hole 923A is located in Section 153-923A-14R-1. It occurs above a cataclastic zone located in Section 153-923A-15R-1 and intensifies toward it (see below).

**Cataclastic Zones**

Cataclastic zones in the core recovered from Hole 923A are concentrated in Sections 153-923A-15R-1 and 15R-2, but a few less developed cataclastic zones are also found toward the top of the core. The first cataclastic zone encountered at Hole 923A occurs in rock from the top of the first core (Section 153-923A-1W-1, Piece 1) and was probably recovered from rubble. The sample contains branching veins of pale-green actinolite that alternate with lenses of neoblastic

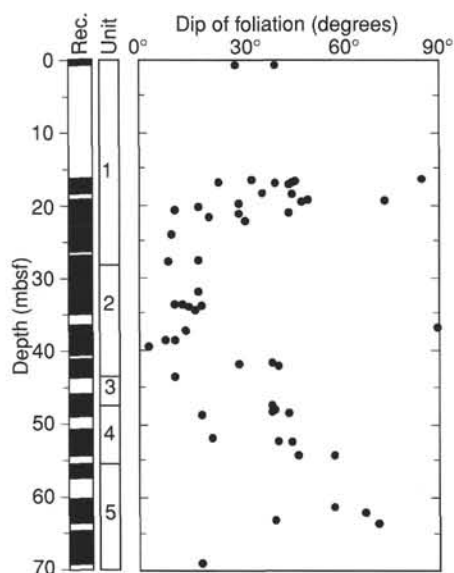


Figure 45. Downhole variations in the dip of magmatic and crystal-plastic foliations in Hole 923A.

plagioclase, clay minerals, prehnite(?), and chlorite. They cut a strong shape preferred orientation fabric in the gabbroic rocks, defined by elongate plagioclase and pyroxene grains. Strong, localized microfracturing is associated with the actinolite veins. In the piece below, there is no cataclasis but instead a dense fracture array is found together with alteration phases including epidote and actinolite.

A similar cataclastic zone occurs in Section 153-923A-13R-1. Grains around the microfractures are smaller than nearby grains. The microfractures overprint a strong crystal-plastic foliation. Branching veinlets of actinolite and chlorite dissect the heterogeneously altered microgabbro surrounding the cataclastic zone. In this example, chlorite and clay minerals pervade the microfractures. This cataclastic zone appears to have preserved textures formed during a previous stage of strain localization where distributed fracturing associated with a focused hydrothermal alteration but only limited grain-size reduction has occurred.

Below these intervals the strongest development of cataclastic zones is found in Section 153-923A-15R-1 (Pieces 5 to 14; Fig. 46). This interval comprises several zones 0.5 to 1 cm wide of finer grained minerals with branching networks or "swarms" of actinolite, chlorite, and minor albite veins. Epidote, prehnite, and secondary plagioclase are distributed through these zones. The cataclastic zones and veins dip about 20°. A slickenside lineation occurs at this location (Section 153-923A-15R-1, Piece 8) on a fracture surface that parallels a chlorite vein dipping about 50°. This area of cataclastic zones extends more than 1 m and is located above a zone of strongly elongated porphyroclastic fabric at the base of the core section (Section 153-923A-15R-1, Piece 15). A weak cataclasis is also present in the core section below (Section 153-923A-15-2, Piece 1). A diffuse zone of actinolite veining occurs at the top of Piece 1 of this section. Igneous textures and crystal-plastic fabric are locally preserved within the broad cataclastic zone.

Cataclastic zones are also encountered in Section 153-923A-16R-2 and also are associated with actinolite and chlorite veins (Pieces 1, 5, and 6) and in Section 153-923A-16R-3 where a weak cataclastic texture has developed in a pegmatitic gabbro. This cataclastic zone is located adjacent to a shear zone along the contact between a fine-grained granoblastic gabbro and the pegmatitic gabbro (Section 153-923A-16R-3, Pieces 7–8). A weak cataclasis is also associated with a fault in Section 153-923A-16R-4 (Piece 4).

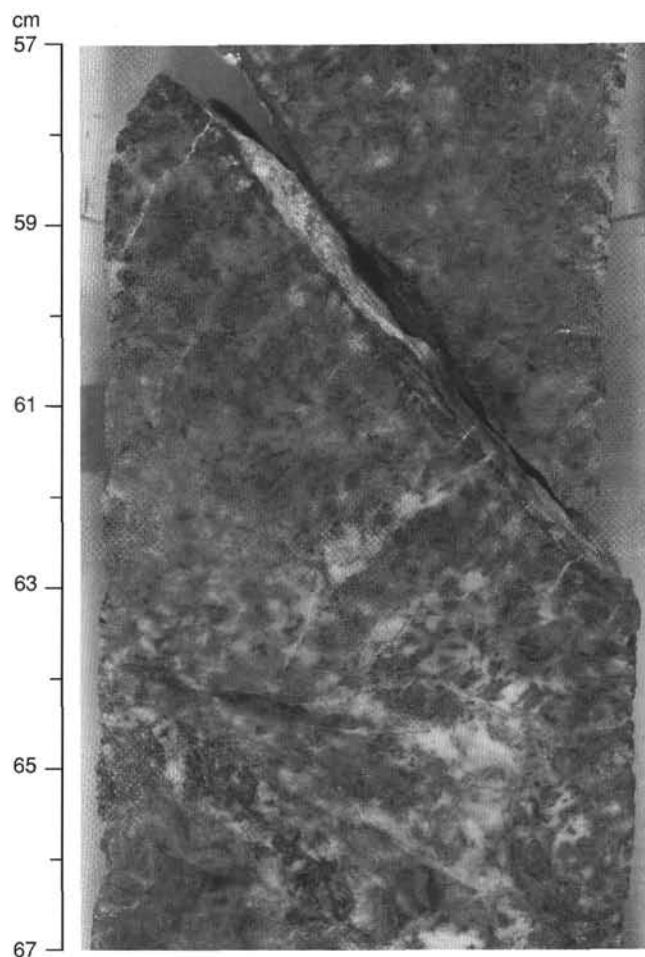


Figure 46. Sample 153-923A-15R-1 (Piece 10, 57–67 cm). Cataclastic zone with swarm of thin fractures containing chlorite, actinolite, zoisite, and clay minerals. Core breakup at top of piece has occurred along one of these fractures.

### Faults and Joints

Although the broad cataclastic zone described above in Section 153-923A-15R-1 may represent a major fault zone, there are a few discrete, minor faults with discernible displacements that dissect the core. One fault has localized just above the boundary of lithologic Units 1 and 2 and dips at about 60° (Section 153-923A-7R-1, Piece 10). An apparent normal separation of about 1 cm offsets a moderately-dipping, grain-size variation which is interpreted as a primary igneous feature. In several other locations, narrow (1–2 mm) veins preserve penetrative, strong mineral lineations in chlorite and actinolite fill. These are evident on tops and bases of adjacent sub-pieces that have separated along these veins (e.g., Section 153-923A-14R-1, Piece 10). Two gently dipping faults (15° and 30°) occur in Section 153-923A-5R-1. The one that dips 15° has a normal displacement of a few millimeters and is filled with chlorite and actinolite. Similar lineated vein fabrics are found in Section 153-923A-15R-1 (Piece 8) within a cataclastic zone, and in Sections 153-923A-15R-3 (Piece 2), 16R-1 (Piece 5), and 16R-4 (Piece 8) (Fig. 47).

In core from near the base of the hole a minor fault cuts a subvertical magmatic vein with apophyses that penetrate between clinopyroxene grains. The fault is subhorizontal, dipping 7°. A reverse separation of about 11 mm is estimated for this fault on the cut core face with a right-lateral apparent displacement on the top of the core piece, determined from the separation of the magmatic vein. Plagioclase and smectite seal the fault. Another fault in Section 153-923A-16R-4 (Piece 8) is steeply dipping (68°), 7 mm wide, and contains

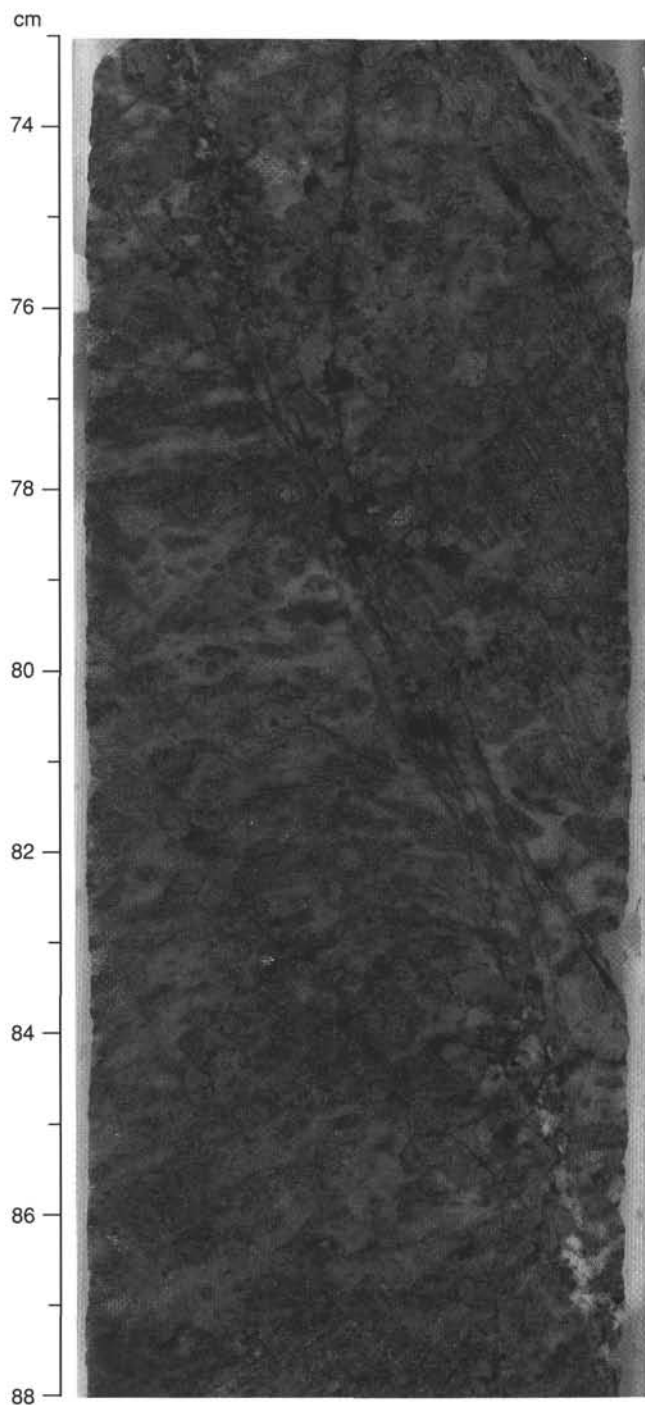


Figure 47. Sample 153-923A-16R-4 (Piece 8, 73–88 cm). Closely-spaced, thin chlorite and actinolite veins (dark) that cut the crystal-plastic foliation of the gabbroic host rock. The apparent deflection of this foliation suggests a normal component of displacement along a crystal-plastic shear zone subparallel to the chlorite-actinolite vein set. A vein of a lighter gabbroic material, also subparallel to this shear zone, is visible in the upper left and lower right corner of photograph. It could be a felsic vein, or a zone of enhanced hydrothermal alteration of the host gabbroic rocks.

anastomosing strands of chlorite veins. In the “footwall” of this fault the crystal-plastic foliation is deflected downwards, suggesting a normal displacement component.

Only minor jointing is evident in Hole 923A. The majority of joints are steeply dipping and their surfaces are coated with clay and iron oxide minerals, and in some areas with minor chlorite (e.g., Sections 153-923A-2R-2, Piece 7, 7R-1, and 7R-2). The strongest jointing occurs in Section 153-923A-8R-1 where several joints, with opposing dips of about  $60^\circ$  dissect Piece 6. Additional joints are located in Sections 153-923A-8R-1 (Piece 6), 9R-1, 9R-2 (Piece 7), 9R-3 (Piece 3), 10R-1 (Piece 4), and 10R-2 (Pieces 1C and 1D).

#### *Veins*

Gabbroic rocks recovered in cores from Hole 923A display several generations of veins, which overprint magmatic and solid-state plastic fabrics. Veins occur as both discrete veins and vein arrays and networks and result in moderate to extensive alteration in the host rock immediately adjacent to them. The main vein types in Site 923A rocks include felsic veins, actinolite  $\pm$  chlorite veins, and associated veins of chlorite + iron oxide  $\pm$  iron hydroxide minerals, and epidote-bearing veins.

#### *Felsic Veins*

Felsic veins occur as millimeter- to centimeter-scale veins with sharp to diffuse boundaries that are commonly associated with zones of alteration of varying widths in the host rock. Their dips range from subhorizontal to subvertical. They consist of plagioclase + actinolite  $\pm$  clinopyroxene  $\pm$  chlorite  $\pm$  quartz  $\pm$  epidote and may contain other accessory minerals. Actinolite or other amphibole crystals commonly form the core and albitized plagioclase the margins of the veins. Locally they also contain abundant iron oxide and sulfide minerals. Sample 153-923A-15R-3 (Piece 3, 76–90 cm), for example, displays two subparallel and steeply dipping ( $70^\circ$ ) felsic veins (up to 20 mm wide) that are composed of clinopyroxene, secondary plagioclase, iron oxide and sulfide minerals, and euhedral apatite crystals. Clinopyroxene is partially replaced by actinolite and rimmed by chlorite. These veins have nearly 3-cm-wide alteration halos and are cut by chlorite  $\pm$  actinolite veinlets with dips of  $30^\circ$  to  $40^\circ$ . Similarly, a felsic vein in Sample 153-923A-16R-4 (Piece 1, 2–8 cm) crosscuts a coarse-grained gabbro and contains actinolite  $\pm$  chlorite in the lens-shaped core and altered plagioclase in the margins. Farther down in the section (Piece 4) a subvertical felsic vein, with thin, irregular apophyses extending between the clinopyroxene grains, shows similar mineral compositions and is cut and offset by a subhorizontal ( $7^\circ$  dip) fault. The vein shows 11 mm of separation across this fault and a reverse sense of movement on the cut face of the core. The 2-mm-wide fault plane is filled with plagioclase and smectite.

#### *Actinolite $\pm$ Chlorite Veins*

These are the most common vein types in the core from Hole 923A. Individual veins and subparallel vein arrays are green and dark green to black and display planar to irregular geometries with locally well-developed overlapping segments. The veins range from less than 1 mm to several millimeters wide, and their dip angles range from subhorizontal to subvertical. Where actinolite  $\pm$  chlorite veins cut olivine and clinopyroxene they commonly produce irregular dark green patches. In places they contain symmetric alteration zones and halos. Generally they cut across the crystal-plastic foliation and lineation in gabbroic rocks at oblique to high angles (e.g., Sections 153-923A-2R-1, Pieces 4–5, and 8–9) and 2R-2, Pieces 1–2, and 5–8). They also cut the shear zones (Section 153-923A-16R-2, Piece 2). Some actinolite  $\pm$  chlorite veins are cut and offset along faults by as much as several millimeters (e.g., Section 153-923A-5R-1, Piece 2). Locally, some actinolite  $\pm$  chlorite veins crosscut other actinolite  $\pm$  chlorite veins. Two steeply dipping ( $65^\circ$ ) actinolite veins appear to cut

across, for example, a gently dipping ( $10^\circ$ ) diffuse actinolite  $\pm$  chlorite vein in Section 153-923A-10R-3 (Piece 5).

There is also a distinct family of veins composed of chlorite, clay and oxide minerals. These consist of thin, branching and anastomosing veinlets locally occurring along with actinolite  $\pm$  chlorite veins. On the outer surface of the cores, these veins produce diffuse yellow stains (e.g., Section 153-923A-7R-1, Piece 2A).

#### *Epidote-bearing Veins*

These veins are rare compared actinolite  $\pm$  chlorite veins and occur as irregular veins and veinlets with widely varying widths and orientations. They contain plagioclase, actinolite, quartz, and/or prehnite in addition to epidote (see "Metamorphic Petrology," this chapter). A 2-mm-wide epidote veinlet in Section 153-923A-1W-1 (Piece 2) with a 15-mm-wide alteration halo that is composed of epidote and plagioclase cuts and offsets a 1-mm-wide actinolite  $\pm$  chlorite vein.

#### *Brittle Features*

Examination of the distribution of brittle structures in the gabbroic rocks recovered from Hole 923A shows that most of the brittle features are observed in rocks from the base of the hole (Fig. 44). Only weak brittle features such as narrow cataclastic zones, minor zones of semi-brittle textures, and isolated joints appear in rocks near the top of the core. A minor normal fault is located at the boundary between Unit 1 and Unit 2 (Section 153-923A-7R-1, Piece 12). In Unit 2 only very weak brittle deformation is evident in the form of joints, from the top of Unit 2 until Section 153-923A-10R-3. Below this section where distributed fracturing, semi-brittle textures, and cataclasis become more pronounced. At the boundary between Units 2 and 3 there is evidence for weak cataclasis with the development of semi-brittle textures in Core 153-923A-8R, concentrated near the top of Unit 3. Distributed fractures are localized directly above the contact between Units 3 and 4 and also between Units 4 and 5 (Section 153-923A-13R-3, Pieces 6 and 7). Brittle features become more concentrated in lithologic Unit 5 where distributed fractures and minor faults are present in the base of Section 153-923A-14R-1. These may be related to the broad cataclastic zone in Section 153-923A-15R-1 (Pieces 5 to 13) (Fig. 46). Below this zone, each section of Core 153-923A-16R contains one or more brittle structures, including minor actinolite/chlorite bearing faults (Sections 16R-1, Piece 5, and 16R-4, Piece 8), distributed fractures (Section 16R-3, Piece 8), and weak cataclasis (Sections 16R-2, Pieces 5–6, and 16R-4, Piece 4).

## PALEOMAGNETISM

Paleomagnetic measurements were made on the archive half-cores and 40 minicores taken from Hole 923A, which was drilled approximately 200 m north of Site 921.

### Whole-core Measurements

Susceptibility values for whole cores from Hole 923A generally range from 0.01 to 0.1 SI (Fig. 48). The upper four cores (Cores 153-923A-1W to 4R) include several intervals of high susceptibility, reflecting the greater abundance of oxide gabbros in this portion of the section (see "Igneous Petrology," this chapter). Olivine gabbros, which comprise the majority of the recovered core, are characterized by lower susceptibility. The marked susceptibility low ( $\sim 10^{-3}$  SI) at approximately 61 mbsf corresponds to a highly altered olivine gabbro in Section 153-923A-15R-1.

Measurements of the archive half-cores from Hole 923A provide a nearly continuous record of downhole remanence variations as a result of the high recovery ( $\sim 75\%$ ). The natural remanent magnetization (NRM) of archive half-cores from Site 923 is similar to that of gabbros from Sites 921 and 922. Approximately half the cores have

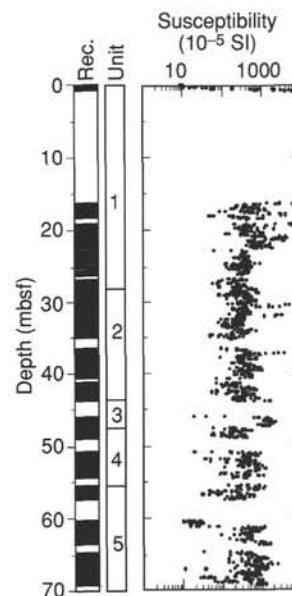


Figure 48. Whole-core susceptibility data for Hole 923A.

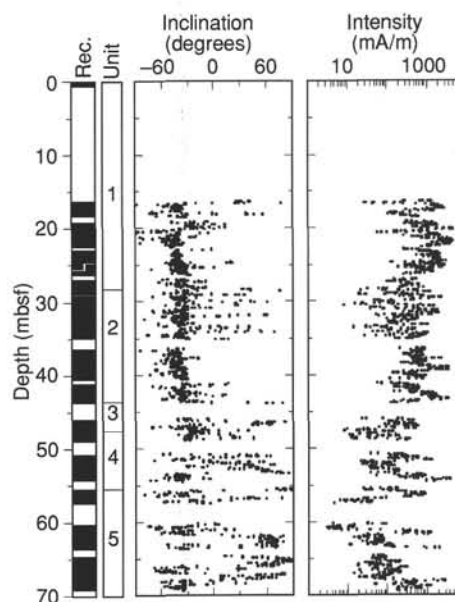


Figure 49. Downhole remanence data for archive half-cores from Hole 923A after demagnetization at 20 mT. Inclinations in the upper 45 m are predominantly negative and near the expected reversed dipole inclination ( $-41^\circ$ ) at the site. Below this depth, inclinations are scattered and include several intervals of apparent normal polarity.

magnetizations too high to yield reliable NRM data; however, the archive half-core data suggest a range of NRM values between 0.5 A/m and  $>3.0$  A/m. Demagnetization of the archive half-cores to 20 mT yields predominantly negative inclinations to a depth of approximately 45 mbsf (Fig. 49). The mean inclination (approximately  $-40^\circ$ ) in this interval is comparable to the expected reversed dipole inclination ( $-41^\circ$ ) at the site. Below this depth, the inclination data are highly scattered and include several apparent polarity reversals. This downhole trend in inclination is similar to that observed in Site 921, particularly in Hole 921E. The inclination variation with depth is paralleled by changes in intensity, with higher values ( $\sim 0.5$  A/m) in

Table 9. Summary of magnetic properties of discrete samples from Site 923.

Core, section, interval (cm)	Piece	Depth (mbsf)	Rock type	NRM			K (SI)	AMS		
				Dec.	Inc.	Int.		P	L	F
153-923A-										
2R-1, 27-30	4	16.67	Gneissic amphibolite	349.5	79.0	0.51	0.00416	1.042	1.02	1.020
2R-2, 2-5	1	17.59	Lineated olivine gabbro	207.8	-32.8	0.72	0.00361	1.066	1.035	1.030
2R-2, 89-92	8	18.46	Lineated olivine gabbro	0.1	31.0	0.30	0.00397	1.096	1.051	1.043
3R-1, 34-37	3	19.54	Gneissic olivine gabbro	196.1	9.4	0.59	0.00379	1.106	1.089	1.015
3R-1, 95-98	5B	20.15	Gneissic olivine gabbro	208.7	-35.1	6.17	0.00425	1.095	1.052	1.041
3R-2, 34-37	2A	21.03	Gneissic gabbro	239.3	15.6	0.72	0.00623	1.106	1.031	1.073
4R-1, 118-121	7B	22.38	Gabbro	265.6	-31.1	2.52	0.00585	1.076	1.017	1.059
4R-1, 121-124	7B	22.41	Gabbro	269.9	-32.5	2.52	0.00548	1.095	1.039	1.054
5R-2, 109-112	2	25.00	Gabbro	292.6	-33.6	1.76	0.00284	1.096	1.074	1.020
5R-2, 114-117	3	25.05	Gabbro	14.9	-10.9	1.11	0.00398	1.098	1.062	1.034
6R-1, 22-25	7	24.92	Olivine gabbro	325.9	-8.4	0.75	0.00583	1.144	1.086	1.054
7R-1, 81-84	9	27.71	Olivine gabbro	269.0	-0.6	0.71	0.00418	1.168	1.122	1.041
7R-2, 1-4	1	28.29	Olivine gabbro	190.7	82.6	1.27	0.00729	1.121	1.049	1.068
7R-2, 4-7	1	28.32	Olivine gabbro	126.5	80.9	0.56	0.00300	1.183	1.021	1.159
8R-1, 29-32	5A	29.29	Olivine gabbro	201.6	-12.5	0.61	0.00283	1.077	1.049	1.026
8R-3, 10-13	1	31.91	Gabbro	127.9	-80.4	0.35	0.00386	1.117	1.039	1.075
9R-1, 130-133	4A	33.20	Olivine gabbro	252.7	39.4	0.36	0.00245	1.109	1.067	1.040
9R-2, 70-73	8A	34.08	Poikilitic olivine gabbro	293.8	76.3	0.89	0.00606	1.173	1.118	1.049
10R-1, 106-109	5D	37.56	Olivine gabbro	95.8	6.4	0.46	0.00317	1.110	1.053	1.053
10R-2, 39-41	1C	38.16	Olivine gabbro	278.8	-24.8	0.75	0.00378	1.169	1.107	1.056
10R-3, 44-47	3	39.63	Gabbro	279.2	-9.2	0.81	0.00515	1.137	1.034	1.099
11R-1, 69-71	8	41.89	Gneissic gabbro	207.8	6.1	0.38	0.00203	1.098	1.041	1.055
11R-2, 58-61	5	43.14	Gabbro	194.9	-29.7	1.46	0.00255	1.080	1.047	1.032
12R-1, 126-129	5B	47.26	Poikilitic olivine gabbro	212.3	85.2	1.49	0.01212	1.273	1.059	1.202
12R-2, 18-21	1	47.62	Gabbro	205.7	82.0	0.30	0.00182	1.127	1.088	1.037
12R-2, 41-44	2	47.85	Olivine gabbro	171.8	72.6	0.80	0.00742	1.168	1.074	1.088
13R-1, 114-117	13	51.94	Gneissic olivine gabbro	222.5	80.6	1.04	0.00496	1.090	1.049	1.039
13R-2, 113-116	7	53.38	Olivine gabbro	214.3	73.5	1.85	0.00816	1.067	1.007	1.060
13R-2, 116-119	7	53.41	Olivine gabbro	217.5	71.5	1.96	0.00853	1.061	1.022	1.037
13R-3, 50-53	6	54.22	Gabbro	209.9	-42.4	6.77	0.00125	1.046	1.021	1.024
14R-1, 55-58	8	56.05	Troctolitic olivine gabbro	228.4	69.5	0.89	0.00730	1.086	1.039	1.045
14R-2, 6-9	1	56.98	Olivine gabbro	300.1	75.6	0.10	0.00123	—	—	—
15R-1, 93-96	14	61.23	Olivine gabbro	79.6	70.3	1.49	0.00960	1.091	1.043	1.046
15R-3, 4-7	1	62.88	Olivine gabbro	167.9	68.8	1.46	0.00608	1.140	1.066	1.070
15R-3, 7-10	1	62.91	Olivine gabbro	166.0	67.3	1.28	0.00530	1.178	1.090	1.081
16R-2, 2-5	1A	65.98	Olivine gabbro	188.8	71.1	0.40	0.00342	1.167	1.077	1.083
16R-3, 74-77	5	67.87	Olivine gabbro	165.1	63.8	0.96	0.00660	1.131	1.083	1.044
16R-3, 77-80	5	67.90	Olivine gabbro	182.8	76.5	0.52	0.00463	1.144	1.042	1.098
16R-4, 60-63	7	68.98	Olivine gabbro	305.0	60.2	0.26	0.00359	1.050	1.019	1.030
16R-4, 63-66	7	69.01	Olivine gabbro	153.5	85.7	1.30	0.01224	1.041	1.026	1.015

Notes: Table includes volume susceptibility ( $K$ ), natural remanent magnetization (NRM), magnetic fabric parameters ( $P = K_1/K_3$ ,  $L = K_1/K_2$ ,  $F = K_2/K_3$ , where  $K_1$ ,  $K_2$ , and  $K_3$  are the maximum, intermediate, and minimum axes of the susceptibility ellipsoid, respectively). Rock names (see "Igneous Petrology," this chapter) are defined for whole piece and may not be descriptive of minicore samples.

the upper portion of the hole and generally lower values ( $\sim 0.1$  A/m) below a depth of approximately 45 mbsf. The NRM intensities are reasonably consistent throughout the hole. Thus, the reduced magnetizations after 20 mT demagnetization in the lower part of the hole probably reflect the lower stability, and hence relatively larger normal polarity overprints, of gabbros in this interval.

### Discrete Sample Measurements

Basic magnetic properties (NRM and initial susceptibility) were determined for 40 discrete samples taken from Hole 923A (Table 9). The mean NRM intensity for these discrete samples (geometric mean =  $0.86$  A/m  $\pm 0.4$  log unit; arithmetic mean =  $1.23 \pm 1.4$  A/m) is indistinguishable from the mean intensity of gabbros at Sites 921 and 922 (Fig. 50). As noted in gabbros from Sites 921 and 922, the mean intensity of these reversely magnetized gabbros from Site 922 probably represents a minimum estimate of their in-situ magnetization as a result of normal polarity overprints (e.g., drilling remanence). Volume susceptibilities from the discrete samples generally range from  $10^{-2}$  to  $10^{-3}$  SI, resulting in a mean Koenigsberger ratio ( $Q$ , the ratio of remanent to induced magnetization) of  $6.37 \pm 0.4$  log units (arithmetic mean =  $11.69 \pm 27.9$ ).

The majority of discrete samples from Site 923 have multiple components of magnetization, with the highest stability component typically being of reversed polarity (Fig. 51). Only one measured sample has a univectorial remanence decay (Sample 153-923-13R-3, 50-53 cm). This sample has the highest NRM intensity of any Site 923 gabbro, although it is not mineralogically distinct (see "Igneous Petrology," this chapter).

Most samples have a steeply oriented, low-stability component that is probably related to drilling. This drilling related overprint is removed by AF demagnetization at 10-15 mT (e.g., Fig. 51).

After removal of the drilling-related overprint, one or two additional higher stability magnetization components are typically recognized. An intermediate stability component ( $B$  component) of normal polarity is identified in approximately half of the samples. With few exceptions, the  $B$  magnetization component is only present in samples from the lower portion of Hole 923A (Cores 153-923A-12R to 16R). This component has a mean inclination of  $55.0^\circ$  ( $\alpha = 5.3^\circ$ ,  $n = 18$ ; McFadden and Reid, 1982), slightly steeper than the present field inclination at the site (Fig. 52). This component may represent a relatively recent magnetization (e.g., a viscous remanence), although the steeper than expected inclination suggests that this component may not have been completely isolated from the steeper, drilling-related remanence.

The highest stability component of magnetization ( $C$  component) is generally of reversed polarity, with a mean inclination ( $-37.0^\circ$ ;  $\alpha = 7.2^\circ$ ,  $n = 31$ ) that is statistically indistinguishable from the reversed dipole direction at the site (Fig. 52). This highest stability component decays toward the origin only in approximately 20% of the samples. These samples generally do not contain a  $B$  magnetization component (e.g., Fig. 51B). The remaining samples exhibit more complex demagnetization behavior, with no clearly defined characteristic remanence direction. The remanence directions during demagnetization for many of these samples lie along great circle paths (Fig. 53). The sample shown in this figure (Sample 153-923A-7R-2, 4-7 cm) is typical: a steep, drilling-related remanence is removed by

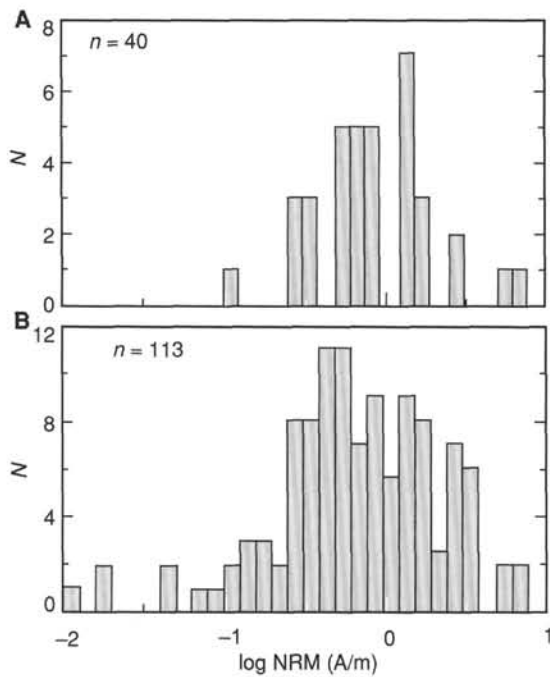


Figure 50. Comparison of NRM intensities from (A) Site 923 with the distribution of all gabbroic samples from (B) Sites 921–923.

approximately 20 mT and the remaining demagnetization steps define a great circle path consistent with a final reversed polarity magnetization. The final demagnetization steps in this sample have negative inclinations (Fig. 53B) although the final magnetization component cannot be isolated.

In addition to samples that are evidently complexly magnetized, some samples (particularly from depths >45 mbsf in Hole 923A) exhibit relatively simple demagnetization behavior with little evidence of a high-stability reversed polarity magnetization. The remanence in these apparent normal polarity samples often decays along a trajectory toward the origin, with only the highest demagnetization steps revealing a negative inclination (Fig. 54). The magnetization directions for this sample (Sample 153-923-15R-3, 7–10 cm) during demagnetization, however, lie along a great circle path similar to that observed for samples with better defined, high stability reversed polarity magnetizations. In a few samples, no final negative inclination is evident at all. The low magnetic stability (median destructive fields of 5–10 mT) and continuous variation between samples with well defined reversed polarity magnetizations and those of apparent normal polarity, suggests that the apparent normal polarity magnetizations in Hole 923A may represent a low-stability overprint which has almost completely obscured the original reversed polarity remanence.

Anisotropy of magnetic susceptibility was determined for all samples from Site 923 (Table 9). The degree of anisotropy is comparable to that of gabbros from Sites 921 and 922 (Fig. 55). As noted for the samples from Sites 921 and 922, however, there is no strong tendency toward either oblate or prolate magnetic fabrics. The heterogeneous nature of anisotropy between closely spaced samples precludes the recognition of any downhole characterizations or correlations with lithologic units. The highest degree of anisotropy in Hole 923A occurs in a sample from Section 153-923A-12R-1, an interval lacking any deformation features or magmatic structures that might have produced the strongly developed magnetic fabric. Resolution of the origin of the magnetic anisotropy will be the subject of shore-based investigations.

### Discussion of Paleomagnetic Results

Results from Site 923 generally are similar to those obtained from Site 921, located approximately 200 m to the south. In particular, both

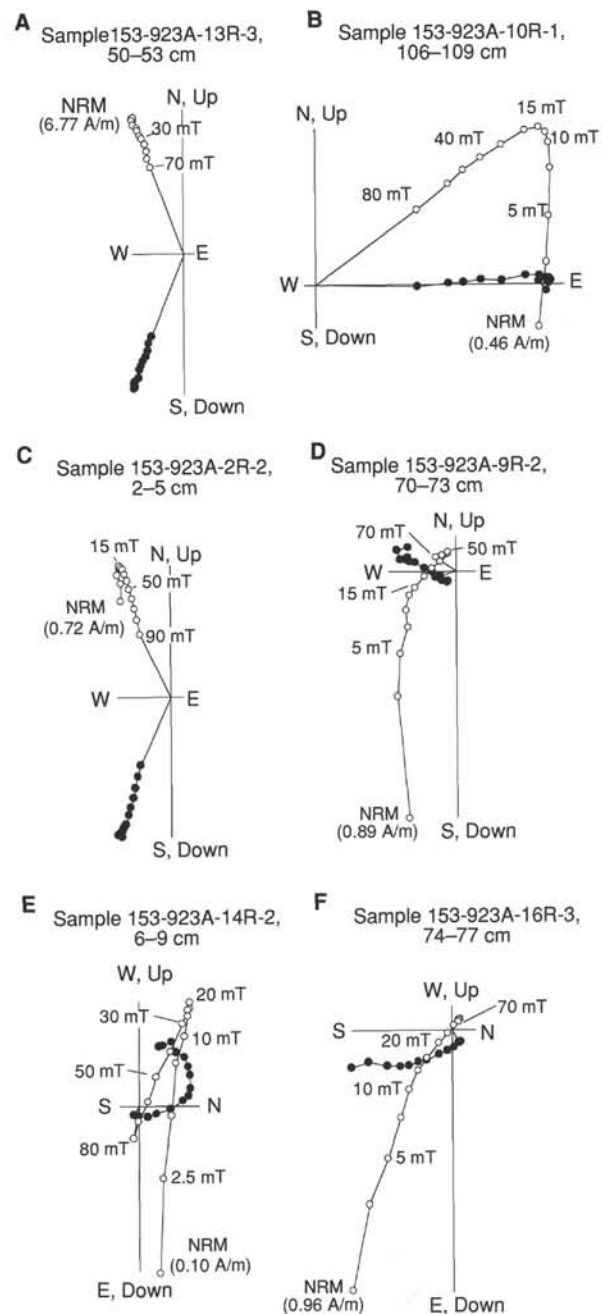


Figure 51. Vector endpoint diagrams for AF and thermal demagnetization of representative discrete samples from Site 923. A. Demagnetization behavior illustrating high-stability magnetization and univectorial decay toward origin. The majority of samples have a high stability magnetization component of reversed polarity (B, C, D, F), with a variable steeply inclined low-stability component probably related to drilling. Filled (open) circles are projections of the vector onto the horizontal (vertical) plane. NRM intensity for each sample given in parentheses.

sites exhibit predominantly reversed polarity with more complex magnetizations in the lower portion of each hole. These regions of complex magnetization include multiple apparent polarity transitions, with polarity shifts noted both within individual pieces and at piece boundaries. Gabbros with apparent normal polarity at the base of Hole 923A are tentatively considered to represent significant low-stability overprints that obscure any pre-existing reversed polarity remanence. In contrast, the high magnetic stability to both AF and

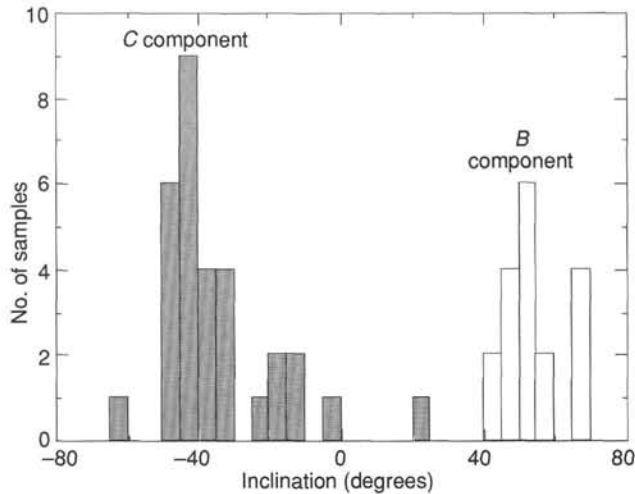


Figure 52. Inclination distribution for magnetization components recognized in samples from Hole 923A. B component is of normal polarity. The highest-stability C component is typically of reversed polarity although this component generally does not represent the characteristic magnetization direction.

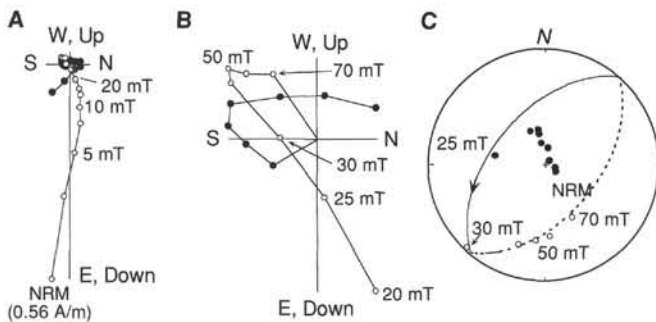


Figure 53. Vector endpoint diagram and equal area plot for Sample 153-923A-7R-2, 4–7 cm. Filled (open) circles in (A) and (B) are projections of the vector onto the horizontal (vertical) plane. Following removal of a drilling remanence (by ~20 mT), the remanence directions during demagnetization lie along a great circle path consistent with the presence of a higher stability reversed polarity component. C. Lower hemisphere projections shown by filled circles and solid line. Arrows indicate progression of magnetic vector during demagnetization.

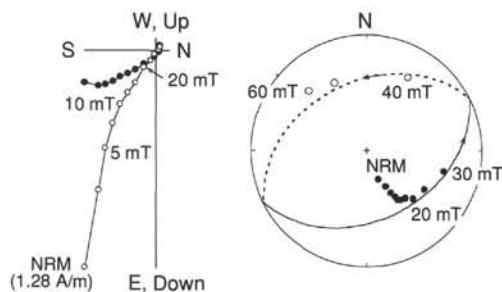


Figure 54. Vector endpoint diagram and equal area plot for sample illustrating possible origin of apparent normal polarity samples in Sample 153-923A-15R-3, 7–10 cm. Filled (open) circles are projections of the vector onto the horizontal (vertical) plane. Following removal of a drilling remanence (by ~10 mT), the remanence directions during demagnetization lie along a great circle path consistent with the presence of a higher stability reversed polarity component. Lower hemisphere projections shown by filled circles and solid line. Arrows indicate progression of magnetic vector during demagnetization.

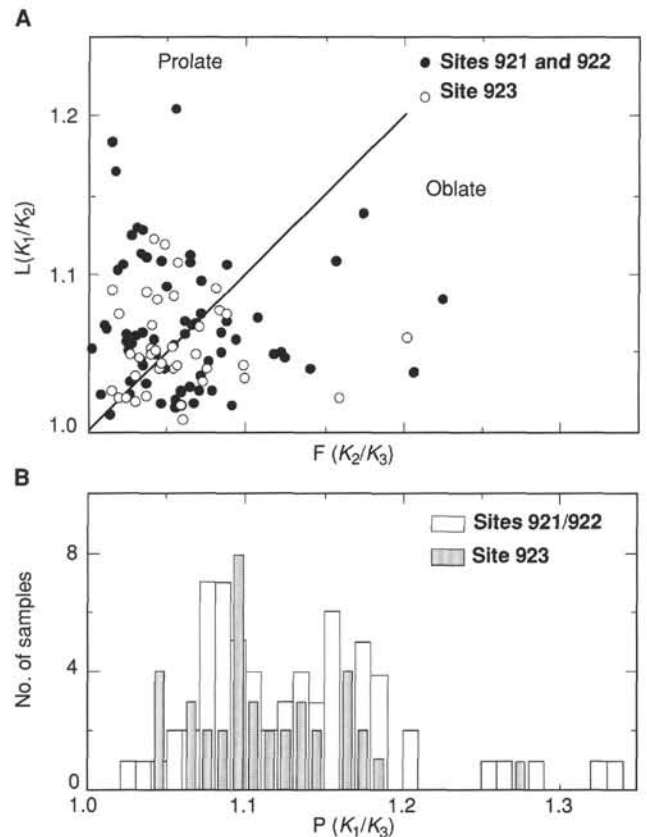


Figure 55. Comparison of magnetic fabric of gabbros from Site 923 and Sites 921 and 922. A. Magnetic fabric lineation (L) vs. foliation (F) illustrating dominantly triaxial susceptibility ellipsoid shape. B. Anisotropy degree (P) for Site 923 gabbros.

thermal demagnetization, and the isolation of similar components by both techniques, in normal polarity gabbros from Site 921 suggest that some primary normal polarity magnetizations are present at this site. Shore-based studies will determine the origin of the magnetization at these sites. However, the presence of reversed polarity magnetizations strongly supports the presence of some gabbroic material older than 0.78 Ma, the age of the last magnetic reversal (Cande and Kent, 1992).

### PHYSICAL PROPERTIES

Thirty-four minicores were sampled from Hole 923A and analyzed for horizontal compressional-wave velocity ( $V_p$ ), resistivity, and a determination of index properties (bulk density, grain density, water content, porosity, and dry density; Table 10). Thermal conductivities were determined from 27 half-round archive sections of core (Table 11). Bulk whole-core densities were measured using the gamma-ray attenuation porosity evaluator (GRAPE) component of the multisensor track. Descriptions of experimental methods are provided in the “Physical Properties” section of the “Explanatory Notes” (this volume) and in “Explanatory Notes” of the Leg 147 *Initial Reports* (Shipboard Scientific Party, 1993).

The following discussion incorporates a summary of index properties for this site, an examination of downhole variations in these properties, and consideration of relationships between examined physical properties. While the measurements are believed to accurately characterize the samples studied, the coarse grain size and small-scale variability characteristic of gabbroic rocks does limit the extent to which results from the analysis of minicores can be extrapolated to larger scale downhole characteristics at each location.

**Table 10. Index properties for Site 923 gabbroic rocks including compressional-wave velocity ( $V_p$ ), resistivity, alteration estimate, rock type, and unit identification from visual core descriptions.**

Core, section, interval (cm)	Piece	Depth (mbsf)	$V_p$ (m/s)	Resistivity ( $\Omega$ m)	FF	Wet-bulk density ( $g/cm^3$ )	Dry-bulk density ( $g/cm^3$ )	Grain density ( $g/cm^3$ )	Void ratio	Porosity (%)	Water content (%)	Alteration estimate (%)	Rock type	Unit
153-923A-														
2R-1, 27-29	4	16.67	6532	528	2641	2.949	2.944	2.959	0.0052	0.519	0.180	85	GA/GG	1
2R-2, 2-4	1	17.59	6098	211	1053	2.893	2.883	2.913	0.0107	1.058	0.375	6	LOG	1
2R-2, 89-91	8	18.46	6587	285	1424	2.971	2.968	2.978	0.0033	0.333	0.115	(7)*	LOG	1
3R-1, 34-36	3	19.54	6379	444	2222	2.976	2.972	2.983	0.0040	0.398	0.137	(5)*	GOG	1
3R-1, 95-97	5B	20.15	5722	265	1325	2.914	2.910	2.923	0.0044	0.436	0.153	2	AGOG	1
3R-2, 34-36	2A	21.03	5736	485	2425	2.933	2.929	2.941	0.0041	0.408	0.142	5	GG	1
4R-1, 118-120	7B	22.38	6467	1098	5488	3.005	3.000	3.014	0.0048	0.479	0.163	18	G	1
4R-1, 121-123	7B	22.41	6180	629	3146	3.000	2.997	3.007	0.0033	0.324	0.111	18	G	1
5R-2, 109-111	2	24.92	6344	1408	7041	2.992	2.989	2.998	0.0030	0.297	0.101	(5)*	G	1
5R-2, 114-116	3	25	5735	380	1901	2.980	2.978	2.983	0.0016	0.161	0.055	(5)*	G	1
6R-1, 122-124	7	25.05	6487	542	2708	2.961	2.959	2.965	0.0021	0.212	0.073	2	OG	1
7R-1, 81-83	9	27.71	6525	171	857	3.010	3.005	3.018	0.0041	0.411	0.140	2	OG	1
8R-1, 29-31	5A	29.29	6564	111	555	2.838	2.836	2.841	0.0018	0.181	0.065	8	OG/G/T	2
8R-3, 10-12	1	31.91	6539	97	484	2.976	2.974	2.980	0.0022	0.217	0.075	4	G	2
9R-1, 130-132	4A	33.2	6558	81	405	2.988	2.986	2.993	0.0025	0.246	0.084	12	OG	2
9R-2, 70-72	8A	34.08	6387	62	310	2.938	2.935	2.943	0.0027	0.270	0.094	17	POG	2
10R-1, 106-108	5D	37.56	6181	167	837	2.759	2.752	2.769	0.0061	0.603	0.224	2	OG	2
10R-2, 39-41	1C	38.16	6262	166	830	2.952	2.950	2.957	0.0025	0.246	0.085	2	OG	2
11R-1, 69-71	8	41.89	6423	134	671	2.988	2.984	2.997	0.0043	0.425	0.146	6	GG	2
11R-2, 58-60	5	43.14	6471	153	765	3.010	3.003	3.023	0.0067	0.663	0.226	5	G	2
12R-1, 126-128	5B	47.26	5875	543	2714	2.893	2.883	2.910	0.0092	0.907	0.322	22	POG	3
12R-2, 18-20	1	47.62	6511	115	576	2.951	2.949	2.956	0.0025	0.246	0.085	2	G	4
12R-2, 41-43	2	47.85	6095	234	1171	2.978	2.976	2.982	0.0021	0.207	0.071	2	OG	4
13R-1, 114-116	13	51.94	6452	197	987	2.985	2.983	2.990	0.0024	0.239	0.082	3	GOG	4
13R-2, 113-115	7	53.38	6529	112	561	2.902	2.897	2.912	0.0049	0.489	0.172	2	OG	4
13R-2, 116-118	7	53.41	6184	123	616	2.890	2.888	2.894	0.0021	0.214	0.076	2	OG	4
13R-3, 50-52	6	54.22	5469	255	1275	3.002	2.996	3.015	0.0064	0.633	0.216	(5)*	G	4
14R-1, 55-57	8	56.05	5412	156	780	2.887	2.881	2.897	0.0055	0.550	0.195	5	TOG	5
14R-2, 6-8	1	56.98	5662	176	878	2.870	2.863	2.882	0.0065	0.646	0.231	10	OG	5
15R-3, 7-9	1	62.91	5619	169	845	2.864	2.862	2.868	0.0021	0.212	0.076	5	OG	5
16R-2, 2-4	1A	65.98	5402	604	3021	2.858	2.844	2.882	0.0133	1.313	0.472	5	OG	5
16R-3, 74-76	5	67.87	5725	330	1648	2.934	2.928	2.945	0.0058	0.576	0.201	1	OG	5
16R-4, 60-62	7	68.98	5663	201	1007	2.926	2.917	2.943	0.0087	0.858	0.301	4	OG	5
16R-4, 63-65	7	69.01	5650	623	3113	3.017	3.013	3.025	0.0041	0.412	0.140	4	OG	5

Notes: \* = not measured in this sample (nearby value). G = gabbro, OG = olivine gabbro, T = troctolite, GA/GG = gneissic amphibolite/gneissic gabbro, LOG = lined olivine gabbro, GOG = gneissic olivine gabbro, AGOG = augen gneissic olivine gabbro, POG = poikilitic olivine gabbro, TOG = troctolitic olivine gabbro. FF = formation factor.

## Data

Bulk densities, porosity, water content, and void ratio have been determined (with salt volume corrections for a salinity of 0.032) from wet and dry mass and volume measurements of minicores sampling the predominantly gabbroic rock recovered at Site 923 (Table 10). Bulk densities range from 2.76 to 3.02  $g/cm^3$  with a median value of 2.95  $g/cm^3$ . Grain densities are only slightly higher (2.77 to 3.03  $g/cm^3$ , median value 2.96  $g/cm^3$ ), reflecting the characteristic low porosity (0.16% to 1.31%, median value 0.41%) of these rocks.  $V_p$  ranges from 5402 to 6587 m/s, with a median value of 6223 m/s. The densities and velocities of these rocks are similar to those observed in metagabbro exposed in fracture zones of the Atlantic (e.g., compilation of Christensen, 1982), and to those gabbroic rocks from Sites 921 and 922. The rocks display thermal conductivities ranging from 1.9 to 3.1  $W/m^{\circ}C$  with a median value of 2.6  $W/m^{\circ}C$ , which is within the range of variability observed in gabbroic material by Clark (1966).

Figure 56 shows the variations in resistivity, velocity, porosity, bulk density, thermal conductivity, and alteration as a function of depth in Hole 923A. No samples were taken from the first core recovered, but moderately dense sampling of the relatively continuous core recovered from the remainder allows discussion of variations downhole at this location.

Unit 1 (below 16.5 mbsf) is characterized by an increase in resistivity and bulk density, a decrease in porosity, and relatively constant thermal conductivity to about 25 mbsf. Compressional-wave velocity ( $V_p$ ) and degree of alteration fluctuate with depth with no discernible trend in this interval. From 25 to 33 mbsf, resistivity decreases while velocity remains approximately constant. Porosity and extent of alteration estimated from visual core descriptions (see also "Igneous" and "Metamorphic Petrology" sections, this chapter) show a gentle increasing trend in the interval from 25 to 33 mbsf. Thermal conductiv-

**Table 11. Thermal conductivity for archive half-round core pieces and alteration, rock type, and unit identification from visual core descriptions.**

Core, section, interval (cm)	Piece	Depth (mbsf)	Thermal conductivity ( $W/m^{\circ}C$ )	Alteration (%)	Rock type	Unit
153-923A-						
2R-1, 13-24	3	16.53	2.569	(85)*	GA	1
2R-2, 86-104	8	18.43	2.653	(7)*	LOG	1
3R-1, 29-38	2A	19.49	2.555	5	GOG	1
3R-1, 34-47	3B	19.54	2.624	(5)*	GOG	1
3R-2, 29-38	2A	20.98	2.723	5	GG	1
4R-1, 118-137	7B	22.38	2.635	18	G	1
5R-2, 90-113	2A	24.81	2.528	(5)*	G	1
5R-2, 114-127	3A	25.05	2.670	(4)*	G	1
6R-1, 125-142	13	25.95	2.589	2	OG	1
7R-1, 80-102	9	27.70	2.285	2	OG	1
8R-1, 23-40	5A	29.23	2.350	8	OG/G/T	2
8R-3, 1-16	1	31.82	2.606	4	G	2
9R-1, 120-135	4A	33.10	3.094	12	OG	2
10R-1, 101-115	5D	37.51	2.994	2	OG	2
10R-3, 42-56	3	39.61	2.809	(2)*	G	2
11R-1, 62-83	8	41.82	2.812	6	GG	2
11R-2, 49-67	5	43.05	2.303	5	G	2
12R-2, 1-21	1	47.45	2.486	2	G	4
12R-2, 23-45	2	47.67	2.961	2	OG	4
13R-1, 106-119	13	51.86	2.908	5	GOG	4
13R-2, 99-120	7	53.24	2.319	2	OG	4
13R-3, 49-63	6	54.21	2.805	(5)*	G	4
14R-1, 54-67	8	56.04	2.232	5	TOG	5
14R-2, 1-14	1	56.93	2.816	10	OG	5
15R-1, 90-104	14	61.20	2.718	34	OG	5
16R-2, 1-18	1A	65.97	1.889	5	OG	5
16R-4, 58-72	7	68.96	2.330	4	OG	5

Notes: \* = not measured in this sample (nearby value). G = gabbro, OG = olivine gabbro, T = troctolite, GA = gneissic amphibolite, LOG = lined olivine gabbro, GOG = gneissic olivine gabbro, AGOG = augen gneissic olivine gabbro, TOG = troctolitic olivine gabbro.

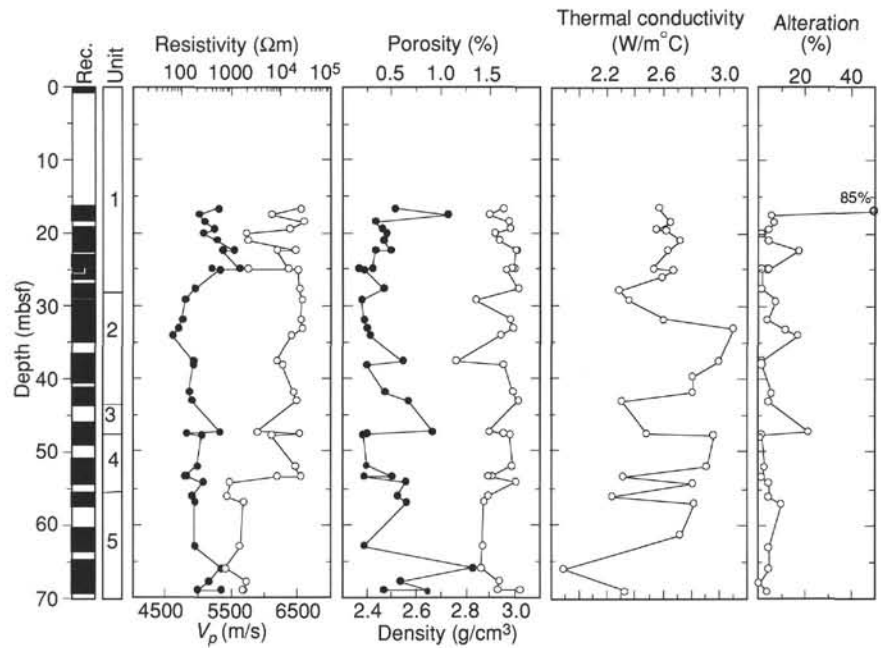


Figure 56. Physical property determinations adjacent to bars indicating core recovery (black) and unit identification as functions of depth for Hole 923A. Circles represent locations of physical properties determinations. First panel from left: left curve is resistivity (filled circles), right curve is compressional wave velocity ( $V_p$ ) (open circles). Second panel: left curve is porosity (filled circles), right curve is density (open circles).

ity increases steadily from about 2.3 to 3.1 W/m°C, and the maximum values observed correspond with more highly altered (12%) olivine gabbro within Unit 2. With the exception of one lower density minicore sampled from an olivine gabbro, gabbro, and troctolite piece (Sample 153-923A-8R-1, Piece 5A, 29–31 cm; bulk density 2.84 g/cm<sup>3</sup>), bulk densities remain relatively constant at about 3.0 g/cm<sup>3</sup> to 33 mbsf. The transition to Unit 2 at 28.2 mbsf occurs with the lower density olivine gabbro, gabbro, and troctolite that also display low thermal conductivity.

From around 33 mbsf (within Unit 2), resistivity and porosity appear to generally increase with depth, whereas velocity and thermal conductivity generally decrease with depth to the base of Unit 2. Bulk-density measurements remain around 2.9–3.0 g/cm<sup>3</sup> with a decrease to less than 2.8 g/cm<sup>3</sup> corresponding with a local high in porosity at about 39 mbsf.

The moderately altered (22%), moderately porous (0.9%) poikilitic olivine gabbro sampled at the base of Unit 3 (Sample 153-923A-12R-1, Piece 5B, 126–128 cm) shows relatively high resistivity and low velocity, bulk density, and thermal conductivity compared to the underlying Unit 4. The varitextured gabbro and olivine gabbro of Unit 4 display variable physical properties, particularly in the lowermost sections of core recovered from this unit.

Minicores from Unit 5 are characterized by considerably lower velocities (averaging 5500–5600 m/s) than was observed in the overlying Units 2, 3, and 4 (6300–6500 m/s). Unit 5 is characterized by densities of less than 2.9 g/cm<sup>3</sup> for all but the base of the section, where density increases to near 3.0 g/cm<sup>3</sup>. Thermal conductivity generally decreases with depth in this unit, with a pronounced low of about 1.9 W/m°C at 66 m depth that corresponds with a pronounced porosity high (1.3%), a local velocity low (5400 m/s), and an increase in resistivity in the olivine gabbro Sample 153-923A-16R-2 (Piece 1A, 2–4 cm). Extent of alteration appears to be relatively low and constant in samples from this unit (estimated from visual core descriptions to be 4%–5%).

### GRAPE Assessment

Variations in density with depth were determined by GRAPE at Hole 923A (Fig. 57). As was the case at Site 920, GRAPE densities for this hole are systematically low although the major trends recorded by the discrete sample analysis remain. Spurious GRAPE

determinations generally correspond with ends of core pieces or gaps between pieces. However, in sections with relatively good recovery it appears that the GRAPE may provide a good resolution in density variations with depth where the core is characterized by relatively continuous and long (>15 cm) piece lengths (e.g., 36.5–41, 61–63, and 65–69 mbsf). This again indicates that, with appropriate calibration and volume corrections, GRAPE measurements could be of some utility in future high-recovery hard-rock legs.

### Comparative Analysis of Site 923 Physical Properties Measurements

The compressional-wave velocities measured in core recovered from the upper 53 m of Hole 923A are relatively high, ranging from 5722 to 6587 m/s with a mean value of 6301 m/s and a median value of 6405 m/s. This median velocity is high for the upper crust although still falling within the range generally associated with seismic Layer 2. These velocities are comparable to those observed in gabbroic rocks with similar densities and low to moderate porosities recovered from Hole 735B in the southwest Indian Ocean (Robinson, Von Herzen, et al., 1989) or from the Hess Deep area (Gillis, Mével, Allan, et al., 1993).

The lowermost part of Unit 4 and all of Unit 5 are characterized by material displaying much lower compressional-wave velocities (5402–5725 m/s, mean value 5575 m/s, and median 5634 m/s). While minicore samples from the upper and lower parts of the core (above and below 53 mbsf) show the same range of observed densities, the median density for the faster upper part is 2.97 g/cm<sup>3</sup>, whereas the lower part displays a median density of only 2.91 g/cm<sup>3</sup>. The lower part of the core also shows slightly greater porosities (median value of 0.6%) than are observed in the upper part (median value of 0.33%), although porosity varies considerably throughout the entire recovered core sampled at Site 923.

Compressional-wave velocity ( $V_p$ ) generally increases with increasing density (Fig. 58), particularly in the olivine gabbro and variably deformed gabbro. However, relatively high-density, low-velocity material also occurs in core recovered from gabbroic rock located at the base of Unit 4 (Sample 153-923A-13R-3, Piece 6, 50–52 cm) and in olivine gabbro located near the base of Unit 5 (Sample 153-923A-16R-4, Piece 7, 63–65 cm). Undeformed gabbroic rock (Gabbro [2%–5%] and Gabbro [18%]) in Fig. 58, upper

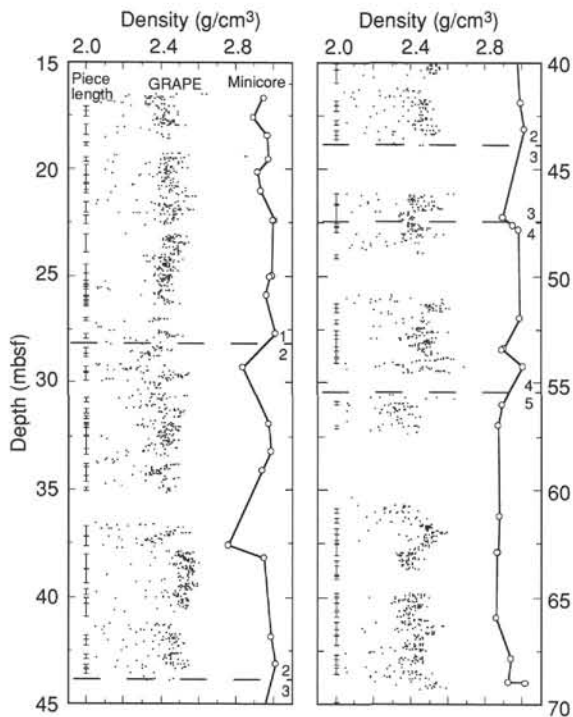


Figure 57. GRAPE data from Hole 923A shown in two panels with 5 m overlap between panels (40–45 m). Length of core pieces shown as bars on left of panels; GRAPE data are shown as dots, and discrete minicore density determinations are shown as open circles connected by fine lines. All GRAPE determinations less than 2 g/cm<sup>3</sup> have been removed from the profile. Unit boundaries indicated by horizontal dashed lines bracketed by unit numbers.

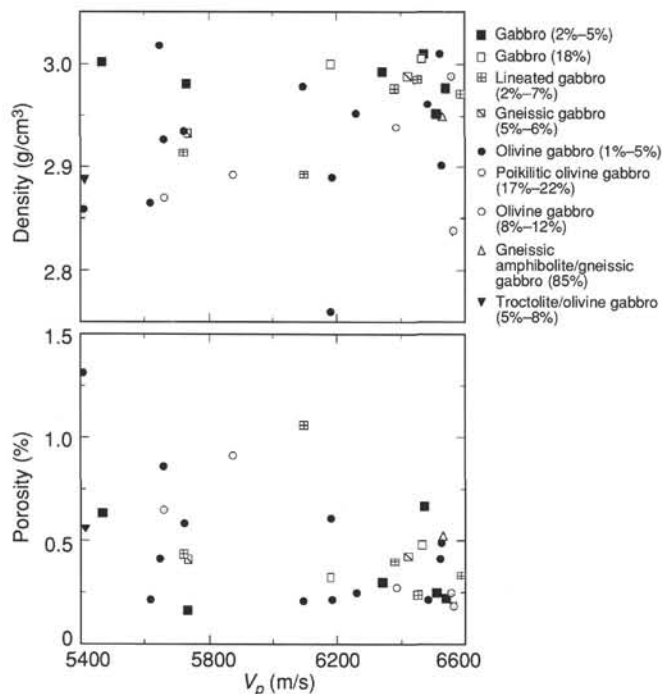


Figure 58. Velocity ( $V_p$ ) vs. density and velocity ( $V_p$ ) vs. porosity for rocks recovered at Site 923. Parenthetic values indicate extent of alteration from visual core descriptions.

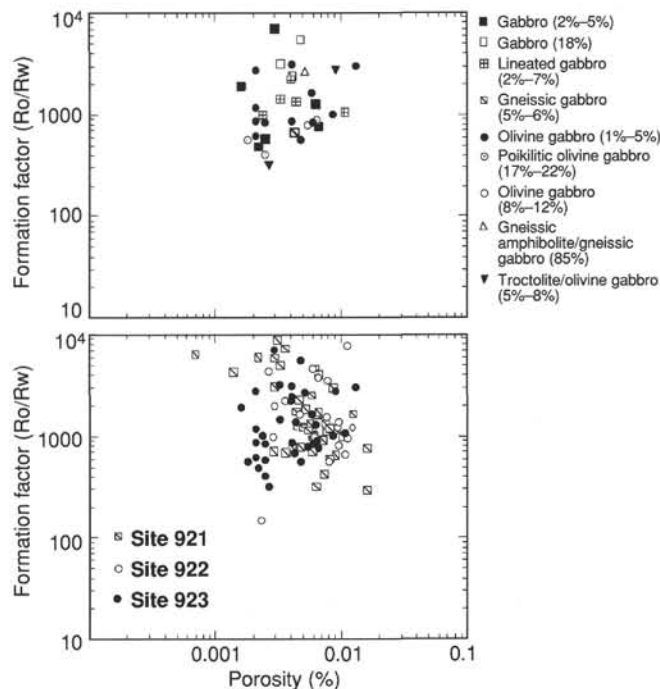


Figure 59. Formation factor (ratio of rock and pore water resistivity) vs. porosity (corrected for salt) for rocks recovered at Site 923, and formation factor (ratio of rock and pore water resistivity) vs. porosity (corrected for salt) for rocks recovered at Sites 921, 922, and 923. Parenthetic values indicate extent of alteration from visual core descriptions.

panel) does not show any discernible velocity-density relationship. Decreasing compressional-wave velocity ( $V_p$ ) is weakly related to increasing porosity (Fig. 58), with no obvious dependence on rock type as determined from visual core descriptions.

Formation factor (ratio of rock and pore water resistivity) and porosity (shown as a ratio of rock volume corrected for salt) of gabbroic rock from Site 923 are shown in Figure 59. Site 923 samples display considerable scatter that does not appear to be related to rock type as determined from the visual core descriptions (Fig. 59). Some of the scatter may be due to limitations in experimental procedures. However, changes in resistivity trends downhole (Fig. 56) generally coincide with variations in other observed physical properties and probably reflect changes in rock properties with depth in the core. If this is the case, it would appear that mechanisms for electronic conduction in rocks recovered from Site 923 are variable.

## REFERENCES\*

- Auzende, J.M., Cannat, M., Gente, P., Henriot, J.P., Juteau, T., Karson, J.A., Lagabrielle, Y., and Tivey, M.A., 1993. Deep layers of mantle and oceanic crust exposed along the southern wall of the Kane Fracture Zone: submersible observations. *C.R. Acad. Sci. Ser. 2*, 317:1641–1648.
- Bideau, D., Hebert, R., Hekinian, R., and Cannat, M., 1991. Metamorphism of deep-seated rocks from the Garret Ultrafast Transform (East Pacific Rise near 13°25'S). *J. Geophys. Res.*, 96:10079–10099.
- Campbell, I.H., 1977. A study of cumulate processes and macrorhythmic layering in the Jimberlana Layered Intrusion of western Australia: Part I: The upper layered series. *J. Petrol.*, 18:183–215.

\* Abbreviations for names of organizations and publications in ODP reference lists follow the style given in *Chemical Abstracts Service Source Index* (published by American Chemical Society).

- Cande, S.C., and Kent, D.V., 1992. A new geomagnetic polarity time scale for the Late Cretaceous and Cenozoic. *J. Geophys. Res.*, 97:13917–13951.
- Christensen, N.I., 1982. Seismic velocities. In Carmichael, R.S. (Ed.), *Handbook of Physical Properties of Rocks*: Boca Raton, FL (CRC Press), 2:1–228.
- Clark, S.P. (Ed.), 1966. *Handbook of Physical Constants*. Mem.—Geol. Soc. Am., 97.
- Gillis, K.M., Mével, C., Allan, J.F., et al., 1993. *Proc. ODP, Init. Repts.*, 147: College Station, TX, (Ocean Drilling Program).
- Ito, E., and Anderson, A.T., Jr., 1983. Submarine metamorphism of gabbros from the Mid Cayman Rise: petrographic and mineralogic constraints on hydrothermal processes at slow-spreading ridges. *Contrib. Mineral. Petrol.*, 82:371–388.
- Jackson, E.D., 1961. Primary textures and mineral associations in the ultramafic zone of the Stillwater Complex, Montana. *Geol. Surv. Prof. Pap. U.S.*, 358.
- Karson, J.A., and Dick, H.J.B., 1983. Tectonics of ridge-transform intersections at the Kane Fracture Zone. *Mar. Geophys. Res.*, 6:51–98.
- McFadden, P.L., and Reid, A.B., 1982. Analysis of paleomagnetic inclination data. *Geophys. J. R. Astron. Soc.*, 69:307–319.
- Mével, C., Cannat, M., Gente, P., Marion, E., Auzende, J.-M., and Karson, J.A., 1991. Emplacement of deep crustal and mantle rocks on the west median valley wall of the MARK area (MAR 23°N). *Tectonophysics*, 190:31–53.
- Robinson, P.T., Von Herzen, R., et al., 1989. *Proc. ODP, Init. Repts.*, 118: College Station, TX (Ocean Drilling Program).
- Shipboard Scientific Party, 1993. Explanatory notes. In Gillis, K., Mével, C., Allan, J., et al., *Proc. ODP, Init. Repts.*, 147: College Station, TX (Ocean Drilling Program), 15–42.
- Spear, F.S., 1980. NaSi-CaAl exchange equilibrium between plagioclase and amphibole, an empirical model. *Contrib. Mineral. Petrol.*, 72:33–41.
- , 1981. An experimental study of hornblende stability and compositional variability in amphibolite. *Am. J. Sci.*, 281:697–734.
- Wadsworth, W.J., 1961. The ultrabasic rocks of southwest Rhum. *Philos. Trans. R. Soc. London B*, 244:21–64.

Ms 153IR-105

**NOTE: For all sites drilled, core-description forms (“barrel sheets”), and core photographs can be found in Section 3, beginning on page 277. Thin-section data are given in Section 4, beginning on page 665. The CD-ROM (back pocket, this volume) contains the complete set of spreadsheets with piece-by-piece data for all structural features identified and measured. A set of summary spreadsheets that are linked to the igneous and metamorphic spreadsheets are also contained on the CD-ROM. Keys, summary tables, checklists, and thin-section summaries and notes are also archived. Compressed versions of the figures created for this volume, compatible with Macintosh computers, are located in the directories labeled REPT92X in the “Structure” directory. Scanned TIFF images of all the SVCD drawings are archived in the “STRCDRAW” file. Apparent dip data and true strike and dip data for all measurable features are contained in the “STR\_DIP” subdirectory. This directory also contains the LinesToPlane documentation and program that converts the apparent dip data to true strike and dip in an archived form. GRAPE, MST, and index properties are also reported on the CD-ROM.**